

Winter 2009

# Chipless RFID sensor tag system with microstrip transmissionline based ID generation schemes

Sudhir Shrestha

Follow this and additional works at: <https://digitalcommons.latech.edu/dissertations>

 Part of the [Electrical and Computer Engineering Commons](#)

---

CHIPLESS RFID SENSOR TAG SYSTEM WITH  
MICROSTRIP TRANSMISSIONLINE BASED  
ID GENERATION SCHEMES

by

Sudhir Shrestha, B.E.

A Dissertation Presented in Partial Fulfillment  
of the Requirement for the Degree of  
Doctor of Philosophy in Engineering

COLLEGE OF ENGINEERING AND SCIENCE  
LOUISIANA TECH UNIVERSITY

March 2009

UMI Number: 3351362

### INFORMATION TO USERS

The quality of this reproduction is dependent upon the quality of the copy submitted. Broken or indistinct print, colored or poor quality illustrations and photographs, print bleed-through, substandard margins, and improper alignment can adversely affect reproduction.

In the unlikely event that the author did not send a complete manuscript and there are missing pages, these will be noted. Also, if unauthorized copyright material had to be removed, a note will indicate the deletion.

**UMI**<sup>®</sup>

---

UMI Microform 3351362

Copyright 2009 by ProQuest LLC.

All rights reserved. This microform edition is protected against unauthorized copying under Title 17, United States Code.

ProQuest LLC  
789 E. Eisenhower Parkway  
PO Box 1346  
Ann Arbor, MI 48106-1346

LOUISIANA TECH UNIVERSITY

THE GRADUATE SCHOOL

January 15, 2009

Date

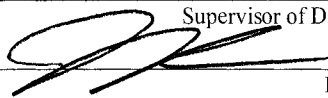
We hereby recommend that the dissertation prepared under our supervision  
by Sudhir Shrestha

entitled CHIPLESS RFID SENSOR TAG SYSTEM WITH MICROSTRIP TRANSMISSION  
LINE BASED ID GENERATION SCHEMES

be accepted in partial fulfillment of the requirements for the Degree of  
Doctor of Philosophy in Engineering



Supervisor of Dissertation Research



Head of Department

Department

Recommendation concurred in:



Advisory Committee

Approved:

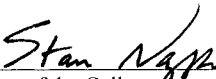


Director of Graduate Studies

Approved:



Dean of the Graduate School



Dean of the College



## ABSTRACT

This dissertation presents a chipless radio frequency identification (RFID) sensor tag system consisting of passive chipless RFID sensor tags and specialized reader. The chipless sensor tags are fabricated on a flexible substrate and contain an ID generation circuit, a sensor, and a microstrip antenna. The ID generation circuit consists of meandered microstrip transmission lines and uses a novel reflection and delay based ID generation scheme. The scheme, using an input RF pulse, constructs an on-off keying (OOK) or pulse position modulated (PPM) signal pattern representing a unique ID code. Two transmission lines and OOK representation are used and the generation of ten different ID codes are demonstrated. The integrated ID generation circuit, sensor, and antenna use a single transmission line and PPM representation, and demonstrate the generation of eight different ID codes. However, the presented schemes allow the generation of higher combinations of bits.

A practical method to measure radar cross section (RCS) parameters of antennas that provides complete and more accurate information on scattering properties of antennas, essential for chipless sensor tag design, is presented. The new method uses minimum mean square error estimation solution of a derived received backscattered signal power equation and provides load independent structural-mode RCS, antenna-mode RCS, and relative phase factor of the measured antenna. Two configurations of the chipless sensor tags configuration-I (conf-I) and configuration-II (conf-II) are presented.

In conf-I tags, sensors are connected as a load to the antenna and the sensor information is amplitude modulated in the backscattered signal. The testing with conf-I temperature sensor tag resulted in a 28% amplitude change when the temperature at the tag changes from 27 °C to 140 °C. In conf-II tags, sensors are connected as load to the ID generation circuit and the sensor information is phase modulated in the antenna-mode scattered signal. With the conf-II ethylene sensor tag, a phase change of 33° is observed when the ethylene concentration at the tag changes from 0 to 100 ppm. The specialized reader system is comprised of an analog reader that wirelessly communicates with the sensor tags and a single board computer that computes the sensor information from the received signal. The reader system constructs a 96 bit serialized global trade item number (SGTIN-96) electronic product code (EPC) format unique RFID tag data frame, including 16 bit sensor information, and makes the information available on a secure web interface accessible from cyberspace. The presented sensor tag system has the advantages of passive and chipless sensor tag operation, while offering a wide range of sensors types for integration. Moreover, it offers a viable alternative solution to existing active as well as passive RFID sensor tag systems (eg. SAW based RFID sensor tag systems).

## APPROVAL FOR SCHOLARLY DISSEMINATION

The author grants to the Prescott Memorial Library of Louisiana Tech University the right to reproduce, by appropriate methods, upon request, any or all portions of this Dissertation. It is understood that "proper request" consists of the agreement, on the part of the requesting party, that said reproduction is for his personal use and that subsequent reproduction will not occur without written approval of the author of this Dissertation. Further, any portions of the Dissertation used in books, papers, and other works must be appropriately referenced to this Dissertation.

Finally, the author of this Dissertation reserves the right to publish freely, in the literature, at any time, any or all portions of this Dissertation.

Author 

Date 02/02/2009

## **DEDICATION**

To:

my mother, Chunu Maya Shrestha;

brother-in-law, Narayan Thapa; sister, Sarala Thapa;

brother, Sanjaya Shrestha; sister-in-law, Punam Shrestha;

niece and nephews, Namisha Thapa, Nishan Thapa, Saharsha Shrestha;

and

my beloved wife Ranjana Shrestha.

## TABLE OF CONTENTS

ABSTRACT.....	iii
DEDICATION.....	vi
LIST OF TABLES.....	xii
LIST OF FIGURES.....	xiii
ACKNOWLEDGMENTS.....	xviii
CHAPTER 1 INTRODUCTION .....	1
1.1 Background .....	1
1.1.1 RFID System .....	1
1.1.2 RFID Sensor Tags .....	2
1.1.3 Chipless RFID Sensor Tags .....	3
1.1.4 Chipless RFID Sensor Tag Readers .....	4
1.2 Related Research .....	4
1.3 Research Motivation.....	7
1.3.1 Market Research.....	8
1.3.2 Chip-based and Chipless RFID Tags .....	10
1.3.3 Secure Sensor Information and Application in Harsh Environments .....	11
1.4 Contribution of Dissertation.....	11
1.5 Organization of Dissertation .....	12
CHAPTER 2 SYSTEM OVERVIEW .....	14
2.1 System Overview .....	14
2.2 Chipless Sensor Tag .....	15
2.2.1 Antenna .....	17
2.2.2 Chipless ID Generation Circuit.....	17
2.2.3 Sensor .....	18
2.3 Reader System.....	19
2.3.1 Analog Reader.....	20
2.3.2 Single Board Computer.....	20
2.4 User Interfaces and Authentication.....	21
2.5 Cyber Centric Monitoring .....	22
CHAPTER 3 MEANDERED MICROSTRIP TRANSMISSION LINES .....	24
3.1 Microstrip Transmission Lines.....	24
3.1.1 Wave Propagation in Microstrip Transmission Lines.....	25

3.1.2	Transmission Line Equations and Solutions .....	26
3.1.3	Effective Dielectric Constant and Characteristic Impedance .....	30
3.2	Microstrip Transmission Line Design .....	32
3.3	Meandered Microstrip Transmission Line Design .....	34
3.4	Loss, Dispersion, and Bandwidth .....	35
3.4.1	Losses .....	36
3.4.1.1	Resistive Loss .....	36
3.4.1.2	Dielectric Loss .....	37
3.4.1.3	Radiation Loss .....	37
3.4.2	Dispersion .....	38
3.4.3	Bandwidth .....	39
3.5	Delay and Reflection .....	40
3.5.1	Delay .....	40
3.5.2	Reflection .....	40
3.6	Optimization of Meandered Microstrip Transmission Line Design .....	41
3.6.1	Transmission Line Width .....	42
3.6.2	Meandering Width .....	43
3.6.3	Bend Type .....	44
CHAPTER 4 MICROSTRIP TRANSMISSION LINE REFLECTION AND DELAY		
	BASED ID GENERATION SCHEME .....	46
4.1	Signal Reflection and Delay in Single and Multiple Transmission Lines	
	System .....	46
4.1.1	Single Transmission Line System .....	46
4.1.2	Multiple Transmission Lines System .....	48
4.1.3	Step Impedance Transmission Line System .....	50
4.2	ID Generation using Reflection and Delay in Transmission Lines .....	51
4.2.1	Dual Transmission Lines ID Circuit using OOK Coding .....	51
4.2.2	Step Impedance Transmission Line ID Circuit using OOK Coding .....	53
4.2.3	Phase Modulation Scheme .....	54
4.2.4	Single Transmission Line using PPM Coding .....	55
4.3	Design and Fabrication of Transmission Line Reflection and Delay Based ID	
	Tags .....	57
4.3.1	Tag Design .....	57
4.3.2	Mask Design and Printing .....	59
4.3.3	Photolithography and Etching .....	59
4.4	Measurement Setup .....	60
4.5	Results and Discussions .....	61
4.5.1	Single Transmission Line Circuit .....	61
4.5.2	Dual Transmission Lines ID Circuit .....	63
4.5.3	Step Impedance Transmission Line ID Circuit .....	65
4.6	Antenna Integration .....	67
4.6.1	Antenna Parameters .....	67
4.6.1.1	Resonant Frequency .....	67
4.6.1.2	VSWR .....	67
4.6.1.3	Bandwidth .....	68
4.6.1.4	Gain .....	68

4.6.1.5 Radiation Pattern.....	69
4.6.1.6 Impedance.....	69
4.6.1.7 Size.....	69
4.6.2 Antenna Scattering.....	69
4.6.3 Antenna Scattering Property in Chipless Sensor Tag Design.....	70
CHAPTER 5 RFID TAG ANTENNA SCATTERING PAREMETERS: THEORY AND EXPERIMENTATION FOR A NEW MEASUREMENT METHOD.....	71
5.1 Antenna Backscattering.....	72
5.1.1 Structural-Mode Scattering.....	72
5.1.2 Antenna-Mode Scattering.....	73
5.1.3 Properties of Antenna Backscattering.....	73
5.2 RCS Parameters of Antenna.....	74
5.3 Measurement of RCS Parameters of Antenna.....	75
5.3.1 Conventional RCS Measurement Methods and Challenges.....	75
5.3.2 Need for a New RCS Measurement Method.....	76
5.4 A New Method to Measure RCS Parameters of Antennas.....	77
5.4.1 Theory.....	77
5.4.2 Determination of RCS Parameters using Minimum Mean Square Error Estimation.....	82
5.4.3 Measurement Setup.....	86
5.4.4 Results and Discussions.....	87
5.4.5 Comparison with Previous Measurement Methods.....	90
5.5 Application of RCS Parameters of Antennas in RFID System Design.....	91
5.5.1 Estimation of Received Backscattered Power using Derived Equation.....	91
5.5.2 Chip-based RFID Systems.....	92
5.5.3 RFID Reader Design.....	93
5.5.4 Chipless Sensor Tag Design using Scattering Properties of Antenna.....	93
CHAPTER 6 CHIPLESS SENOSR TAGS.....	94
6.1 Sensor Integrated Antenna Tags (Conf-I Sensor Tags).....	95
6.1.1 Theory.....	95
6.1.2 Design and Fabrication.....	96
6.1.3 Experimental Setup.....	97
6.1.4 Results and Discussions.....	98
6.2 Antenna Scatterings Based ID Generation and Sensor Information Extraction Scheme.....	99
6.2.1 Antenna Scatterings.....	100
6.2.2 Relative Time Domain Delay between Structural-Mode and Antenna-Mode Scattered Pulse Signals.....	100
6.2.3 ID Code Generation using Relative Time Domain Delay.....	101
6.2.4 Relative Phase Difference between Structural-Mode and Antenna-Mode Scattered Pulse Signals.....	102
6.2.5 Sensor Information Extraction using Relative Phase Difference.....	103
6.3 Sensor Requirements.....	103
6.4 Freshness Sensor.....	104

6.4.1 Ethylene Sensor as Freshness Sensor .....	104
6.4.2 Tin-dioxide Nanoparticles Based Ethylene Sensor .....	104
6.4.3 Fabrication of Sensor on the Tag .....	105
6.4.4 Characterization.....	107
6.5 Design and Simulation of Conf-II Tags .....	107
6.5.1 ID Code Generation.....	108
6.5.2 Sensor Information Extraction .....	109
6.6 Fabrication.....	110
6.7 Measurement Setup .....	112
6.8 Results and Discussions .....	113
6.8.1 ID Code Observation.....	113
6.8.2 Phase Change Observation.....	114
6.8.2.1 Results with Discrete Components .....	114
6.8.2.2 Results with Ethylene Sensor.....	117
<b>CHAPTER 7 READER SYSTEM DESIGN AND IMPLIMENTATION .....</b>	<b>120</b>
7.1 Introduction .....	120
7.2 RFID Tag Data Frame Structures.....	122
7.3 Tag ID Standardization Scheme for Chipless RFID Sensor Tags.....	123
7.4 Reader System Components.....	126
7.4.1 Analog Reader.....	126
7.4.2 A Single Board Computer .....	128
7.4.2.1 Hardware Selection.....	129
7.4.2.1.1 Freescale QUICCstart MPC8248.....	129
7.4.2.1.2 Rabbit Coyote BL2500 .....	130
7.4.2.2 Configuration and Programming .....	131
7.4.2.2.1 Freescale SBC .....	131
7.4.2.2.2 Rabbit Core SBC.....	134
7.4.2.3 Connection with the Analog Reader.....	134
7.4.2.3.1 Freescale SBC .....	135
7.4.2.3.2 Rabbit Core SBC.....	136
7.5 Reader System Firmware Development with Rabbit Core SBC.....	137
7.5.1 Initializations .....	138
7.5.2 Web Interface Files .....	139
7.5.3 Input from Analog Reader.....	139
7.5.4 Computation of Sensor Value .....	139
7.5.5 RFID Tag Data Frame Construction .....	140
7.5.6 Information Access through Web Interface and User Authentication .....	140
7.6 System Test Results and Discussions.....	142
7.6.1 Reader Configuration .....	142
7.6.2 System Testing Results .....	143
<b>CHAPTER 8 APPLICATIONS.....</b>	<b>146</b>
8.1 Low Cost Printable RFID Tag Applications .....	146
8.2 RCS Measurement of Antennas for RFID Tag and Reader Design.....	147
8.3 Low Cost Passive Chipless Sensing Applications .....	148
8.4 Cyber Centric Environment Monitoring Applications.....	149



CHAPTER 9 CONCLUSION AND FUTURE WORK.....152

- 9.1 Conclusion.....152
- 9.2 Future Work .....155
  - 9.2.1 Substrate with Higher Delay for Higher Number of Bits.....155
  - 9.2.2 More Flexible Substrates.....156
  - 9.2.3 Tag Printing Techniques .....157
  - 9.2.4 Automatic ID Code and Phase Decoding.....157
  - 9.2.5 Cellular RFID Sensor Tag Deployment Scheme using Mobile Readers .....158

REFERENCES.....161

## LIST OF TABLES

Table 1.1 RFID Tag Revenues by Market in the Year 2008 .....	9
Table 1.2 Price Comparison between Chip-based and Proposed Chipless RFID Tags.....	11
Table 3.1 Design Parameters of Microstrip Transmission Line on FR9151 CU CLAD Substrate.....	34
Table 3.2 Comparison of Input and Output Signals from the Transmission Lines using Corner, Curved, and Mitered Bend Types. ....	45
Table 5.1 Measured RCS Parameters Obtained using Method Presented in this Paper (A) Shown with the Results Obtained using Method Similar to that Described in [56] and [57] (B). Also using the Standard Deviations Shown in Result A, $\sigma_s \pm 2\Delta\sigma_s = (-18.129, -18.493)$ and $\sigma_s$ .....	89
Table 5.2 RCS Parameters Obtained Considering Idealistic Measurement Conditions....	90
Table 7.1 RFID Tag Classifications Based on Tag Capabilities .....	122
Table 7.2 EPC RFID Tag Classifications and Tag Format Structures .....	123
Table 7.3 A Typical SGTIN-96 EPC RFID Tag Data Structure .....	124
Table 7.4 Partitioning of the Serial Number Field to Include Reader ID, Tag ID, Sensor Information.....	125
Table 9.1 High Dielectric Constant Materials .....	156
Table 9.2 More Flexible Substrates for Sensor Tag Fabrication .....	156

## LIST OF FIGURES

Figure 1.1 Schematic diagram of a typical passive RFID system. ....	2
Figure 1.2 Total RFID market projection in US dollars (billion) for the years 2008, 2013, and 2018. ....	9
Figure 1.3 Market projection for chipless RFID tags as a percentage of total market for the years 2006, 2010, and 2016. ....	10
Figure 2.1 Schematic of the chipless RFID sensor tag system. ....	15
Figure 2.2 Schematics of conf-I and conf-II tags. ....	16
Figure 2.3 The monitoring web interface. ....	22
Figure 2.4 Monitoring of reader systems through cyberspace. ....	23
Figure 3.1 Schematic of a microstrip transmission line showing the trace conductor, dielectric layer, and ground plane. ....	25
Figure 3.2 Figures showing electric and magnetic field lines in a microstrip transmission line. ....	26
Figure 3.3 Distributed circuit representation of transmission lines. ....	27
Figure 3.4 Cross sectional view of a microstrip transmission line. ....	30
Figure 3.5 Transmission line trace of same dimensions as shown in Figure 3.4, surrounded by a new medium of dielectric constant $\epsilon_{re}$ . ....	31
Figure 3.6 Substrate parameters of FR9151 CU CLAD used for transmission line fabrication. ....	33
Figure 3.7 Meandered microstrip transmission line design showing various design parameters. ....	35
Figure 3.8 Substrate stacks in the Ansoft Designer simulation tool. ....	42
Figure 3.9 A meandered transmission line design in Ansoft Designer. ....	42

Figure 3.10 Return loss (S11) in decibel (dB) versus the width of the transmission line ( $w$ ) in micrometers.....	43
Figure 3.11 Ansoft Designer simulation setup used for bend type optimization.....	45
Figure 4.1 Pulse reflection in a ground terminated transmission line. ....	48
Figure 4.2 Pulse reflections in two transmission lines with ground terminations. ....	49
Figure 4.3 Pulse reflections in an open terminated step impedance transmission line....	50
Figure 4.4 (a) Schematic representations of two different OOK modulated signal patterns constructed by placing three reflected pulses in six bit positions. (b) Possible bit patterns with three reflected pulses in six bit positions.....	53
Figure 4.5 Reflection pattern representing phase modulated signal.....	55
Figure 4.6 Code generation using reflected pulse and PPM representation .....	56
Figure 4.7 Dual transmission line ID circuit designed in Ansoft Designer for 101010 bit pattern (dimensions: 104 mm $\times$ 53 mm) .....	58
Figure 4.8 A prototype of a dual open transmission line ID circuit (dimensions: 115 mm $\times$ 60 mm). ....	59
Figure 4.9 Experimental setup used to test the ID circuits. ....	61
Figure 4.10 Simulation and experimental results showing input and reflected pulses for open and ground load meandered transmission line. ....	63
Figure 4.11 Simulation and experimental results representing 101010 bit pattern for dual open line ID circuit. ....	64
Figure 4.12 Simulation and experimental results representing 101100 bit pattern for dual open line ID circuit. ....	64
Figure 4.13 Simulation and experimental results showing first three reflections in a (50-25) $\Omega$ step impedance circuit with a 5 mm, 50 $\Omega$ line and a 612 mm, 25 $\Omega$ line. ....	66
Figure 4.14 Simulation and experimental results for a (50-25) $\Omega$ step impedance circuit with a 5 mm, 50 $\Omega$ line and a 306 mm, open 25 $\Omega$ line. ....	67
Figure 5.1 Experimental setup for measuring the return loss of the transmitting antenna at 912 MHz in the presence of a scattering antenna with various loads.....	87
Figure 5.2 Predicted responses (Pr/Pt) given by Equation (11) and observed response in a practical reader like experimental setup. ....	92

Figure 6.1	A fabricated temperature sensor tag sample (antenna dimensions: 5.54 cm × 5.34 cm).....	97
Figure 6.2	Experimental setup for the system testing (anechoic chamber dimensions: 1.8 m × 0.72 m × 0.9 m, reflectivity at 1 GHz: -30 dB). .....	98
Figure 6.3	Normalized backscattered signal amplitudes observed at the reader measured for various temperatures at the sensor tag (17 °C-140 °C).....	99
Figure 6.4	Schematic illustration of code generation using structural-mode and antenna-mode scattered pulses. ....	102
Figure 6.5	Schematic of an ethylene sensor fabricated on the tag.....	106
Figure 6.6	A prototype of a fabricated sensor sample on the tag. ....	106
Figure 6.7	Capacitance of two sensor samples measured using KIETHLEY measurement system.....	107
Figure 6.8	PPM represented ID code generation with two pulse signals. ....	109
Figure 6.9	Simulated phase shift of the reflected signal due to the change in capacitance of the load. ....	110
Figure 6.10	Design of sensor tag in Ansoft Designer showing antenna and transmission line ID circuit. ....	111
Figure 6.11	A fabricated tag sample showing antenna, transmission line, and sensor....	111
Figure 6.12	Schematic of the sensor tag measurement setup. ....	112
Figure 6.13	Experimental results showing received backscattered signal for the no tag condition (representing leakage signal in the reader and noise), and tag with the ID code 10010000 (Tag-I, 011 in PPM), and 10001000 (Tag-II, 100 in PPM), respectively. ....	114
Figure 6.14	(a) Microstrip triangular antenna and meandered transmission line ID circuit for three bit code (110) generation. (b) A (sensor) capacitor integrated at the end of the transmission line. ....	115
Figure 6.15	Experimental results showing received backscattered signal for no tag present versus tags with 2 and 5 pF capacitive loads. ....	116
Figure 6.16	Experimental and simulation results showing the variation in the phase of the received antenna mode scattered pulse at the reader for various load (sensor) capacitance at the tag. ....	117

Figure 6.17	Experimental results showing phase change in antenna-mode scattered pulse with two different ethylene concentrations, 0 ppm and 100 ppm. 100 ps time shift is observed which corresponds to a 33° change in phase (200 ps/division on x-axis, 2 mV/division on y-axis). .....	118
Figure 6.18	Result of phase change in antenna-mode reflected pulse when the ratio of ethylene to air concentration changes from 0 to 80%. .....	119
Figure 7.1	Schematic of cyber enabled RFID system. ....	121
Figure 7.2	An ID tag format example of EPC 96 bit version. ....	123
Figure 7.3	Reader domain concept for construction of unique ID code using reader ID. ....	126
Figure 7.4	Schematic of the reader system showing components of the analog reader and the connection to SBC. ....	127
Figure 7.5	Freescale QUICC start MPC8248 single board computer. ....	130
Figure 7.6	Rabbit Coyote BL2500 single board computer. ....	130
Figure 7.7	Schematic of the SBC connection with host computer for configuration and programming. ....	131
Figure 7.8	Flow chart showing the tasks performed by the SBC to compute the sensor value for integrated sensor-antenna tag.....	133
Figure 7.9	Schematic showing connections of the SBC with the analog reader through the A/D converter and outside world through the ethernet interface. ....	135
Figure 7.10	A modular laboratory prototype of the reader system using the Freescale SBC. ....	136
Figure 7.11	Reader system prototype using Rabbit Core SBC.....	137
Figure 7.12	Schematic of reader operations highlighting the interaction between instructions, user web interface, and memory.....	138
Figure 7.13	The configuration interface used to configure the reader system by providing sensor linear fit parameters for a given sensor type.....	144
Figure 7.14	The monitoring interface showing sensor tag information that includes sensor type, computed temperature at the tag, and the tag ID.....	145
Figure 8.1	The schematic illustration of cyber centric multiple environment monitoring application of the chipless sensor system. ....	150

- Figure 9.1 Schematic of the reader system showing extension for automatic ID and phase reading capability. ....158
- Figure 9.2 The cellular RFID sensor tag deployment concept. (a) Example for reader 003 located in cell 1242 and 009 in cell 1248. (b) Reader 003 moves to cell 1244 and 009 moves to cell 1246. ....159

## ACKNOWLEDGEMENTS

I wish to express my deepest gratitude to my mentor and advisor Dr. Kody Varahramyan for giving me an opportunity to be a part of this exciting research project at one of the finest research institutions in the world, for sharing his profound knowledge with me, for teaching me the research, academic, and professional skills, and for making me wiser.

I would like to express my sincere thanks to Dr. Mangilal Agarwal for his continued support, guidance, and encouragement, as well as his insight and experience, through the course of this research work. I am very grateful to Dr. Rastko Selmic for taking his valuable time to advise me and for being on my advisory committee. I am pleased to thank my advisory committee members, Dr. Scott Gold, Dr. Chad O'Neal, and Dr. Chester Wilson, for taking their valuable time to provide feedback, support, and encouragement for my research. I acknowledge Dr. Li-Hi Zou for his guidance on a part of this work, solving equations for antenna scattering parameters.

I specially thank the Institute for Micromanufacturing (IFM) for providing the research facility, the Center for Secure Cyberspace and Dr. Vir V. Phoha for the support provided, and the IFM staff, Mr. Philip Coane, Ms. Jeanette Futrell, Mr. Adul Khaliq, Mr. John McDonald, Mr. Donald Tatum, Ms. Deborah Woods, and the late Mr. Scott Williams, for their support at various stages of this research work. I am very thankful to Dr. Deeba Balachandran for her suggestion and encouragement, and also my research



group members, Dr. Jie Liu, Mr. Raja Mannam, and Mr. Senaka Kanakamedala for their support and friendship. I would like to thank my seniors, Dr. Aravind Chamarti and Dr. Jeevan Vemagiri for guiding me in the initial stages my this research work, and all other friends at the school and at home for their support and friendship. Last, but not least, I would like to thank my family for their inspiration, continued support, and encouragement.

# CHAPTER 1

## INTRODUCTION

### 1.1 Background

Radio frequency identification has been a key technology for short range wireless auto identification. It has been implemented in many recent technologies, such as product tracking, industrial automation, automatic toll collection, ticketing, public transportation, contact-less smart cards, access control, wireless sensing and information collection, healthcare, and in household applications [1].

#### 1.1.1 RFID System

An RFID system consists of two major units: an interrogator, known as an RFID reader, and a remote unit, known as an RFID tag. The tag has a unique identification code which is used to identify the object it is attached to, similar to a barcode. Unlike barcode technology, an RFID system does not require line of sight, and information can be read at a distance of up to 10 m. Moreover, an RFID tag can convey more extensive information about the object by providing a larger number of bits for information storage. Additionally, using an RFID system, multiple tags can be read simultaneously [1, 2]. RFID tags can be classified as active or passive. The passive tags operate by backscattering the interrogation signal from the reader. The tag information is conveyed to the reader by changing some parameters (eg. amplitude and phase) of the backscattered signal. A schematic diagram of a passive RFID system is shown in Figure 1.1 [1, 3, 4].

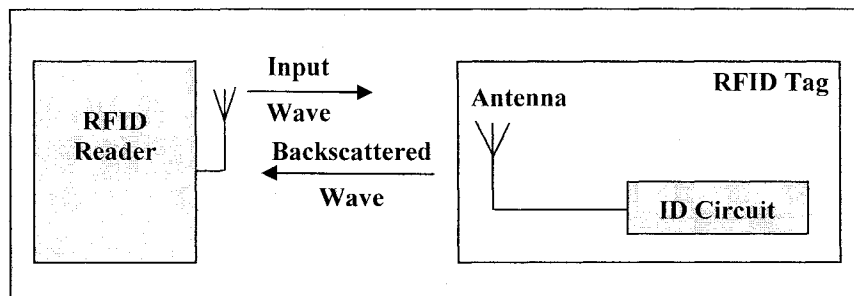


Figure 1.1 Schematic diagram of a typical passive RFID system.

### 1.1.2 RFID Sensor Tags

The battery free operating mechanism of passive RFID tags has attracted many new extensions in the application of RFID systems. Besides the widely used application of RFID technology in wireless object tagging, tracking, and management [1, 5-7], the integration of the sensors on the tags for wireless collection of physical information from the environment for various new applications, such as product monitoring, health care, and household applications, has attracted considerable research interest [8-14]. Various approaches for wireless collection of physical information from the environment with the help of sensor integrated tags have been proposed by many authors [15-20].

RFID sensor tags, in addition to the conventional RFID tag components, typically include a sensor that collects information from the environment. Generally, such tags are in active or semi-passive form, with an on board battery [1, 4, 21, 22]. The battery restricts the minimum size, lifetime, and cost of the tags, and application area of the system. Thus, past research efforts were made on either decreasing the power consumption on wireless sensors tags or harvesting energy from ambient energy sources [23-26]. The more recent approaches to solving the life time and cost issues have been through integration of sensors on passive tags [27-35].

### **1.1.3 Chipless RFID Sensor Tags**

The information exchange between a chip-based RFID tag and a reader takes place through a digital modulated signal, while the information obtained from a sensor is analog. Thus, the integration of a sensor on the chip-based RFID tag requires an on-board analog to digital (A/D) converter on the tag [1]. Because of the size, power, and cost constraints on passive RFID tags, the realization of such tags with integrated sensors has been not only challenging but also limiting their functionality as well as the application area. Moreover, the presence of an electronic component (e.g. microchip) on chip-based tags makes them unusable for applications in a harsh environment, and vulnerable to data alteration by attackers [36-38].

On the other hand, some researchers have been devoting their efforts on developing chipless sensor tag technologies. The chipless sensor tags do not contain any semiconductor chips on the tag and involve innovative sensor integration, as well as ID generation techniques [39-46]. Chipless RFID tags have been investigated, where the ID code generation is realized by non-chip based alternative means, such as using surface acoustic wave (SAW) devices [47-52], transmission lines [43-46], and left handed delay lines [53]. Recently, new SAW tags, such as Z-path SAW RFID tag [49] and tags using time position and phase encoding [51], have been reported. The limitation associated with the SAW tags, consisting of the influence of temperature on the delay, has been utilized in SAW sensor tags [53]. SAW delay line sensors with frequency domain interrogation have also been reported [54]. However, as the SAW devices are responsive to limited stimulants, such as temperature and pressure, the range of realizable SAW sensor tags is limited only to these stimulants.

#### **1.1.4 Chipless RFID Sensor Tag Readers**

Chipless sensor tags do not follow conventional RFID tag and reader communication schemes; thus, the conventional RFID readers cannot communicate with these new sensor tags. While the custom designed readers can obtain information from the chipless sensor tags, the readers do not conform to RFID standards, such as EPC and international standard organization (ISO), which prevents them from being integrated with conventional RFID systems and connecting with cyberspace. This limitation has been a principal challenge in the realization of commercial chipless sensor tag based RFID systems.

### **1.2 Related Research**

Chipless passive tag technologies, such as SAW RFID, strip line RFID, and delay based RFID, have been widely studied to fulfill the lower cost and longer life requirements. SAW based RFID has been the front runner of the chipless RFID tag technologies [47-51]. The SAW based tags operate on the principal of surface acoustic wave propagation delay and reflection inside a SAW device. The interrogation signal from the reader is converted into SAW pulses by an inter-digital transducer (IDT). The SAW pulse then travels along the device that consists of a piezoelectric material and contains reflectors along the propagation path. Each reflector on the device reflects a part of the forward traveling SAW pulse, which travels back to the IDT. The number and the positions of the reflectors are designed in such a way that the reflected SAW pulse pattern represents an ID code. The reflected SAW pulses are converted into an electrical signal by the IDT, which is transmitted back to the reader as an electromagnetic signal with the help of the tag antenna. Recently, new SAW tag technologies, such as Z-path

SAW RFID tag [49] and tags using time position and phase encoding [51] have been reported. These tags use both the position and phase of the reflected signal for encoding, which increases the number of bits generated by the tag. A major drawback of SAW based RFID devices is the influence of temperature and mechanical force on the delay in surface acoustic wave propagation in the piezoelectric material used for SAW devices. Additionally, the energy conversion from electromagnetic waves to surface acoustic waves (for ID generation) and reconversion of surface acoustic waves into electromagnetic waves (for wireless transmission of information to the reader) results in a high insertion loss [1, 40, 55]. The brittleness of the SAW substrates, the need for a separate antenna, and the use of a busy and weather sensitive frequency band (2.4 GHz) are drawbacks of SAW based RFID systems [56].

Recently, a delay based approaches achieving multi-bit digital identification code and using passive components, such as inductors ( $L$ ) and capacitors ( $C$ ), has been successfully demonstrated [39].  $LC$  delay based tags use microstrip inductors and capacitors to achieve delay, and the position of the delayed signal is used to represent a code. In this technique, a pulse signal is delayed in time using  $LC$  delay units, and the delayed pulses in two or more paths are combined at the end of the delay paths forming a pulse signal pattern, which represent an ID code. Transmission line [43-46] and left handed delay line [51] based chipless ID generation techniques have been investigated. The transmission line based ID generation technique uses the inherent delay in transmission line instead of the  $LC$  delay element [39]. ID generation circuits of this technology consist of a long meandering microstrip transmission line and a short straight line. An interrogation input pulse traveling in the meandering line is sequentially tapped

into the shorter line, forming an OOK modulated signal pattern representing an ID code [43-46].

A considerable amount of work has been reported for the analysis and measurement of antenna scattering properties and radar cross section (RCS) parameters [56-69]. Earlier methods for RCS parameter analysis and measurements of antennas were focused on the extraction of the antenna properties from the RCS data [56-61]. Various measurement methods for RCS as separate parameters have been reported by a number of researchers [56-59, 61, 65, 68]. Recently, many RCS parameter measurements and analysis have been motivated for the RFID applications [64-67]. Most of the work reported on scattering properties of antennas for RFID applications have been focused on determining the RCS for different loading conditions using conventional RCS relationships and do not consider measuring the individual parameters of RCS in the form of structural-mode RCS, antenna-mode RCS, and the relative phase.

SAW based sensor tags utilize the influence of certain physical parameters, such as temperature and mechanical stress, on the propagation delay of surface acoustic wave in SAW devices [53]. The change in propagation delay in SAW pulses introduced by a change in temperature is encoded as the sensor information in the generated ID. SAW delay line sensor with frequency domain interrogation has also been reported [54]. Besides SAW, a number of chipless sensor tag systems involving innovative ID generation and sensor integration techniques have been reported by many researchers [39-41]. In [39] and [45] a chipless sensor tag consisting of transmission delay line based ID generation and a sensor integration technique is discussed, where the sensor operates as a switch element between antenna and ID generation circuit. In [40, 41], and [70]

sensor tags with sensor integrated to the antenna are discussed. The sensor is integrated in such a way that the change in sensor parameter changes certain characteristic of the antenna. In [41] and [70], the change in ethylene concentration in the environment changes the capacitance of the integrated sensor, consequently changing the resonant frequency of the antenna. The change in resonant frequency of the antenna is wirelessly detected by the reader.

### **1.3 Research Motivation**

The motivation for this research comes from the idea of developing a reliable and low cost sensor platform which allows integration of a wide variety of sensors (eg. electrical, chemical, biological, etc.) on the tag for a multitude of applications, such as environmental condition monitoring, chemical agent detection, biological agent detection, secure product identification and tracking, and secure sensor data handling through cyberspace, thus leading to the development of marketable products and services for the betterment of humanity. The wireless sensor tags have been traditionally applied as the active or semi-passive tags for the wireless collection of information in a variety of environments. The use of a battery on a tag limits the life of the tag as well as increasing the cost and, consequently, limits the application area. Due to the operation of sensors in the analog domain and passive RFID chips in the digital domain, the efforts to integrate sensors into passive RFID tags have not made any noticeable progress towards the realization of passive sensor tags. These challenges in the development of passive RFID sensor tags have invited many research interests in recent years to investigate passive chipless sensor tags. This dissertation develops a transmission line reflection based ID generation scheme and two configurations of chipless sensor tags that provides a wide



range of sensor types for consideration, from the previously reported transmission delay line based ID generation schemes [43-46], microstrip antennas on flexible substrate [41, 46], and nanoparticles based sensors [41, 70].

For the efficient development of chipless sensor tags, it is of utmost importance that the scattering properties of the tag antenna given by RCS parameters be accurately and entirely determined. Because the previously reported RCS measurement methods are either not practical for the lower UHF frequency bands, such as 915 MHz where most of the RFID system operate, or does not provide entire and accurate information on the RCS parameters, a new method to measure RCS parameters of antennas that can be conducted using a simple measurement setup and that provides accurate and complete information on RCS is presented. Due to the unique communication technique used in chipless sensor tags, the commercially available readers cannot communicate with the developed chipless sensor tags. Thus, the design and development of a reader system that can communicate with the proposed chipless RFID sensor tags and is capable of communicating through cyberspace is presented.

### **1.3.1 Market Research**

As reported in [71] and also shown in Table 1.1, the total RFID market in 2008 constitutes \$2.36B USD,. The market size for chipless RFID tags is projected to reach about \$6B USD by 2013 and \$10B USD by 2018. The projected market size for 2008, 2013, and 2018 is shown in Figure 1.2 [71]. Chipless RFID tags are expected to grow to 8% of the total passive RFID market by 2010 and 45% by 2016, are shown in Figure 1.3, [72].

Table 1.1 RFID Tag Revenues by Market in the Year 2008.

Tag Value (\$million)	2008	Highlights
Airline and Airports	25.9	Excludes passports, cards
Animals and Farming	90.0	Animals
Books, Libraries, Archiving	27.4	Retail books, documents
Financial, Security, Safety	1126.4	Access control, passports
Healthcare and Pharmaceutical	37.7	Drugs, people, assets
Land and Sea Logistics, Postal	38.9	Conveyances, vehicles, postal
Manufacturing	24.0	Assets, tools etc
Military	86.5	Pallets, assets, items etc
Passenger Transport, Automotive	650.7	Card, ticket, clicker, tire
Retail, Consumer Goods	86.5	Pallet, case, apparel, cpg
Other	162.6	Research, education etc
<b>Total Tag Value (\$million)</b>	<b>2357</b>	
<b>Total Tag Value (\$billion)</b>	<b>2.36</b>	

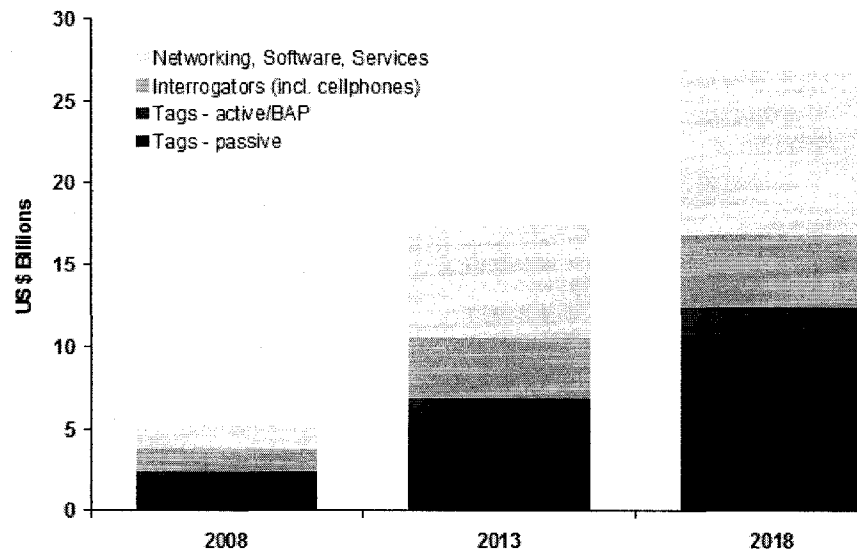


Figure 1.2 Total RFID market projection in US dollars (billion) for the years 2008, 2013, and 2018.

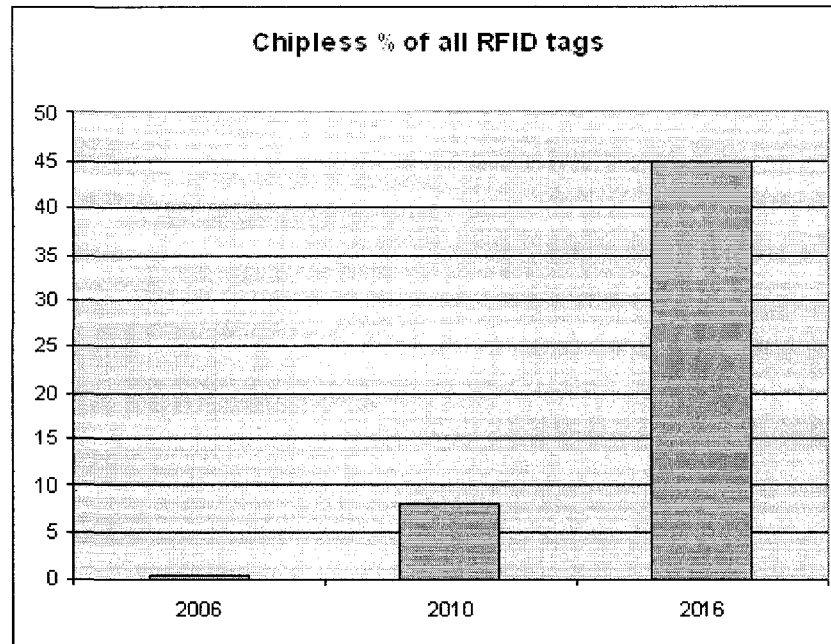


Figure 1.3 Market projection for chipless RFID tags as a percentage of total market for the years 2006, 2010, and 2016.

### **1.3.2 Chip-based and Chipless RFID Tags**

Most of the price on the chip-based RFID tags comes from the price of a semiconductor chips, placement of the chip on the tag, antenna integration, and the packaging of the finished tag. The proposed chipless tags do not contain any semiconductor chip on the tag; thus, they do not require any component placement as well as costly tag packaging processes. The absence of a chip allows the use of a single fabrication process for the proposed tags, thus, the price of the tags is much less as compared to the chip-based RFID tags. The price comparisons between chip-based [74] and proposed chipless RFID tags by each component and process are shown in Table 1.2.

Table 1.2 Price Comparison between Chip-based and Proposed Chipless RFID Tags.

<i>RFID Tag Components</i>	<i>Chip-based RFID Tags (Cents)</i>	<i>Proposed Chipless RFID Tags (Cents)</i>
Chip/ ID Generation Circuit	20	5
Antenna	5	5
Chip Placement	5	0
Chip Connection	5	0
Conversion to package	>10	0
Total	>45	10

### **1.3.3 Secure Sensor Information and Application in Harsh Environments**

The absence of a semiconductor chip (used in chip-based RFID tags) on the chipless RFID sensor tags removes the possibility of improper wireless access and cyber attacks on the sensor tags. For the sensor tags presented, the sensor information is conveyed to the reader as an instantaneous variation in some parameters of the backscattered signal. This is because the alteration of sensor information by attackers is not possible as compared to the chip-based sensor tags where the sensor information can be altered by altering the information stored in the chip. Moreover, the ID generation circuit used in the presented chipless sensor tags is not affected by environmental conditions and can be suited for applications in harsh environments where conventional RFID tags cannot be used.

## **1.4 Contribution of Dissertation**

A transmission line delay and reflection based ID generation scheme for chipless RFID tags application is presented. The scheme presented consists of either multiple

transmission lines in parallel or a step impedance transmission line, and constructs an OOK modulated signal pattern using multiple signal reflections inside the transmission line system. Due to the importance of having complete and accurate information on the RCS parameters of antennas for chipless sensor tag design, and due to the lack of practical measurement techniques providing such information, a new method to measure RCS parameters of antennas is developed and a measurement example is demonstrated.

A chipless RFID sensor tag system consisting of chipless RFID sensor tags and a specialized cyber enabled chipless sensor tag reader is presented. The chipless sensor tags consist of a microstrip antenna and a meandered microstrip transmission line for ID generation, and provide a wide selection of sensor types for consideration. The theory, design, and testing of two such tag configurations, named as conf-I and conf-II, are presented. The conf-I tag consists of a sensor directly connected to the tag antenna constituting a load to the antenna. The change in some parameters of the sensor changes the scattering property of the antenna. The conf-II tags use a single transmission line to generate pulse position modulation (PPM) represented ID code and utilize phase change in the antenna-mode scattered pulse to detect sensor information. The design of a single board computer based chipless RFID sensor tag reader that can communicate over cyberspace is discussed. A firmware with a web based user interface accessible through cyberspace is developed. The system testing results of the developed reader system and the chipless sensor tags is presented.

### **1.5 Organization of Dissertation**

The dissertation is organized into nine chapters. The overview of the developed sensor tag system, including the introduction of important components of the system, is

presented in Chapter 2. The theory, design, and optimization of the meandered microstrip transmission line are presented in Chapter 3. Microstrip transmission line reflection and the delay based ID generation scheme using multiple and step impedance lines are presented in Chapter 4. The principles of operation, design, simulation, and experimental results for the ID generation schemes are discussed.

The theory, solution, and an experimental example of a new method to measure RCS parameters of antennas are presented in Chapter 5. A measurement example with the new measurement method of using a simple measurement setup is discussed. The components, operation mechanism, design, and experimental results on chipless sensor tags are presented in Chapter 6. The design, configuration, and firmware development for the chipless sensor tag reader system are presented in Chapter 7. The applications of the developed RFID tag techniques and the tag system are presented in Chapter 8. The conclusion and the future work plan are discussed in Chapter 9.

## **CHAPTER 2**

### **SYSTEM OVERVIEW**

This chapter presents an overview of the chipless sensor tag system that has been developed. It highlights the system components and their functionalities. The broader overview of the system is discussed in the earlier sections of the chapter, followed by details of the components. The global implication of the system is presented in the later sections.

#### **2.1 System Overview**

As schematically shown in Figure 2.1, the chipless RFID sensor tag system platform consists of two main components, a chipless RFID sensor tags and a single board computer (SBC) based specialized reader system. Chipless sensor tags contain sensors that collect physical information, such as temperature and gas concentration from the environment. The tags wirelessly communicate with the reader at a 915 MHz signal frequency and convey the collected information to the reader. The communication between the tag and the reader takes place by virtue of the backscattering of the interrogation signal transmitted by the reader.

The reader consists of an analog reader and an SBC. The analog reader transmits interrogation signal to the tags, receives the backscattered signal, and feeds the demodulated signal to the SBC. The SBC, after receiving the input form the analog

reader, computes the sensor value, and constructs an EPC standard RFID tag ID, including the computed sensor value, and communicates it to the outside world through cyberspace.

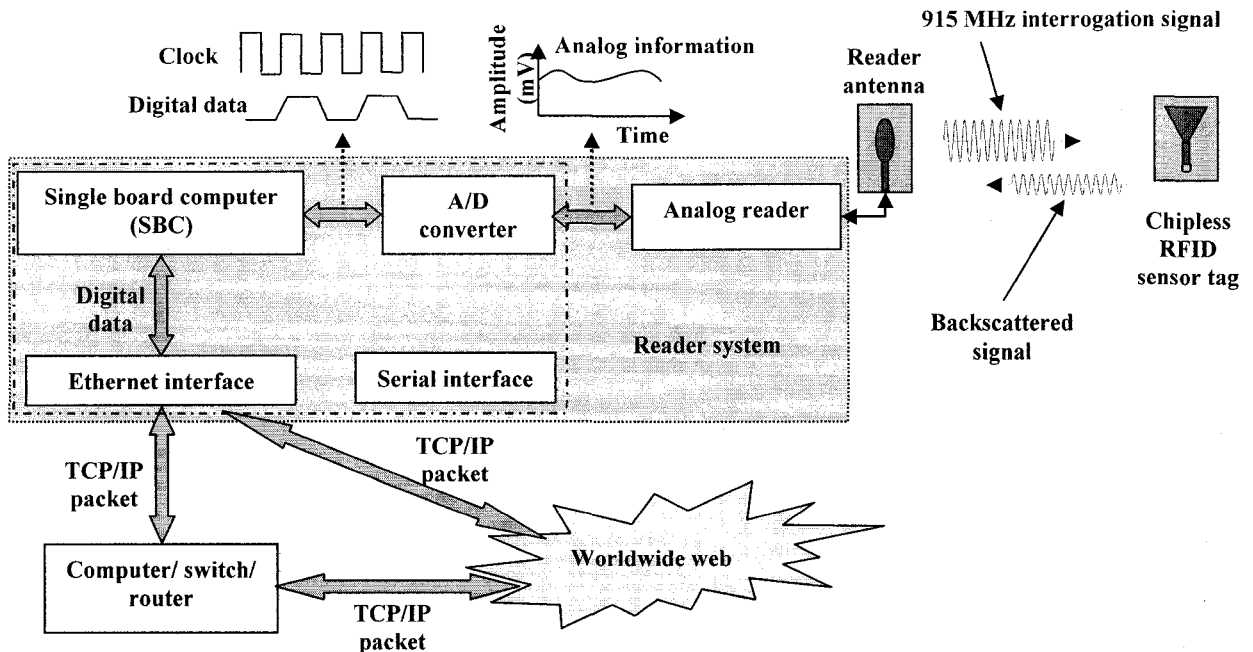


Figure 2.1 Schematic of the chipless RFID sensor tag system.

## 2.2 Chipless Sensor Tag

Generally, chipless sensor tags consist of a planar antenna, a chipless ID code generation circuit, and a sensor. With these components, the presented chipless sensor tag can have two configurations. The first configuration (conf-I) consists of an antenna and a sensor. The second configuration (conf-II) consists of an antenna, a microstrip transmission line reflection and delay based chipless ID code generation circuit, and a sensor. The schematics of conf-I and conf-II tags are shown in Figure 2.2



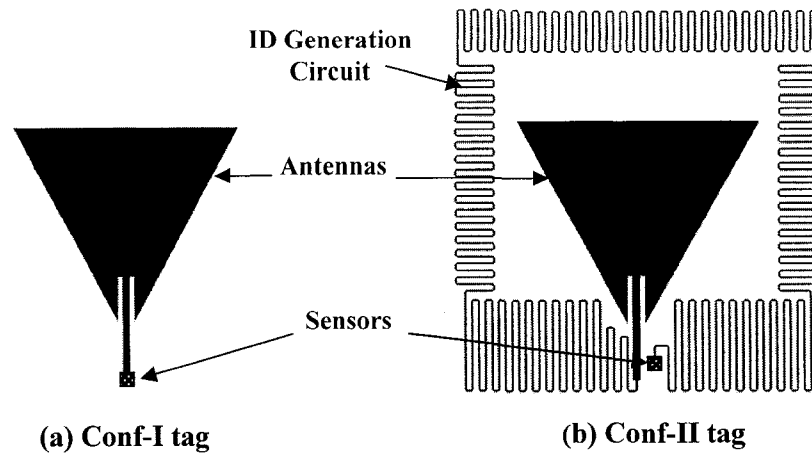


Figure 2.2 Schematics of conf-I and conf-II tags.

In the conf-I tag configuration, a sensor is directly connected to the feed of a planar microstrip triangular antenna where it constitutes a load to the antenna. A schematic of the conf-I tag is shown in Figure 2.2(a). When the sensor senses the presence of the stimulant (sensed material) or change in the quantity of the stimulant, one or more parameters of the sensor changes, which causes the change in the scattering property of the antenna. The change in the scattering property of the antenna appears as a modulation in the backscattered signal amplitude. The reader uses a continuous signal for the interrogation of the conf-I tags and detects the change in the backscattered signal amplitude. From the detected change in the amplitude, the reader computes the sensor parameter change and thereby effectively detects the presence of the stimulant or the change in the quantity of the stimulant in the environment.

The conf-II tag configuration consists of a planar microstrip triangular antenna, a meandered microstrip transmission line, and a sensor. A schematic of the conf-II tag is shown in Figure 2.2(b). The transmission line extends from the feed of the antenna to the sensor, where the sensor is connected as a load to the transmission line. The microstrip

transmission line constitutes the ID code generation circuit for the sensor tag. Similar to the conf-I tag, the presence of the stimulant or the change in the quantity of the stimulant changes one or more parameters of the sensor. Unlike the conf-I tag, the change in the sensor parameter causes the change in the phase (or angle) of the signal reflected at the sensor. The reader uses a pulsed interrogation signal for the conf-II tag, and the change in phase in the reflected pulsed signal is detected at the reader, which gives the measure of the change in the quantity of stimulant at the sensor tag.

### **2.2.1 Antenna**

A triangular microstrip patch antenna with slotted ground plane is used for the sensor tag antenna. The schematic of the antenna is shown in Figure 2.2. The antenna is fabricated on a flexible polyimide substrate using standard photolithography techniques. The antenna has an omnidirectional radiation pattern, 30 MHz bandwidth with center frequency at 915 MHz, voltage standing wave ratio (VSWR) of 1.2, and 5.54 cm × 5.34 cm physical dimensions [46].

### **2.2.2 Chipless ID Generation Circuit**

The chipless ID code generation circuit consists of one or more meandering microstrip transmission lines which, after receiving an input signal, generates a predefined output signal pattern. The generated signal pattern represents an ID code for the tag. The reflection due to impedance mismatches and the signal propagation delay in the transmission lines is used for the ID code generation. Three different configurations of transmission lines are possible, namely, multiple transmission lines with OOK coding, step impedance with OOK coding, and single transmission line with PPM coding. The multiple transmission lines and step impedance configurations can generate a larger

number of bits than the single transmission line configuration. However, due to the difficulties on antenna and sensor integrations with these configurations, the signal transmission line configuration is used to integrate with the chipless sensor tags.

The single transmission line configuration consists of a transmission line extending from the feed of the antenna to the sensor. The propagation delay introduced in a traveling pulse by the length of the line represents a unique PPM identification code for the tag. The structural-mode scattered signal, antenna-mode scattered signal, and the relative phase between the two signals are utilized for ID generation and sensor information detection. The structural-mode scattered signal is associated with the surface of the antenna and does not vary with any variation in the load presented to the antenna. On the other hand, the antenna-mode scattered signal travels through the transmission line length and gets reflected at the sensor, which is caused by the impedance mismatch between the transmission line and the sensor. The change in the reactance of the sensor changes the phase of the reflected signal. At the reader, the relative delay and relative phase between received structural-mode scattered and antenna-mode scattered signals are compared to get the PPM coded tag ID and extract the change in the sensor parameter.

### **2.2.3 Sensor**

The sensor on the tags collects physical information from the environment which is accomplished by detecting the change in one or more parameters of the sensor element caused by the presence of a stimulant in the environment or due to the change in the quantity of the stimulant. The change in the sensor parameter is presented either to the tag antenna or to the ID code generation circuit. Two types of sensors have been considered for the two tag configurations. A resistive sensor (e.g. resistive temperature sensor) is used for the conf-I tag where the change in the sensor parameter is reflected as the change

in amplitude of the backscattered signal. A capacitive sensor (e.g. capacitive ethylene sensor) is used for the conf-II tags, where the change in the sensor capacitance changes the reactance presented to the ID circuit, which in turn changes the phase of the signal reflected at the sensor. A commercial resistive temperature sensor and nano-assembled SnO<sub>2</sub> nanoparticle based capacitive ethylene sensors [70] are used for conf-I and conf-II sensor tags, respectively.

### **2.3 Reader System**

The reader system communicates with the sensor tags and also provides a platform for users to access the sensor information through cyberspace. As seen in Figure 2.1, the system consists of an analog reader and an on-board SBC. The analog reader is responsible for communicating with the sensor tags. It transmits an interrogation signal to the sensor tags, receives the backscattered signal, demodulates, and feeds the received signal to the A/D converter of the SBC.

The SBC plays a bridging role between the special application reader and cyberspace. With the received signal from the analog reader, the SBC computes the sensor value with the help of information provided by a user during the reader configuration (or calibration), and puts the computed sensor value in an electronic product code (EPC) RFID tag standard data structure to construct a unique RFID tag ID. Also included in the tag ID are reader ID, sensor ID, company prefix (company ID), item reference (item ID), and frame headers (pertinent to frame structure). The reader is developed with web based user interfaces accessible through cyberspace, upon authentication. The sensor information, reader ID, and the tag ID are displayed on the

monitoring interface, while the information in the reader can be modified through the configuration interface.

### **2.3.1 Analog Reader**

The analog reader is responsible for the wireless communication between the reader system and the sensor tags. The important components of the analog reader include signal source, filters, amplifiers, leakage cancelation unit, demodulator, circulator, and antenna. With the help of the reader antenna, the interrogation signal is transmitted to the tags, and the backscattered signal from the tags is received. For the conf-I tags, the reader uses a continuous 915 MHz interrogation signal. The received backscattered signal is demodulated and fed to the SBC through the A/D converter input. For the conf-II tags, the analog reader uses a pulsed interrogation signal with 915 MHz carrier frequency. The received backscattered signal from the tags is fed to the oscilloscope for the observation and analysis of the pulse position that represents the ID code and the phase of the signal that gives the sensor information.

### **2.3.2 Single Board Computer**

The single board computer includes the SBC hardware and the firmware developed for the reader system. The SBC hardware is equipped with an 8 bit A/D converter input channel to receive the signal from the analog reader and an ethernet interface to communicate through cyberspace. The firmware of the system includes instructions written to communicate with the analog reader, compute the sensor value from the analog reader input, and communicate the information to users through the web based user interface. During the configuration of the reader system, it takes input of the information needed to compute the sensor value and construct a modified SGTIN-96 format EPC standard unique ID code for the tag [74]. The computed sensor value and the

tag ID are made available on the web based user interfaces to be accessed through cyberspace.

#### **2.4 User Interfaces and Authentication**

The web based user interfaces allow monitoring, accessing, and modifying the information in the reader system through cyberspace. The user web interfaces are categorized into monitoring and configuration interfaces. The monitoring interface displays information on the current analog reader input, sensor type, computed sensor value, reader ID, and the constructed tag ID in the EPC standard format. The configuration web interface displays as well as allows modifying information about sensor type, sensor value computation, reader ID, and tag data format. The web interfaces can be accessed by typing the IP address of the reader system on the address bar of any standard web browser. Whenever the web interface is accessed, the user is asked for authentication by providing a username and password. On the basis of the provided information, the users are grouped into either the monitor or the administrator groups. The administrator group is allowed access to both the monitoring as well as configuration interfaces, while the monitor group is allowed access only to the monitoring interface. A picture of the monitoring interface is shown in Figure 2.3.

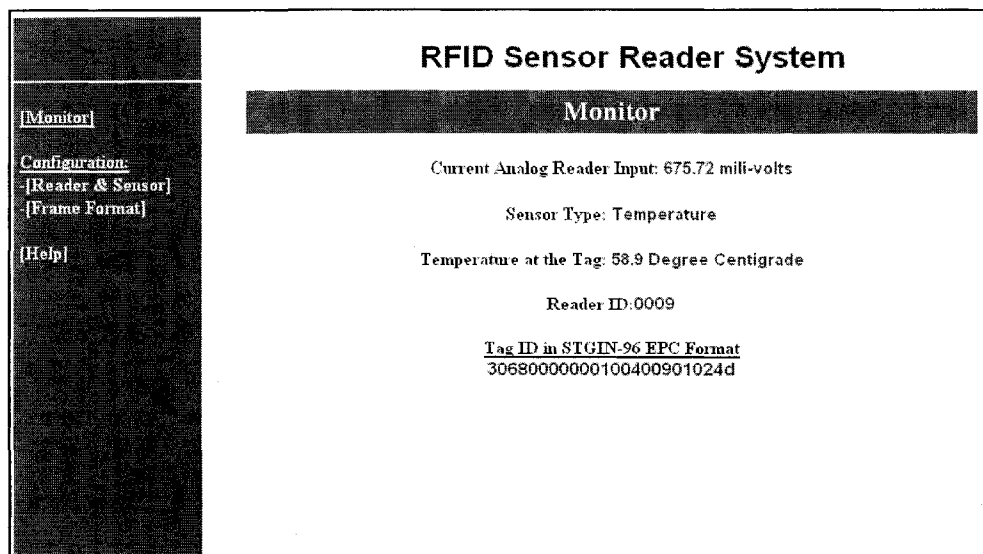


Figure 2.3 The monitoring web interface.

## 2.5 Cyber Centric Monitoring

The reader system can be securely accessed using web based user interfaces through cyberspace and the status of the sensor tags can be monitored remotely. While the application of a single reader system has been discussed thus far, it is also possible to deploy and monitor more than one reader simultaneously. This is made possible due to the fact that a unique reader ID is included in the tag ID. The reader ID is unique among the readers in a given environment, which is globally singled by the company prefix (company ID) and the item reference (item ID). As the different application environments are identified by the specific company prefixes and item references, a reader with a unique reader ID in a given environment has a globally unique ID. This allows for uniquely identifying a reader in a global perspective and, thus, deploying and remotely monitoring a number of reader environments. Such a deployment and monitoring concept is schematically depicted in Figure 2.4 which will be discussed further in Chapter 7.

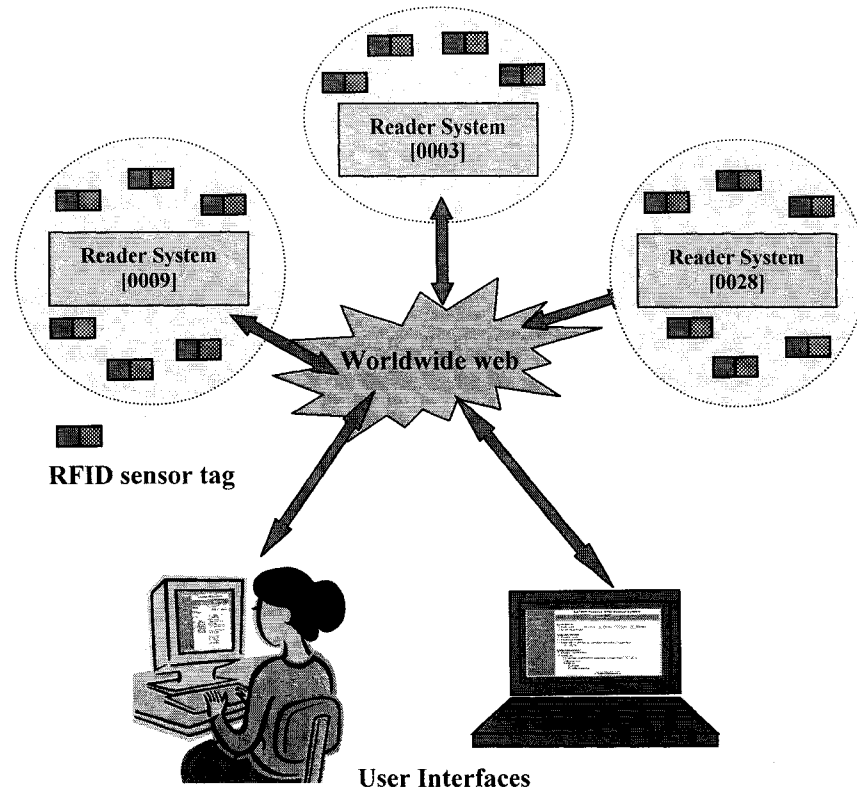


Figure 2.4 Monitoring of reader systems through cyberspace.



## CHAPTER 3

### MEANDERED MICROSTRIP TRANSMISSION LINES

In this chapter, the theory of microstrip transmission lines, practical design considerations, design methodology of meandered microstrip transmission lines, and the optimization of different parameters of meandered transmission line with the help of a simulation tool are discussed.

#### 3.1 Microstrip Transmission Lines

A schematic of a microstrip transmission line is shown in Figure 3.1. A microstrip transmission line is composed of two conductors separated by a dielectric material of dielectric constant  $\epsilon_r$  and relative permittivity  $\mu_r$ . The bottom conductor is much wider than the top conductor. The top conductor, called a trace, is connected to the signal line, while the wider bottom conductor is connected to the signal ground and is called a ground plane [75, 76]. As shown in Figure 3.1, the width and the thickness of the trace are  $w$  and  $t$ , respectively, and the height of the dielectric material is  $h$ .

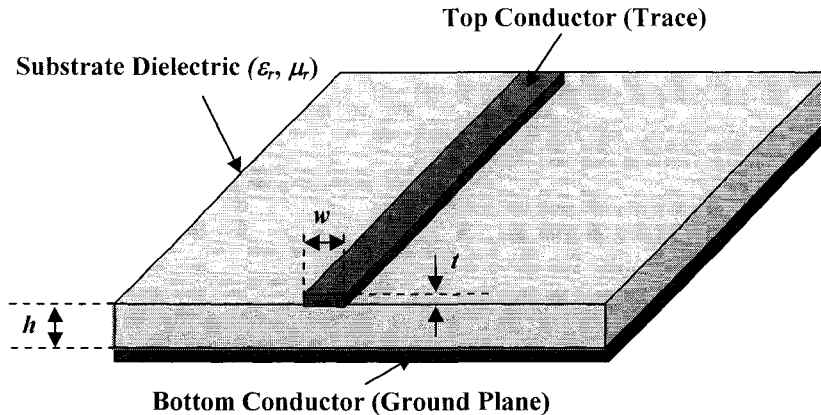


Figure 3.1 Schematic of a microstrip transmission line showing the trace conductor, dielectric layer, and ground plane.

### **3.1.1 Wave Propagation in Microstrip Transmission Lines**

A microstrip transmission line can be closely compared with a coaxial transmission line, a conductor surrounded by a dielectric material. The electromagnetic wave propagation in a coaxial transmission line is in transverse electromagnetic (TEM) mode, where the electric fields are transverse to the magnetic fields. In microstrip transmission lines, the dielectric environment surrounding the metal trace consists of the substrate material between the trace, the ground and air on the sides, and the space above the trace. This creates a dielectric discontinuity around the trace, which gives rise to longitudinal field components which is in contrast to pure transverse fields in coaxial transmission lines. Thus, the propagation in microstrip transmission lines is in a hybrid mode and is called quasi-TEM. The three dimensional view of the electric field lines, magnetic field lines, and cross-sectional view of the electric and magnetic field lines are shown in Figure 3.2(a), Figure 3.2(b), and Figure 3.2(c), respectively [75-77].

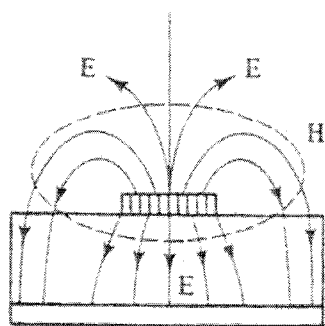
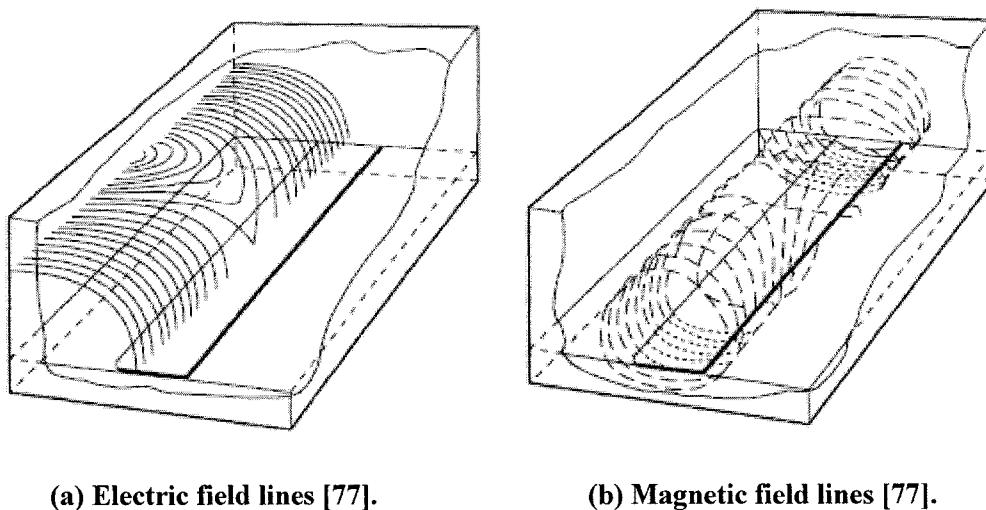


Figure 3.2 Figures showing electric and magnetic field lines in a microstrip transmission line.

### **3.1.2 Transmission Line Equations and Solutions**

A parallel plate transmission line is usually represented by a lumped circuit theory where the impedance elements are assumed to be lumped parameters. This ordinary circuit theory does not hold for higher frequency analysis. At higher frequencies, the series inductance and short capacitance that are distributed along the length of the conductor become significant. It is because at shorter wave lengths (higher frequencies), the physical length of the transmission line is longer than the signal wave length and the lumped parameter equivalent circuit representation of the distributed parameters does not

give accurate results. Thus, here the distributed circuit theory has been utilized to analyze the microstrip transmission line. Using distributed circuit theory, a transmission line can be represented in terms of conductor resistance ( $R$ ), series inductance ( $L$ ), leakage capacitance ( $C$ ), and leakage conductance ( $G$ ), as shown in Figure 3.3 [75], where the parameters ( $R$ ,  $L$ ,  $C$ , and  $G$ ) are expressed in per unit length.

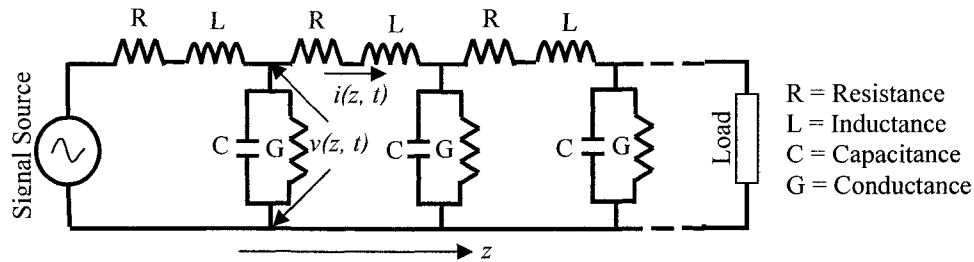


Figure 3.3 Distributed circuit representation of transmission lines.

Considering an elemental section in Figure 3.3, if  $v(z, t)$  is the voltage across the transmission line and  $i(z, t)$  is the current in the line, the transmission line equations in voltage and current forms are given by Equations (3.1) and (3.2), respectively [75].

$$\frac{\partial^2 v}{\partial z^2} = RGv + (RC + LG)\frac{\partial v}{\partial t} + LC\frac{\partial^2 v}{\partial t^2} \quad (3.1)$$

$$\frac{\partial^2 i}{\partial z^2} = RGi + (RC + LG)\frac{\partial i}{\partial t} + LC\frac{\partial^2 i}{\partial t^2} \quad (3.2)$$

Equations (3.1) and (3.2) reveal that the voltage and the current on the line are functions of both position and time. The instantaneous voltage across the line and the current in the line can be expressed in terms of voltage and current phasors,  $V(z)$  and  $I(z)$ , as shown in Equations (3.3) and (3.4), respectively.

$$v(z, t) = \text{Re}V(z)e^{j\omega t} \quad (3.3)$$

$$i(z, t) = \text{Re } I(z)e^{j\omega t} \quad (3.4)$$

Using the phasor voltage and current terms in above equations, the transmission line equations in Equations (3.1) and (3.2) can be expressed in the phasor form as shown in Equations (3.5) and (3.6), respectively [78]

$$\frac{dV^2}{dz^2} = \gamma^2 V \quad (3.5)$$

$$\frac{dI^2}{dz^2} = \gamma^2 I \quad (3.6)$$

where  $\gamma$  is called a propagation constant and is defined by

$$\gamma = \sqrt{ZY} = \alpha + j\beta \quad (3.7)$$

where,

$$Z = R + j\omega L \quad (3.8)$$

$$Y = G + j\omega C. \quad (3.9)$$

In Equation (3.7),  $\alpha$  is the attenuation constant in nepers per unit length and  $\beta$  is the phase constant in radians per unit length. A set of solutions to Equations (3.5) and (3.6) can be written as

$$V = V_+ e^{-\gamma z} + V_- e^{\gamma z} \quad (3.10)$$

$$\bar{I} = Y_0 (V_+ e^{-\gamma z} - V_- e^{\gamma z}). \quad (3.11)$$

$V_+$  and  $V_-$  represent the complex amplitudes in the positive z-direction and the negative z-direction, respectively. In Equation (3.11) the characteristic impedance of the transmission line is defined as

$$Z_0 = \frac{1}{Y_0} = \sqrt{\frac{Z}{Y}} = \sqrt{\frac{R + j\omega L}{G + j\omega C}}. \quad (3.12)$$

Equation (3.12) gives the characteristic impedance of a transmission line independent of its length. The series resistance  $R$  is constant over all the frequency ranges where as the series admittance  $\omega L$  is dependant on frequency and increases with an increase in the frequency of the wave. At very high frequencies,  $\omega L$  becomes dominant over  $R$ , ( $R \ll \omega L$ ), and, similarly,  $\omega C$  becomes dominant over  $G$ , ( $G \ll \omega C$ ). Thus, for very high frequencies, Equation (3.12) can be rewritten as

$$Z_0 = \sqrt{\frac{L}{C}}. \quad (3.13)$$

Similarly, applying the high frequency conditions to Equation (3.7) and comparing real and imaginary parts on the left and right hand sides of the equation, the attenuation constant ( $\alpha$ ) and phase constant ( $\beta$ ) can be obtained, which are shown in Equations (3.14) and (3.15), respectively.

$$\alpha = \frac{1}{2} \left( R \sqrt{\frac{C}{L}} + G \sqrt{\frac{L}{C}} \right), \quad (3.14)$$

$$\beta = \omega \sqrt{LC}. \quad (3.15)$$

The phase velocity of the wave in the transmission line is defined and given by

$$v_p = \frac{\omega}{\beta} = \frac{1}{\sqrt{LC}}. \quad (3.16)$$

The product ( $LC$ ) is independent of the size of the trace ( $w$ ,  $l$ ) and height of the dielectric ( $h$ ), but depends on the relative permeability ( $\mu_r$ ) and relative permittivity ( $\epsilon_r$ ) of the dielectric substrate, as given by

$$v_p = \frac{1}{\sqrt{\mu\epsilon}} = \frac{c}{\sqrt{\mu_r \epsilon_r}}. \quad (3.17)$$

In Equation (3.17),  $c$  stands for the velocity of light in vacuum ( $3 \times 10^8$  m/s). Equation (3.17) reveals that the phase velocity of the wave in a transmission line is smaller than the speed of light in vacuum.

### **3.1.3 Effective Dielectric Constant and Characteristic Impedance**

The characteristic impedance of a microstrip transmission line depends on the trace width ( $w$ ), trace thickness ( $t$ ), substrate height ( $h$ ), relative permeability ( $\mu_r$ ), and permittivity of the substrate ( $\epsilon_r$ ). For convenience, a cross-sectional view of the microstrip transmission line previously shown in Figure 3.3 is shown in Figure 3.4. As a microstrip transmission line is surrounded by two types of dielectric material, the substrate material and the air, the first step in the design of microstrip devices is to find the effective dielectric constant,  $\epsilon_{re}$ , such that the wave propagation properties of the microstrip would be the same when it is surrounded by the new medium of dielectric constant  $\epsilon_{re}$ , as shown in Figure 3.5.

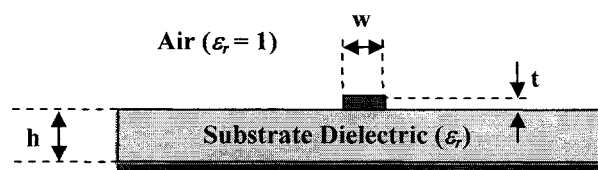


Figure 3.4 Cross sectional view of a microstrip transmission line.

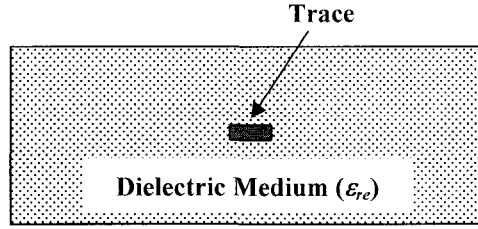


Figure 3.5 Transmission line trace of same dimensions as shown in Figure 3.4, surrounded by a new medium of dielectric constant  $\epsilon_{re}$ .

The effective dielectric constant of the microstrip transmission line shown in Figure 3.4 can be written as shown in Equation (3.18), [76].

$$\epsilon_{re} = \left( \frac{\epsilon_r + 1}{2} \right) + \left( \frac{\epsilon_r - 1}{2} \right) F - \frac{(\epsilon_r - 1)t}{4.6\sqrt{wh}}, \quad (3.18)$$

where,

$$F = \begin{cases} \left[ 1 + \frac{12h}{w} \right]^{-0.5} + 0.04 \left( 1 - \frac{w}{h} \right)^2 & \text{for } w < h \\ \left[ 1 + \frac{12h}{w} \right]^{-0.5} & \text{for } w \geq h \end{cases} \quad (3.19)$$

Considering a nonmagnetic substrate material, the characteristic impedance of the microstrip transmission line is calculated using Equation (3.20), [76]

$$Z_0 = \begin{cases} \left( \frac{60}{\sqrt{\epsilon_{re}}} \right) \ln \left[ 8 \frac{h}{w} + 0.25 \frac{w}{h} \right] & \text{for } w < h \\ \left[ \frac{120\pi}{\sqrt{\epsilon_{re}}} \left[ \frac{w}{h} + 1.393 + 0.667 \ln \left( \frac{w}{h} + 1.444 \right) \right] \right]^{-1} & \text{for } w \geq h \end{cases} \quad (3.20)$$

Conversely, the width of trace ( $w$ ) for a given microstrip substrate can be calculated for any characteristic impedance ( $Z_0$ ) using Equation (3.21), [76].



$$w = \begin{cases} \left( \frac{e^x}{8} - \frac{e^{-x}}{4} \right)^{-1} & \text{for } w < 2h \\ \frac{2h}{\pi} \left[ \frac{377\pi}{2Z_0\sqrt{\epsilon_r}} - 1 - \ln \left( \frac{377\pi}{Z_0\sqrt{\epsilon_r}} - 1 \right) \right] \\ + \frac{h(\epsilon_r - 1)}{2\epsilon_r} \left[ \ln \left( \frac{377\pi}{2Z_0\sqrt{\epsilon_r}} - 1 \right) + 0.293 - \frac{0.517}{\epsilon_r} \right] & \text{for } w \geq 2h \end{cases}, \quad (3.21)$$

where,

$$x = \left( \frac{Z_0}{60} \right) \sqrt{\frac{\epsilon_r + 1}{2}} + \frac{\epsilon_r - 1}{\epsilon_r + 1} \left( 0.226 + \frac{0.12}{\epsilon_r} \right). \quad (3.22)$$

Equations (3.18-3.22) are the practical microstrip transmission line design equations which are used in the following sections to design transmission lines with desired characteristics for a given substrate.

### **3.2 Microstrip Transmission Line Design**

A Pyralux FR9151 CU CLAD substrate [79] was selected for the microstrip transmission line design. The substrate parameters are indicated in the cross sectional view shown in Figure 3.6. As seen in Figure 3.6, the dielectric of the substrate consists of three layers, a Kapton layer sandwiched between the two adhesive layers. The height and dielectric constants of each layer are also indicated in Figure 3.6.

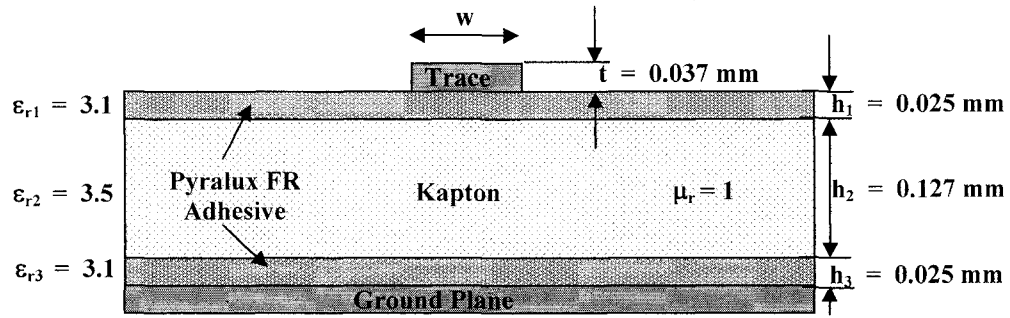


Figure 3.6 Substrate parameters of FR9151 CU CLAD used for transmission line fabrication.

The equivalent dielectric constant of the three layers is calculated using the relationship given in [80], also shown in Equation (3.23).

$$\epsilon_r = \frac{\epsilon_{r1}\epsilon_{r2}(h_1 + h_2)}{\epsilon_{r1}h_2 + \epsilon_{r2}h_1} \quad (3.23)$$

The equivalent dielectric constant of the given substrate is calculated to be 3.375 ( $\epsilon_r$ ), which is used to design the width of the trace for a  $50 \Omega$  ( $Z_0$ ) characteristic impedance with help of Equation (3.21). Here, the impedance of the line is selected to match with the impedance of the antenna as well as that of the other available instrumentation. Provided that the thickness of the substrate is very small (0.177 mm) compared to PCB substrates, the second part of the Equation (3.21) is used for the initial design, assuming that the width of the trace is greater than twice the thickness of the substrate ( $w \geq 2h$ ). The width is calculated to be 0.4304 mm ( $w$ ). The result confirms the assumption made ( $0.4304 > (2 \times 0.177)$ ). Using the calculated values, the effective dielectric constant for the microstrip transmission line is obtained using Equations (3.18) and (3.19), and found to be 2.6058 ( $\epsilon_{re}$ ). The phase velocity ( $v_p$ ) of the wave in the transmission line is obtained using Equation (3.17) and found to be  $1.858 \times 10^8$  m/s

(185.8 mm/ns), which gives the wavelength of a 915 MHz ( $f$ ) signal in the transmission line to be 203.06 mm ( $\lambda_t = v_p/f$ ). The calculated parameter values are shown in Table 3.1.

Table 3.1 Design Parameters of Microstrip Transmission Line on FR9151 CU CLAD Substrate.

<i>Parameter Name</i>	<i>Symbol</i>	<i>Value</i>
Substrate height	$h$	0.177 mm
Equivalent dielectric constant	$\epsilon_r$	3.375
Impedance of the line	$Z_0$	50 $\Omega$
Width of the line	$w$	0.4304 mm
Effective dielectric constant	$\epsilon_{re}$	2.6058
Phase velocity	$v_p$	$1.858 \times 10^8$ m/s (185.8 mm/ns)
Signal frequency	$f$	915 MHz
Signal wavelength in the line	$\lambda$	203.06 mm

### **3.3 Meandered Microstrip Transmission Line Design**

Transmission lines are usually meandered in circuit designs to save space on the substrate and minimize circuit costs. The important parameters for a meandered transmission line design are meandering length ( $M_l$ ), meandering width ( $M_w$ ), and the bend type. A meandered transmission line can be considered as a collection of a number of small straight transmission line elements connected in series. The length of each element is called the meandering length, while the separation between the two consecutive elements is called the meandering width. The meandering length and width of a microstrip transmission line are indicated Figure 3.7. The rule of thumb in meandered transmission line design is that the meandering length should be smaller than the quarter wavelength of the signal wave ( $\lambda/4$ ) and the separation (meandering width) should be more than twice the transmission line width ( $w$ ). As shown in Table 3.1, the

wave length of the signal in the transmission line is 203.06 mm and the width of the line is 0.403 mm. Thus, for the initial design, the meandering length and meandering width are selected as 50 mm ( $< (203.06/4)$  mm) and 3 mm ( $> (2 \times 0.430)$  mm), respectively.

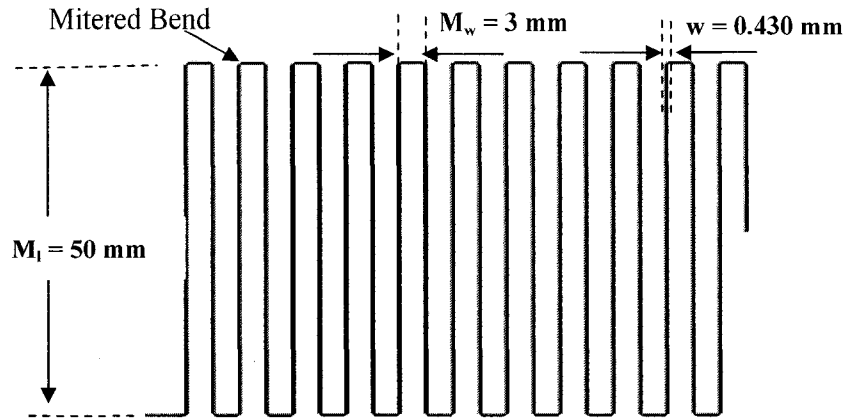


Figure 3.7 Meandered microstrip transmission line design showing various design parameters.

Generally, three types of bend are used in the meandered microstrip transmission lines, corner, curved, and mitered. A mitered bend type has been selected for the transmission line design. The selected design parameters will be optimized with the help of a simulation tool in Section 3.6.

### **3.4 Loss, Dispersion, and Bandwidth**

The loss, dispersion, and bandwidth of a transmission line become more critical for higher signal frequency designs. The losses in the transmission line result in reduced signal power and, consequently, smaller tag read distance. The dispersion limits the maximum length of the line that can be used for a particular signal pulse width, while bandwidth restricts the maximum carrier frequency that can be used for interrogation.

### 3.4.1 Losses

The losses in a transmission line originate principally from three sources; the finite conductivity of the trace conductor called resistive loss, the finite conductivity of the dielectric material called dielectric loss, and the antenna effect of the transmission line called radiation loss.

**3.4.1.1 Resistive Loss** The resistive loss originates from the finite conductivity of the microstrip conductor forming the trace line, which causes energy dissipation in the form of heat. Also, at UHF frequencies, the current density in the conductor is concentrated only in a thin layer of the microstrip line, which exacerbates the resistive loss. The attenuation constant ( $\alpha_c$  in decibel per centimeter) for a wide microstrip line ( $w > h$ ) is given as [75]

$$\alpha_c \approx \frac{8.686R_s}{Z_0 w} \text{ for } (w/h) > 1, \quad (3.24)$$

where,  $R_s$  is the surface skin resistance in square/m given by

$$R_s = \sqrt{\frac{\pi f \mu}{\sigma_c}}. \quad (3.25)$$

The skin depth,  $\delta$  cm, is given by

$$\delta = \sqrt{\frac{1}{\pi f \mu \sigma_c}}, \quad (3.26)$$

where,  $\sigma_c$ ,  $\mu$ , and  $f$  represent the conductivity of the trace conductor, permeability of the dielectric material, and the frequency of the signal, respectively. Equation (3.24) shows that the attenuation decreases with the increase in characteristic impedance as well as with the width of the line.

**3.4.1.2 Dielectric Loss** Dielectric loss in the microstrip transmission line arises due to the imperfect dielectric material. A non-ideal dielectric material has a finite conductivity, which causes signal leakage from the trace to the ground through the dielectric material and, thus, causes attenuation in the signal traveling in the transmission line. The dielectric loss is usually expressed as the dielectric loss tangent ( $\tan\theta$ ), which is related to the conductivity ( $\sigma_d$ ) of the dielectric material as

$$\tan\theta = \frac{\sigma_d}{\omega\epsilon}. \quad (3.27)$$

The dielectric loss tangent ( $\tan\theta$ ) is related to the dielectric attenuation constant ( $\alpha_d$  in decibel per centimeter) as

$$\alpha_d = 4.343\omega\sqrt{\mu\epsilon} \tan\theta. \quad (3.28)$$

The dielectric attenuation constant can also be expressed in terms of the effective permittivity ( $\epsilon_{re}$ ) and the conductivity of the substrate as

$$\alpha_d = 1.634 \times 10^3 \frac{q\sigma_d}{\sqrt{\epsilon_{re}}}, \quad (3.29)$$

where,  $q$  is called a the filling factor and is given by

$$q = \frac{\epsilon_{re} - 1}{\epsilon_r - 1}. \quad (3.30)$$

Equation (3.29) shows that the dielectric loss is higher for higher conductivity substrate materials.

**3.4.1.3 Radiation Loss** The radiation loss in the microstrip transmission line occurs due to the fact that a part of the signal flowing in the line is radiated into space due to the antenna effect of the lines. The radiation loss depends on the substrate thickness, dielectric constant of the substrate material, and the structure of the lines. The ratio of

radiated power to the total dissipated power in an open-terminated microstrip line is given as

$$\frac{P_{rad}}{P_t} = 240\pi^2 \left( \frac{h}{\lambda_0} \right)^2 \frac{F(\epsilon_{re})}{Z_0} \quad (3.31)$$

where,  $F(\epsilon_{re})$  is known as radiation factor and defined as

$$F(\epsilon_{re}) = \frac{\epsilon_{re} + 1}{\epsilon_{re}} - \frac{\epsilon_{re} - 1}{2\epsilon_{re}\sqrt{\epsilon_{re}}} \ln \frac{\sqrt{\epsilon_{re} + 1}}{\sqrt{\epsilon_{re} - 1}}. \quad (3.32)$$

Equation (3.31) shows that the radiation loss decreases when the characteristic impedance of the line increases. Also the radiation loss is smaller for lower dielectric permittivity and smaller substrate thickness.

### 3.4.2 Dispersion

The dispersion is a form of signal distortion caused by the frequency dependence of the signal propagation delay in the transmission line. The distortion occurs because the different frequency components of a signal arrive at different times at the output when compared to the input. In a microstrip transmission line, it occurs primarily due to the frequency dependence of the substrate effective dielectric constant. The variation in effective dielectric constant due with the frequency of the signal is given by [81]

$$\epsilon_{re}(f) = \epsilon_r - \frac{\epsilon_r - \epsilon_{re}}{1 + (f/f_{50})^m} \quad (3.33)$$

where,

$$f_{50} = \frac{f'}{0.75 + \left( 0.75 - \frac{0.332}{\epsilon_r^{1.73}} \right) \frac{w}{h}}, \quad (3.34)$$

$$f' = \frac{c \tan^{-1} \left( \epsilon_r \sqrt{\frac{\epsilon_{re} - 1}{\epsilon_r - \epsilon_{re}}} \right)}{2\pi h \sqrt{\epsilon_r - \epsilon_{re}}}, \quad (3.35)$$

and,

$$m = 1 + \frac{1}{1 + \sqrt{w/h}} + 0.32 \left( \frac{1}{1 + \sqrt{w/h}} \right)^3 \text{ for } (w/h) \geq 0.7, \quad (3.36)$$

where  $f$ ,  $f_{50}$ , and  $f'$  are in gigahertz and  $c$  is the velocity of light in free space in meters per second. The dispersion characteristics have been calculated analytically using Equation (3.33-3.36). The results show that the frequency dependent dielectric constant ( $\epsilon_{re}(f)$ ) varies by 0.02%, 0.37%, and 7.36% when the frequency varies from 0.5 to 1.5 GHz, 3 to 11 GHz, and 1 to 100 GHz, respectively. Because the variation in the dielectric constant is negligible at the frequency range 902 to 928 MHz, the transmission line is considered to be non-dispersive for the proposed application.

### 3.4.3 Bandwidth

The attenuation of the signal in a transmission line is a function of the frequency, and the attenuation is higher for the higher frequencies. This limits the range of signal for which the transmission line can be used. Cut-off frequency,  $f_c$ , for a microstrip transmission line is given by

$$f_c = \frac{Z_0}{2\mu_0 h}, \quad (3.37)$$

where,  $Z_0$  is the microstrip line characteristic impedance,  $\mu_0$  is the free space permeability, and  $h$  is the height of dielectric material. For the given substrate, the cut-off frequency is calculated to be 111 GHz. This shows that the bandwidth of the transmission line circuit is not a limiting factor for the application under consideration.



## 3.5 Delay and Reflection

### 3.5.1 Delay

The delay in a transmission line is introduced due to the time taken by a signal to travel through the length of the line. Thus, it is rightly named as the signal propagation delay. The delay can also be thought of as the result of the inherent capacitive and inductive elements of a transmission line that are shown in the distributed components equivalent circuit in Figure 3.4. The propagation delay in a transmission line depends on the speed of the signal in the transmission line. For the given substrate, it has been calculated to be 158 mm/ns. Thus, a 158 mm length of the designed transmission line introduces 1 ns delay in the signal propagating through the transmission line.

### 3.5.2 Reflection

Consider a case where a signal source is connected at one end of a transmission line and a load of known impedance ( $Z_L$ ) is connected at the other end. The signal from the source travels along the transmission line and the power is dissipated at the load. However, not all the signal power flowing through the transmission line is delivered to the load. A part of the signal power will be reflected back, if the characteristic impedance of the transmission line and the impedance of the load are not matched. The amount of reflection depends on the amount of mismatch between the characteristic impedances of the transmission line and the load. Complete reflection of power occurs, if the end of the transmission line is open or ground terminated [76]. The reflection of the signal has been utilized in many applications, such as the time domain reflectometer (TDR) measurement technique, shunt-stub-line impedance matching [83], and transmission line characterization [84, 85]. The amount of the reflection depends on the degree of

mismatch between the transmission line characteristic impedance ( $Z_0$ ) and the load impedance ( $Z_L$ ), measured as the signal reflection coefficient  $\tau$  given by

$$\tau = \frac{|Z_L - Z_0|}{|Z_L + Z_0|}. \quad (3.38)$$

Equation (3.38) reveals that if the impedances of transmission line and the load are exactly equal, the reflection coefficient becomes zero ( $\tau = 0$ ), which implies that all the signal power flowing towards the load is delivered to the load and no signal reflection occurs. This is called a matched condition. While for other extreme cases with zero or infinite load impedance, the reflection coefficient is unity ( $\tau = 1$ ), which implies that all the signal power flowing towards the load is reflected back.

### **3.6 Optimization of Meandered Microstrip Transmission Line Design**

The calculated design parameters of a meandered microstrip transmission line, ie. the transmission line width, meandering width, and the bend type are optimized with the help of Ansoft Designer simulation software [86]. Using the given substrate information, stacked layers of metal, adhesive, and dielectric is created in the simulation environment. A snapshot of those created stacked layers is shown in Figure 3.8. Using the calculated design parameters of the transmission line ( $w = 0.43$  mm,  $M_l = 50$  mm, and  $M_w = 3$  mm), a simulation model of a meandered transmission line model is designed on the created substrate. The designed simulation model of the transmission line is shown in Figure 3.9.

	Name	Type	Material	Drag Mode	Thickness
—	Trace	signal	copper	middle align	37um
▨	Adhesive	dielectric	Pyralux...		25um
▨	Dielectric	dielectric	Kapton		127um
▨	Adhesi...	dielectric	Pyralux...		25um
■	Ground	metalized...	copper	middle align	0mil

Figure 3.8 Substrate stacks in the Ansoft Designer simulation tool.

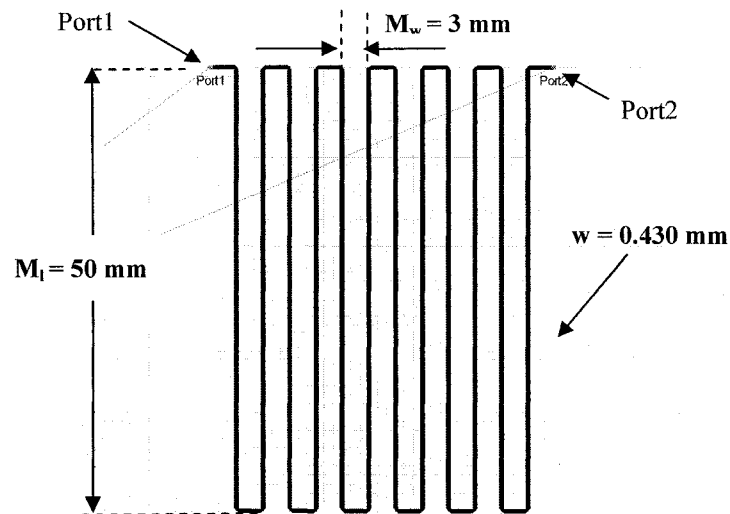


Figure 3.9 A meandered transmission line design in Ansoft Designer.

As shown in the simulation model in Figure 3.9, the two ends of the transmission line are defined as the two ports (port1 and port2) such that, in the next simulations level, the transmission line can be simulated as a two port device. Using the designed simulation model, the transmission line width, meandering width, and the bend type are optimized.

### 3.6.1 Transmission Line Width

The characteristic impedance of a meandered transmission line differs from a straight line. A set of simulations are conducted to optimize the width of the meandered line for a  $50 \Omega$  characteristic impedance. In the circuit level of the simulation

environment, two microwave ports with  $50\ \Omega$  impedances are connected at the two ports of the transmission line design, and scattering parameters (S-parameters) are simulated for a 915 MHz carrier signal. The S11 parameter measures the return loss of the two port device at port1. The return loss at port1 (S11) is minimum when the impedances of the microwave port and the transmission line are best matched. To find the best match transmission line width, the width of the line is varied from  $400\ \mu\text{m}$  ( $0.40\ \text{mm}$ ) to  $500\ \mu\text{m}$  ( $0.50\ \text{mm}$ ), and the S11 parameter is measured. The obtained result for S11 in decibel (dB) versus width of the line in micrometers is shown in Figure 3.10. It is observed that the return loss is smallest ( $-54.68\ \text{dB}$ ) for a  $453\ \mu\text{m}$  ( $0.453\ \text{mm}$ ) transmission line width.

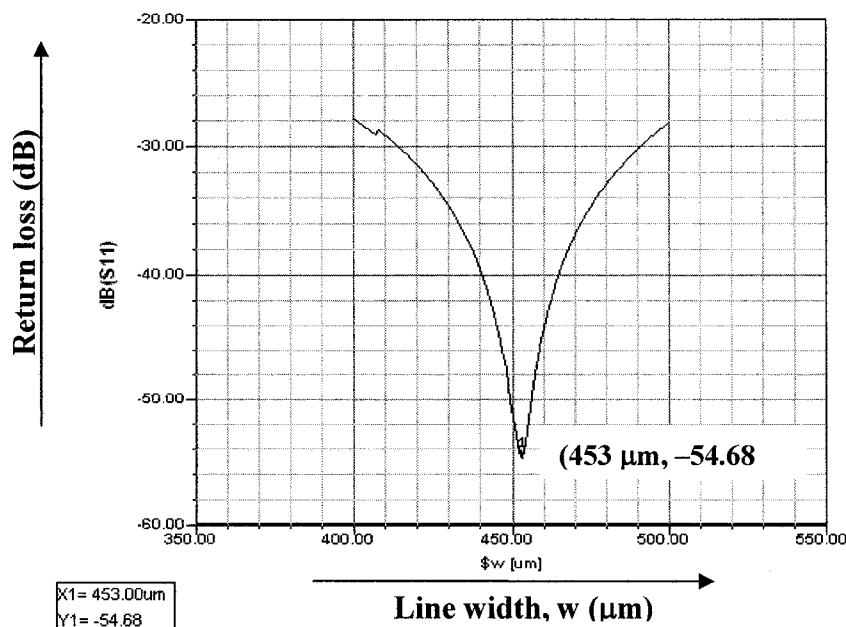


Figure 3.10 Return loss (S11) in decibel (dB) versus the width of the transmission line ( $w$ ) in micrometers.

### 3.6.2 Meandering Width

The simulations were conducted to test the different meandering line widths without introducing distortion in the signal. A smaller line width is desirable to reduce

the dimension of the circuit on the substrate. But a smaller meandering line width increases the coupling between the two parallel lines (cross-talk), which in turn increases the signal distortion. The transmission line design was simulated for 3 mm, 2 mm, and 1 mm widths, using a similar setup discussed for bend type optimization, and the output signal was observed for each case. It was observed that the width can be reduced to 1 mm without any distortion in the output signal. It should be noted that the minimum meandering width condition, twice the line width, still holds for 1 mm ( $> (2 \times 0.452)$  mm).

### **3.6.3 Bend Type**

Simulations are conducted separately for three bend types; corner, curved, and mitered. A pulse signal with 915 MHz carrier is used for the simulation. The pulse is generated with the help of a signal source, pulse generator, and a switch. The circuit level simulation design in Ansoft Designer is shown in Figure 3.11. The single source is connected at the input of the switch, which is operated by the pulse generator. The output of the switch is a 3.3 ns rectangular pulse with a 915 MHz carrier signal. The generated pulse signal is fed to port1 of the transmission line and the output signal is observed at port2 with the help of a 50  $\Omega$  microwave port. The output signal is observed at the microwave port for the corner, curved, and mitered bend types. The input signal, bend type, and the observed output signals for different bend types are compared in Table 3.2. It is observed that the output signal is less distorted in the case of the mitered bend type compared to the corner and the curved bend types. Thus, the mitered bend type is considered for the transmission line circuit designs presented in this dissertation.

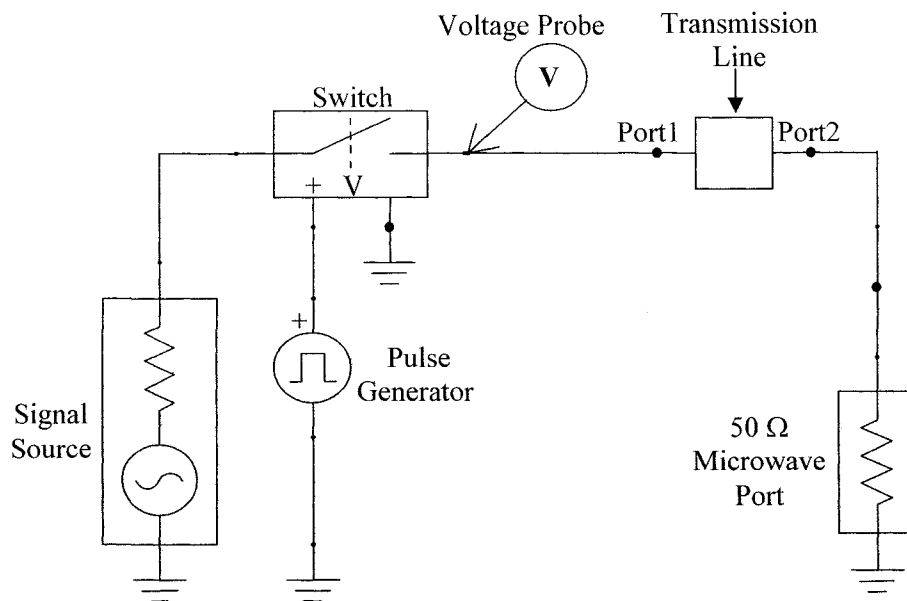
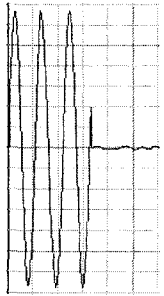

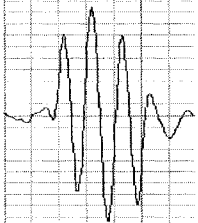

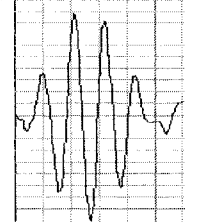

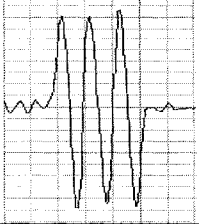


Figure 3.11 Ansoft Designer simulation setup used for bend type optimization.

Table 3.2 Comparison of Input and Output Signals from the Transmission Lines using Corner, Curved, and Mitered Bend Types.

<i>Input Signal</i>	<i>Bend Type</i>	<i>Output Signal</i>
	 <u>Corner</u>	
	 <u>Curved</u>	
	 <u>Mitered</u>	

## CHAPTER 4

### **MICROSTRIP TRANSMISSION LINE REFLECTION AND DELAY BASED ID GENERATION SCHEME**

The transmission line reflection and delay based ID generation scheme reported in [87] is discussed in this chapter. The proposed scheme, after receiving a sinusoidal interrogation input pulse, constructs an OOK modulated composite signal pattern that represents a unique ID code. The circuit considered consists of open or ground terminated multiple transmission lines of different lengths, and utilizes reflection, due to impedance mismatch, and length dependent propagation delay to construct OOK modulated signal patterns. The proposed scheme also allows a larger number of bits to be generated. The new scheme eliminates the need for isolators and circulators used in previously reported delay based ID generation schemes [43-46].

#### **4.1 Signal Reflection and Delay in Single and Multiple Transmission Lines System**

##### **4.1.1 Single Transmission Line System**

The fraction of signal power propagating through a transmission line that is delivered to a load connected at the end of the transmission line depends on the characteristic impedance of the transmission line and the impedance of the load. The signal power is completely delivered to the load if the two impedances are exactly equal,

that is, if the two are matched. When the two impedances are not matched, not all the signal power flowing through the transmission line is delivered to (or absorbed by) the load, but some part of the signal is reflected back. The magnitude of the power reflection depends on the magnitude of the mismatch between the two impedances. The amount of the reflection is characterized by a quantity called a reflection coefficient, which is denoted by  $\tau$  and given by

$$\tau = \frac{Z_L - Z_T}{Z_L + Z_T}, \quad (4.1)$$

$$|\tau| = 1 \text{ for } Z_L = 0, \text{ or } Z_L \gg Z_T, \quad (4.2)$$

where,  $Z_T$  and  $Z_L$  are the transmission line characteristic impedance and load impedance, respectively. Equation (4.2) suggests that all the signal power flowing through a transmission line with open or shorted end (infinite or zero impedance) is reflected back from the termination. Figure 4.1 shows a simple schematic consisting of a pulse generation system, a transmission line with a shorted load, and an oscilloscope. A signal generator, pulse generator, and a high speed switch constitute the pulse generation system which generates a rectangular pulse with a sinusoidal carrier signal (called a sinusoidal pulse). As illustrated in Figure 4.1, if the sinusoidal pulse signal is fed into one end of a transmission line, denoted as the input port, with the other end connected to ground (shorted), the pulse flows from the input, along the transmission line, to the shorted end and gets reflected at the termination. The reflected pulse travels back to the input end. The transmission line has its own inherent propagation delay and losses. The delay is due to the time required for the signal to propagate along the transmission line, and the loss is due to the radiation loss, dielectric loss, and a small amount of metal line loss. Therefore,



two pulses appear in the oscilloscope connected at the input port of the setup, as shown in Figure 4.1. The first pulse is the input pulse. The second pulse, reduced in amplitude and delayed in time with respect to the input pulse, is the reflected pulse.

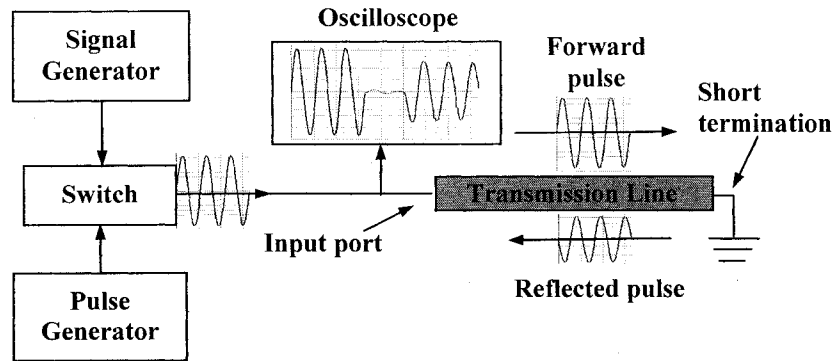


Figure 4.1 Pulse reflection in a ground terminated transmission line.

The angle (phase) of the reflected pulse also depends on the characteristic impedance of the transmission line and the impedance of the load as given by

$$\phi = \angle \left( \frac{Z_L - Z_T}{Z_L + Z_T} \right), \quad (4.3)$$

$$\text{For } Z_L = 0, \phi = \pi, \text{ and } Z_L = \infty, \phi = 0. \quad (4.4)$$

Thus, for a short termination, the phase of the reflected signal is opposite as compared to the input signal ( $\phi = \pi$ , from Equation (4.4)) while it is the same as the input signal for an open termination ( $\phi = 0$ , from Equation (4.4)). The phase of any other termination is determined by Equation (4.3).

#### **4.1.2 Multiple Transmission Lines System**

The sinusoidal pulse reflection phenomena in a single transmission line with an unmatched load termination has been discussed in the preceding section. Now two

parallel transmission lines connected to a common input port, and having open (or ground) termination, is considered. A schematic diagram of two parallel meandered transmission lines with a common input port is shown in Figure 4.2. Referring to the example shown in Figure 4.2, if a pulse signal is fed to a system of two open (or ground) terminated transmission lines, the input signal travels in both transmission lines and eventually gets reflected at the terminations and, thus, producing two delayed reflected pulses at the input port. The positions of the reflected pulses depends on the length of the respective transmission lines. In addition, the reflection from one transmission line serves as the secondary input pulse for the other line. Therefore, a secondary reflected pulse follows the two initial reflected pulses. Again, this secondary reflection serves as input for tertiary reflections and so on. The amplitude of the successive reflected pulses diminishes as the reflected signal divides at transmission line branches, and also is due to transmission line losses. The same principles apply for a system of three or more lines.

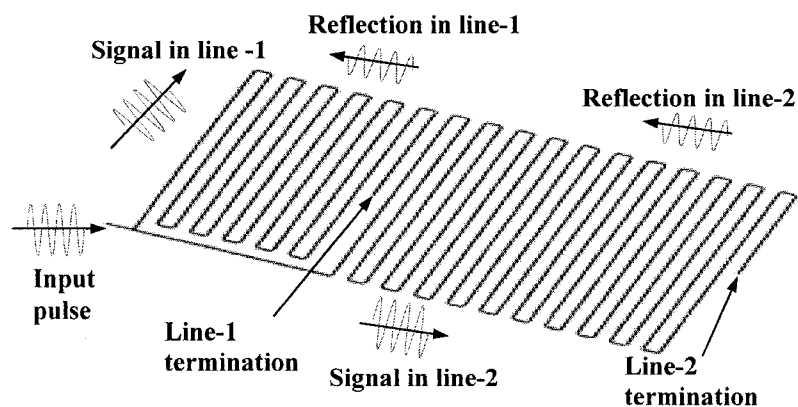


Figure 4.2 Pulse reflections in two transmission lines with ground terminations.

### 4.1.3 Step Impedance Transmission Line System

Reflection and delay in a step impedance transmission line system is described with the help of a single transmission line system as shown in Figure 4.3. The step impedance transmission line system consists of a single transmission line with discontinuous impedance along the line. In the example shown in Figure 4.3, a small transmission line having an impedance  $Z_{T1}$  ohm is followed by an open terminated line having impedance  $Z_{T2}$  ohm ( $> Z_{T1}$ ). If a pulse signal is fed to the transmission line system, as shown in Figure 4.3, the pulse signal travels along the  $Z_{T1}$  line until it reaches the ( $Z_{T1}$ - $Z_{T2}$ ) interface. At the ( $Z_{T1}$ - $Z_{T2}$ ) interface, some part of the signal power is reflected while the remaining signal power travels into the  $Z_{T2}$  line. The transmitted signal travels along the  $Z_{T2}$  line until it is finally reflected back from the open termination. Some portion of the backward travelling signal is again reflected at the ( $Z_{T2}$ - $Z_{T1}$ ) interface. The same phenomenon continues and multiple reflections occur inside the line such that a number of reflected pulses, delayed in time, appear at the input port.

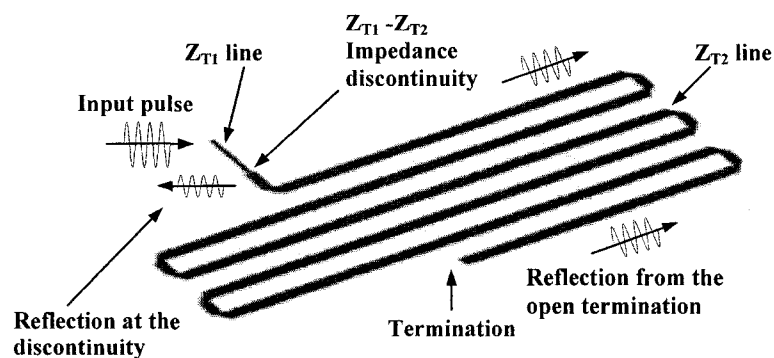


Figure 4.3 Pulse reflections in an open terminated step impedance transmission line.

## **4.2 ID Generation using Reflection and Delay in Transmission Lines**

In the previous section, it has been discussed that a sinusoidal pulse signal, reflected from an unmatched transmission line termination, is delayed in time with respect to the input pulse due to the inherent signal propagation delay. Additionally, in a multiple transmission line system or step impedance transmission line system, a number of delayed reflected pulses appear at the input terminal due to multiple reflections inside the transmission line. The number of reflections depends on the number of transmission lines or number of impedance steps, while the delay depends on length. By proper design of the transmission line system, reflected pulses can be placed at any desired position to form a predefined signal pattern that represents a unique ID code. The ID generation technique and ID circuit design are discussed in this section.

### **4.2.1 Dual Transmission Lines ID Circuit using OOK Coding**

The proposed dual transmission line ID generation circuit scheme consists of ground or open terminated transmission lines with a common feed point. As the delay in a reflected pulse depends on the length of the transmission line, the reflected signal can be placed at any desired position by properly designing the transmission line length. The lengths of the transmission lines are designed so that the reflection pattern forms a composite signal that follows a predefined digital modulation scheme and represents a unique ID code. For every input pulse in the circuit consisting of two transmission lines with a common feed, two primary, a secondary and higher order reflected pulses are received. The first three reflections, consisting of two primary reflections from the two lines and the third due to superposition of the two secondary reflections, are used for ID code generation. The relative positions of the reflected pulses depend on the delay and

therefore the lengths of the transmission lines. The OOK modulated pattern has been considered for the design of the reflected signal pattern representing the ID codes.

Dual transmission line ID circuits consist of different combinations of two transmission line lengths to construct OOK modulated signal patterns. Two different OOK modulated signal patterns representing **101010** and **110100** bit patterns, constructed by placing three reflected pulses in six bit positions are shown in Figure 4.4 (a), which is a schematic representation of the code generation concept. In practice, consecutive reflected pulses are more attenuated than shown in Figure 4.4 (a), and higher order reflections are not considered for code generation, thus limiting the use to only the first three pulses. The presence of a pulse represents binary **1** and its absence represents binary **0**. With this representation, ten different OOK modulated signal patterns, representing ten different ID codes can be constructed, as shown in Figure 4.4(b). It should be noted that only three 1s are considered in any sequence for code generation. If  $n$  positions are considered with three reflected pulses, taking the first bit as a starting bit,  $(n-2) \times (n-1)/2$  bit sequences can be constructed, where  $n$  is greater than or equal to the number of reflected pulses. For  $n$  positions, to get the maximum number of ID code sequences, the number of reflected pulses, here defined as  $I$ , is given by  $I = n/2$  when  $n$  is even, and it is given by  $I = (n+1)/2$  when  $n$  is odd. If three positions are considered with three reflected pulses, only four bit sequences can be obtained. Therefore, six bit positions are adopted to achieve more bit sequences with the same number of (two) transmission lines.

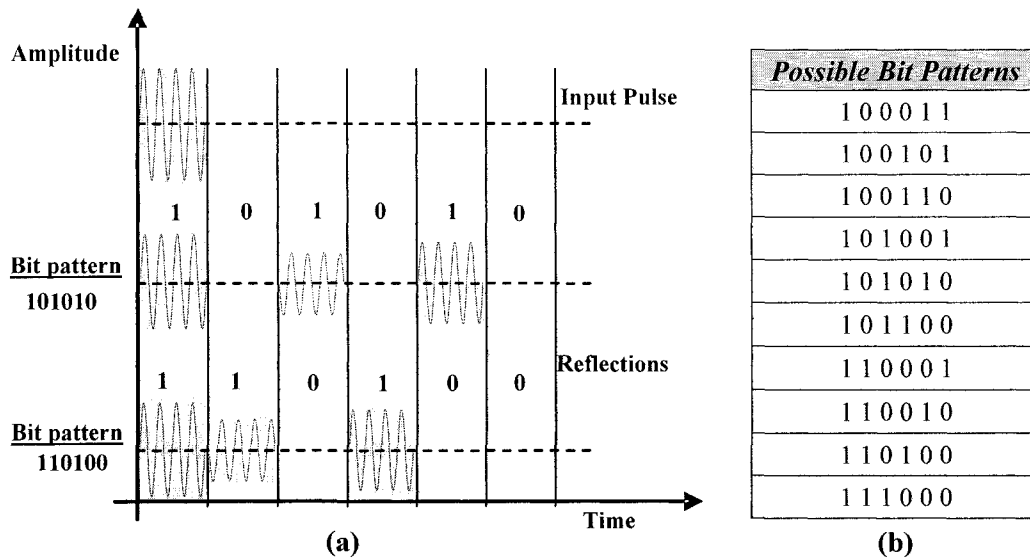


Figure 4.4 (a) Schematic representations of two different OOK modulated signal patterns constructed by placing three reflected pulses in six bit positions. (b) Possible bit patterns with three reflected pulses in six bit positions.

#### 4.2.2 Step Impedance Transmission Line ID Circuit using OOK Coding

The step impedance transmission tag ID circuit consists of single transmission line having abrupt impedance discontinuities along the line. As the impedance of a microstrip transmission line for a given substrate depends on its width, a varying impedance microstrip transmission line can be obtained by simply varying the width along the length of the line, as discussed in Section 4.1.3. With an appropriate selection of transmission line widths and lengths, the reflected pulses can be placed at any desired position to construct OOK modulated signal patterns.

Step impedance transmission line ID circuits consist of different combinations of transmission line impedances in series, such that the impedance change is abrupt. The cases considered are a  $50 \Omega$  line followed by a  $25 \Omega$  line, open or ground terminated. ID

circuits are designed by considering the first three reflected pulses. An ID circuit with a 5 mm long  $50 \Omega$  transmission line, followed by 612 mm long  $25 \Omega$  open transmission line places reflected pulses separated by 3.4 ns. The reflection pattern represents an OOK modulated **101010** bit pattern with 3.4 ns bit width. The design is based on 1 ns delay for a 90 mm long transmission line. An ID circuit with a 5 mm long  $50 \Omega$  line followed by a 306 mm long  $25 \Omega$  open transmission line places the first three pulses reflections in sequence, resembling a **111000** bit pattern in six bits representation. Simulation and experimental results for these two ID circuits are discussed in Section 4.5.2.

#### **4.2.3 Phase Modulation Scheme**

The phase of the reflected pulses depends on the type of terminating load. An open load results in a reflected pulse of the same phase as the input pulse while it is of opposite phase for the case of a shorted load. Similarly, the phase of a reflected pulse from an impedance discontinuity depends on impedances. If the impedance is increasing at the discontinuity, the reflected pulse will have same phase as the original pulse, and if it is decreasing, the phase will be opposite. The reflected pulses of different phases can be placed in desired position by designing the length and the load termination of the transmission line ID circuit to form a phase modulated signal pattern. The signal pattern can be used to modulate the code of the circuit as phase modulation. An example ID circuit that generates a phase modulated signal pattern is designed in the Ansoft Designer, and the simulation results are shown in Figure 4.5. With a predefined bit width of 3.278 ns, the presence of the phase reversal is considered to represent a binary “1” and the absence of phase reversal is considered to represent a binary “0.” With the three reflected pulses, the pattern generated a two bits ID, “11” in the example shown in Figure 4.5. Although the phase modulation results in a smaller ID combination, the phase modulated

signal pattern is less prone to noise and false triggering. The construction of a phase modulated signal pattern requires perfect pulse shape with sharp transitions at the rising and falling edges of the pulses, which has not been possible with the currently designed ID circuit and, thus, the generated pattern lacks an identifiable phase transition point. Therefore, the phase modulated ID circuit has not been considered further. However, it is possible that phase of the reflected pulse can be utilized for information excretion about the terminating load.

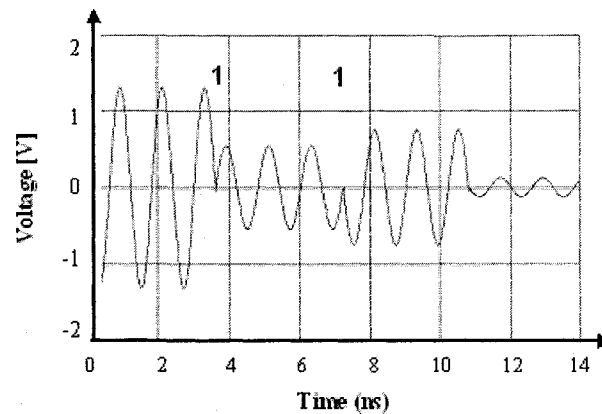


Figure 4.5 Reflection pattern representing phase modulated signal.

#### **4.2.4 Single Transmission Line using PPM Coding**

The reflected pulse can be placed in a fashion to generate a pulse position modulated (PPM) signal pattern. In this technique, a single transmission line circuit is considered and the generated signal pattern consists of two signal pulses. The transmission lines can be designed to place the reflected signal pulse in a predefined position where a position of the second pulse with respect to the first pulse, represent a unique ID code. The ID code generation, using two pulses and the respective PPM code, is shown in Figure 4.6.



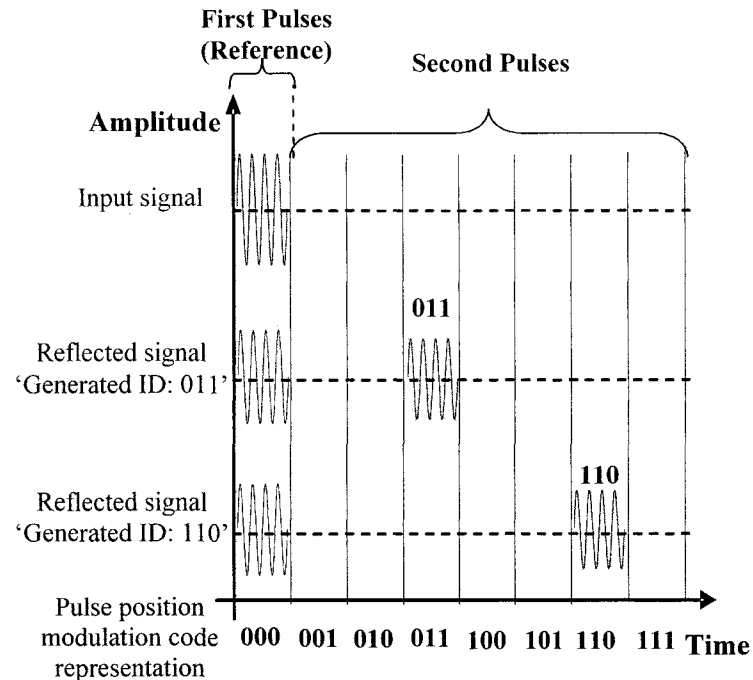


Figure 4.6 Code generation using reflected pulse and PPM representation.

In this technique, the first pulse is taken as the reference pulse, and the position of the second pulse with respect to the first pulse determines the code represented by the pattern. In Figure 4.6, PPM codes represented by the respective positions of the pulses are indicated below the horizontal axis (time-axis). For example, the position of second pulse in the fourth bit position with respect to the first bit position represents an 011 ID code. Similarly, the position of the second pulse in the seventh bit position represents an 110 ID code. The number of different bit patterns that can be generated with a PPM modulated pattern is less than the number of bit patterns with an OOK modulated pattern. Additionally, this technique does not take the secondary reflections into account, which tends to cause error in identification. However, the simplicity of the circuit using this technique is more attractive in applications, such as sensor tag, where the problems associated with secondary reflections are small.

### **4.3 Design and Fabrication of Transmission Line Reflection and Delay Based ID Tags**

The transmission line reflection and delay based ID tags are designed in Ansoft Designer simulation software [86]. The designed tag structures are transferred into a transparent mask and the tags are fabricated using standard photolithographic techniques.

#### **4.3.1 Tag Design**

The meandered microstrip transmission line is adopted for the tag design. A dual line ID circuit design is shown in Figure 4.7. Meandered line length ( $M_l$ ) of 50 mm and gap width ( $M_w$ ) of 3 mm are adopted, except for the second line of the two transmission line circuit, where the meandered length of the second line ( $M_l$ ) is selected to be 53 mm. The width of the trace ( $w$ ) is calculated to obtain the 50  $\Omega$  characteristic impedance of the transmission line. The characteristic impedance of a meandered line deviates from that of a straight line, and the analytical width of line for the meandered transmission line is optimized by running simulations on impedance versus meandered line width  $w$ . As the only restriction on transmission line impedance selection is the matching with the impedance of the input system, the impedance of the transmission line can be changed to match the input system impedance. Based on the simulations results observed with different bend types, the mitred bend type is adopted for the transmission line design. ID circuits for OOK modulated signal patterns are designed considering the presence of the reflected pulse as binary “1” and its absence as binary “0.”

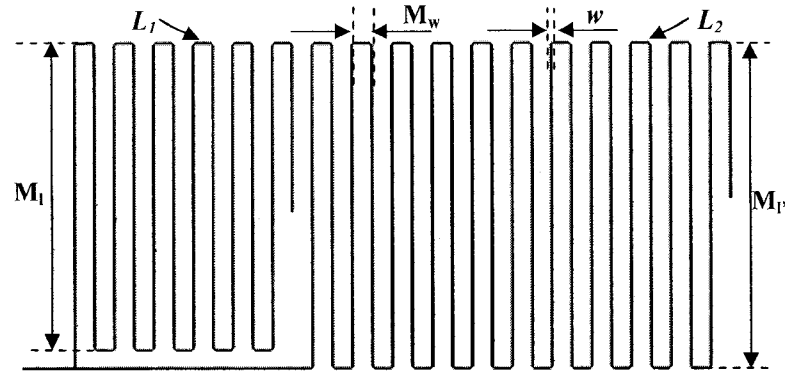


Figure 4.7 Dual transmission line ID circuit designed in Ansoft Designer for 101010 bit pattern (dimensions: 104 mm  $\times$  53 mm).

For any bit pattern, the length of the first or shorter transmission line ( $L_1$ ) and that of the second or longer line ( $L_2$ ) are given by Equations (4.5) and (4.6), respectively.

$$L_1 = (i' - i) \times T \times l, \quad (4.5)$$

$$L_2 = (i' - 1) \times T \times l, \quad (4.6)$$

where,  $i$  and  $i'$  are the numbers representing the position of the second and the third pulses, respectively. The length of transmission line required for 1 ns reflection delay  $l$  is in millimetre, and the bit width  $T$  is in nanoseconds. For six bit design,  $i$  can take 2 through 5 while  $i'$  can take 3 through 6. Equations (4.5) and (4.6) are true for any number of bits, as long as the ID circuit consists of two transmission lines and three pulses are considered.

Now consider a **101010** bit pattern. Using the convention discussed,  $i = 3$ , and  $i' = 5$ . Taking bit width,  $T = 3.4$  ns and  $l = 90$  mm/ns, Equations (4.5) and (4.6) give  $L_1 = 612$  mm and  $L_2 = 1224$  mm. For **101100** bit pattern, lengths of lines  $L_1$  and  $L_2$  are 306 mm and 918 mm, respectively.

### **4.3.2 Mask Design and Printing**

Pyralux FR9151 CU CLAD [79] is used as the substrate to fabricate the ID circuit samples with conventional photolithographic techniques. The circuit masks are designed in Ansoft Designer and converted to postscript format with LinkCAD software [88]. A standard photolithographic technique for PCB is followed in order to transfer the mask patterns onto the substrate.

### **4.3.3 Photolithography and Etching**

At first, positive photoresist PR-1813 is spin coated on a substrate surface. The substrate is then soft baked. The spin coating and soft baking cycle is repeated for the other side of the substrate. The photoresist is then patterned by exposing to UV light through the mask and developed in MF-321 developer solution. The developed pattern on the substrate is then hard baked and etched in chloride solution using a hot bath bubble etching setup to produce the desired copper pattern. Conductive epoxy is used to make ground connections to the ground plane. Epoxy is carefully applied through drilled holes at the desired locations and then dried. SMA jacks are then attached by soldering to provide signal connections and for testing. A fabricated dual open line ID circuit prototype is shown in Figure 4.8.

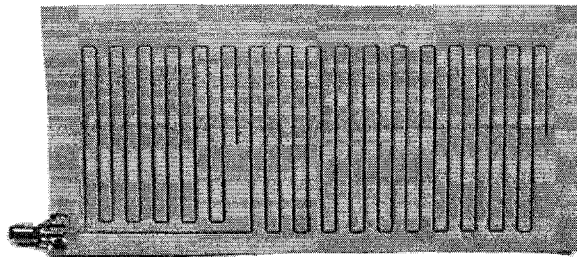


Figure 4.8 A prototype of a dual open transmission line ID circuit (dimensions: 115 mm × 60 mm).

#### 4.4 Measurement Setup

The schematic diagram of the experimental setup used to test the ID circuits is shown in Figure 4.9, which consists of a signal source, an oscilloscope, and a high isolation coaxial circulator (manufacturer: JQL Electronics Inc., part no: JCC0800T0960S10). The signal source further consists of a signal generator, pulse generator, and a mixer (used as a RF switch) and generates an interrogator input pulse with a sinusoidal carrier. The input pulse signal is generated by operating the switch with a pulse from a narrow width pulse generator. A 915 MHz sinusoidal signal is used as the carrier signal and an interrogation input pulse of 4 ns is generated. The generated pulse signal is analyzed for frequency spectrum coverage in MATLAB using fast fourier transform. The bandwidth was found to be 140 MHz. However, the allowed bandwidth for 915 MHz in ISM band is 26 MHz. It should be noted that for this work a 915 MHz carrier is adopted for the practicality of demonstrating an example of the proposed scheme with the available laboratory instrumentation. The range of frequencies used to generate ID code using the proposed scheme is not limited to 915 MHz. The frequency regime migration with the proposed microstrip lines can be done without much modification to the system design.

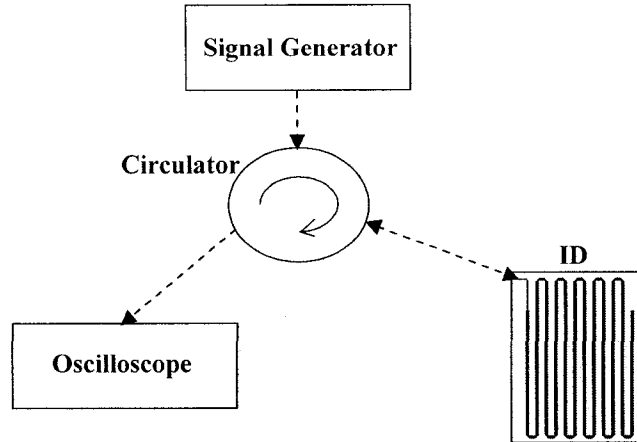


Figure 4.9 Experimental setup used to test the ID circuits.

In the simulation and designs, a 3.278 ns rectangular pulse with 915 MHz sinusoidal carrier is used as the input signal. But the practical generated input pulse has finite rise time and fall time, resulting in a wider pulse width (4 ns). The signal source, ID circuit, and the oscilloscope are connected through the circulator, as shown in Figure 4.9. The circulator has three ports (port 1, 2, and 3), where it presents a low attenuation path from port 1 to port 2, and port 2 to port 3, while providing a high attenuation path from port 1 to port 3, and port 2 to port 1. The input pulse is fed to port 1. The ID circuit is connected at port 2, and the signal is observed at port 3 by means of an oscilloscope. Thus, the circulator directs the input signal from the source to the ID circuit and the reflected signals to the oscilloscope.

## **4.5 Results and Discussions**

### **4.5.1 Single Transmission Line Circuit**

A single meandered transmission line circuit is designed and simulated (in Ansoft Designer) to observe pulse reflection and delay in the transmission line. The circuit consists of a 639 mm long, 50  $\Omega$  meandered microstrip transmission line. A pulse signal

is fed from one end of the transmission line and the reflection is observed at the same end, with the other end open or ground terminated.

The single transmission line circuit, as discussed, is fabricated using the fabrication methods discussed in the tag design and fabrication section. A pulse signal is fed at the input port of the circuit and the reflections for different loading condition are observed at the other end using a slightly modified setup, as shown in Figure 4.9. In the modified setup, the signal is observed just before the ID circuit, by using a T-connector, and the oscilloscope is replaced with a  $50\ \Omega$  load. The intention of this modification is to observe both the input and reflected pulses so as to compare the delay and attenuation.

Figure 4.10 shows the experimental and simulation results, showing input and reflected pulses for both open and ground load cases. It is observed that each input pulse is followed by a reflected pulse, which is attenuated and delayed with respect to the input pulse. The reflected signal is attenuated due to the losses in the transmission line while the delay is due to the inherent propagation delay in the transmission line. It is also observed that for the case of the open load condition, the reflected pulse is in the same phase as the input pulse, while in the ground load condition, the phase is opposite. The simulation results and the experimental results observed are in good agreement.

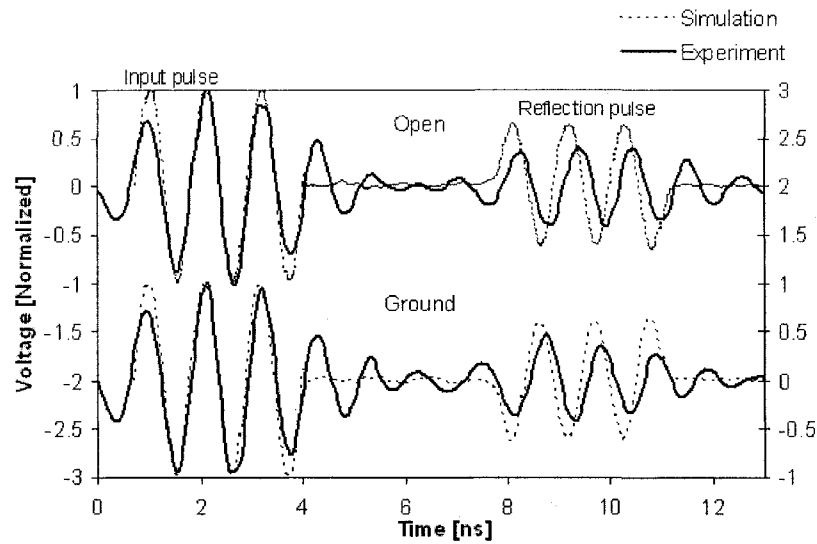


Figure 4.10 Simulation and experimental results showing input and reflected pulses for open and ground load meandered transmission line.

#### 4.5.2 Dual Transmission Lines ID Circuit

Dual open transmission line ID circuits for **101010** ( $L_1 = 612$  mm,  $L_2 = 1224$  mm) and **101100** ( $L_1 = 306$  mm,  $L_2 = 918$  mm) bit patterns are designed and fabricated using the method described in Section 4.3 and tested using the set up discussed in Section 4.4. The simulation of the design is carried out in Ansoft Designer. The simulation and experimental results for the **101010** and **101100** bit patterns are shown in Figure 4.11 and Figure 4.12, respectively. Three prominent cycles of the sinusoidal signal in the input pulse are considered for comparing the simulation and experimental results. The first pulse (pulse 1) is due to the reflection from the shorter line ( $L_1$ ) and the second pulse (pulse 2) is from the longer line ( $L_2$ ). The third pulse (pulse 3) represents the composite of two secondary reflections from the two lines.



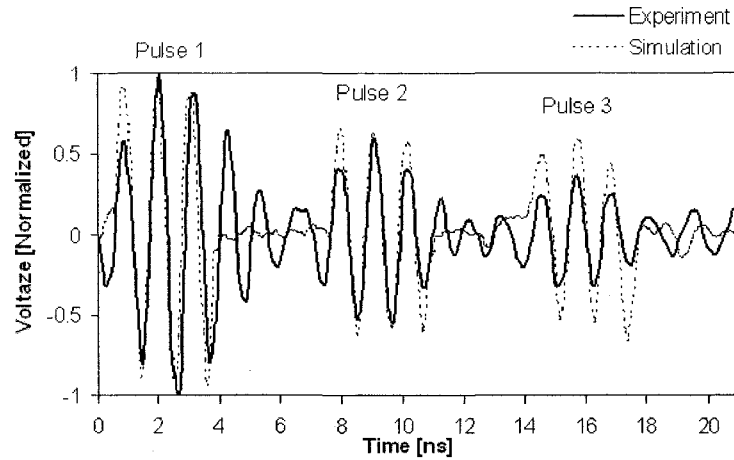


Figure 4.11 Simulation and experimental results representing 101010 bit pattern for dual open line ID circuit.

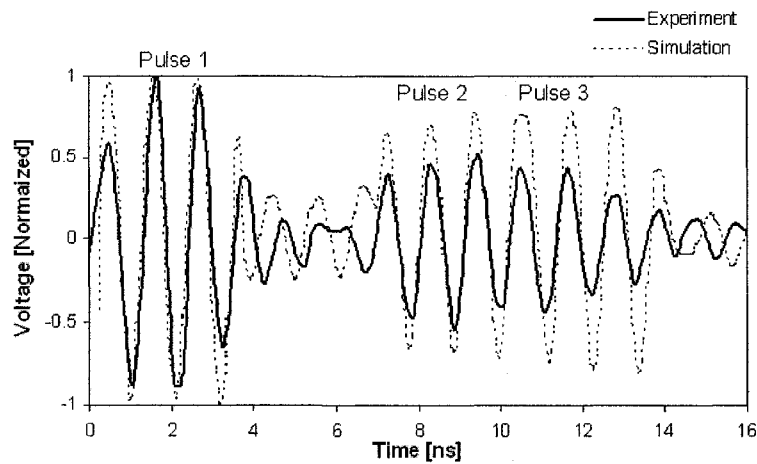


Figure 4.12 Simulation and experimental results representing 101100 bit pattern for dual open line ID circuit.

In Figure 4.12, the third pulse just follows the second pulse; as a result, the second and the third pulses appear to be continuous. The experimental reflection patterns in both cases considered are in good agreement with the simulation reflection patterns. The position of the experimental reflection pulses coincides with the simulation reflections. Some slight deviations and differences in amplitude can be attributed to the presence of

noise in the off state of the pulse signal. The output signal pattern is the composite of many reflections and the noise of the first reflection becomes comparable to the consecutive reflected pulses as the order of reflection increases. The greater deviation in the third pulse as compared to the other two pulses can be attributed to this fact. The differences between the amplitudes of different cycles within the third pulse in Figure 4.12 is due to the addition of the trailing cycles of the second pulse to the initial cycles of the third pulse. Similar results are observed for the ground termination, but the phases of the reflected pulses are reversed, as is explained for the single transmission line case in Section 4.5.1.

#### **4.5.3 Step Impedance Transmission Line ID Circuit**

The simulation and experimental results for a step impedance ID circuit consisting of a 5 mm, 50  $\Omega$  line followed by a 612 mm, 25  $\Omega$  open line are shown in Figure 4.13. It is observed that the experimental result is in close agreement with the simulation result. The first pulse is due to the reflection at the (50-25)  $\Omega$  interface and the second pulse is due to the reflection at the open termination of the 25  $\Omega$  line. The third pulse is due to the secondary reflection of some part of the backward travelling first reflection at the (25-50)  $\Omega$  interface, as described earlier.

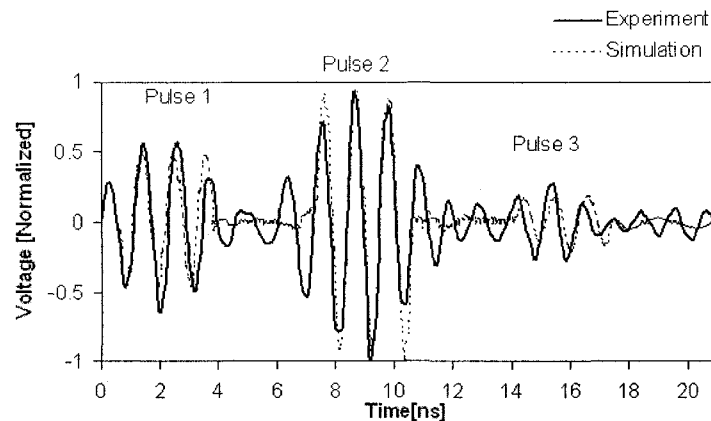


Figure 4.13 Simulation and experimental results showing first three reflections in a (50-25)  $\Omega$  step impedance circuit with a 5 mm, 50  $\Omega$  line and a 612 mm, 25  $\Omega$  line.

The simulation and experimental results for a (50-25)  $\Omega$  step impedance circuit with a 5 mm, 50  $\Omega$  transmission line, and a 306 mm, 25  $\Omega$  open transmission line are shown in Figure 4.14. The result consists of three reflected pulses. The phases of the first and second pulses are opposite. The phase change is abrupt in the simulation, as the pulses are assumed ideal. But the phase change in the experimental result is gradual, due to the imperfect practical interrogation input pulse and the presence of noise. The deviation between the experimental and simulation results from 2 to 4 ns (at the end of first pulse) can also be attributed to this fact. The second and third experimental pulses are in good agreement with the simulation pulses. If a pulse represents a binary **1** and a space represents binary **0**, the signal pattern in Figure 4.13 represents **101010** and that in Figure 4.14 represents **111000** bit patterns in a six bit design. Similar results are observed for a ground termination of a 25  $\Omega$  line, but the phase of reflected pulse from the ground termination is reversed.

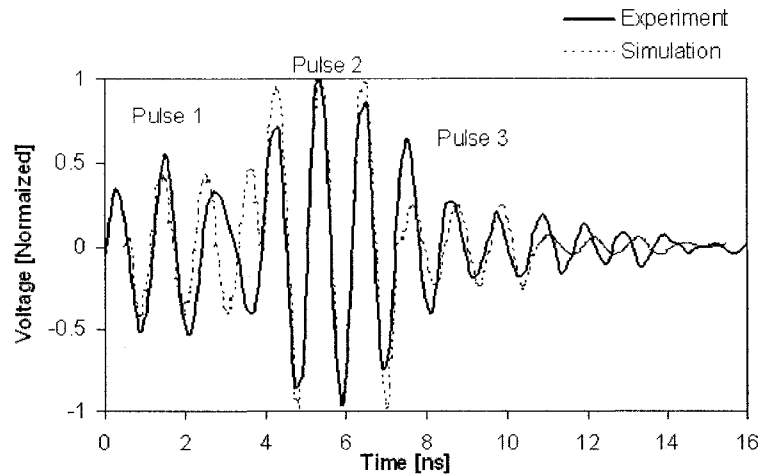


Figure 4.14 Simulation and experimental results for a  $(50\text{-}25)\ \Omega$  step impedance circuit with a 5 mm,  $50\ \Omega$  line and a 306 mm, open  $25\ \Omega$  line.

## 4.6 Antenna Integration

The theory, design, simulation, fabrication, and testing aspects of the microstrip transmission line reflection and delay based ID generation scheme have been discussed thus far. The antenna parameters, which are important for integration into an ID circuit to realize a complete RFID tag, are discussed in this section.

### 4.6.1 Antenna Parameters

**4.6.1.1 Resonant Frequency** At the resonant frequency, an antenna has the highest efficiency of power transmission and reception. This is the frequency where the antenna is designed to operate at its best. For the operation in the UHF ISM band (902 MHz to 928 MHz), an antenna having a 915 MHz resonating frequency is desirable.

**4.6.1.2 VSWR** VSWR stands for voltage standing wave ratio and it is related to the return loss of the antenna. A smaller VSWR corresponds to a more efficient power transmission; thus an antenna having a smaller VSWR (less than two) is desirable for RFID applications. The VSWR for an antenna is frequency dependant and it is smallest at

the resonant frequency. The VSWR ( $S$ ) of the antenna is related to the voltage reflection coefficient ( $\Gamma$ ) at the antenna feed, as given by Equation (4.7).

$$S = \frac{1 + |\Gamma|}{1 - |\Gamma|}. \quad (4.7)$$

Equation (4.7) reveals that the VSWR of an antennas is always greater or equal to one, one being the perfect condition when all the signal power flowing into the antenna port is radiated into space. The VSWR requirement for RFID applications is,  $S \leq 2$ , which corresponds to  $\Gamma \leq 0.33$ .

**4.6.1.3 Bandwidth** Bandwidth of an antenna is the range of frequencies where the performance of the antenna meets the minimum requirements for a given application. For the RFID application, the required bandwidth is the frequency spectrum 902 MHz to 928 MHz and the antenna is required to have a VSWR less than two over the given spectrum.

**4.6.1.4 Gain** Gain measures the ability of an antenna to radiate in a particular direction compared to an isotropic antenna which radiates equally in all directions. Higher gain signifies a more efficient radiation in a desired direction. The gain of an antenna is expressed relative to the isotropic antenna in decibels (dBi), which signifies the magnitude the transmitter power is increased for the highest power radiated direction (or power added when measured in dB). The total power transmitted by an antenna is measured as the effective radiated isotropic power (EIRP), as given by Equation (4.8).

$$E = P_t + G_a, \quad (4.8)$$

where,  $E$  is EIRP in decibels (dB),  $P_t$  is transmitter output power in decibels (dB), and  $G_a$  is antenna gain in decibels relative to an isotropic antenna (dBi).

**4.6.1.5 Radiation Pattern** The radiation pattern is the geometrical distribution of power transmitted by the antenna into space. An omnidirectional radiation pattern signifies that the antenna radiates equal power in all directions in a particular plane. An omnidirectional radiation pattern is desirable for the RFID application.

**4.6.1.6 Impedance** Impedance of an antenna is defined as viewed from the feed of the antenna. As impedance matching between the tag and the antenna is of great importance for an efficient power transfer, it is desirable to have a matching antenna with the tag. The transmission line based ID tag circuits are designed to have  $50 \Omega$  impedance. Thus,  $50 \Omega$  input impedance is required for an antenna to integrate with the proposed RFID tags.

**4.6.1.7 Size** The size of an antenna signifies the geometrical volume occupied by the antenna. Because the size and the cost of a tag are associated with the size of the antenna, it is desirable to have a smaller size for a defined set of parameters. Usually, planar antennas are used for the RFID application limiting the size to the geometrical area of the antenna.

#### **4.6.2 Antenna Scattering**

When an antenna is illuminated by an electromagnetic wave, some part of the signal is absorbed by the antenna, which is defined as antenna absorption, is delivered to the load, while the remaining part of the signal which is reflected back into space is defined as antenna scattering. The reflection phenomena can be further divided into optical reflection and scattering reflection. Optical reflection is a simple reflection due to the fact that the EM wave encountered some obstacle in the propagation path. The scattering reflection is caused because of the antenna function of the conductor. The scattering reflections stem from two sources: the structure of the antenna and the load

connected to the antenna, named respectively as structural-mode and antenna-mode scatterings. The RFID system relies on the antenna-mode scattering and operates in the controlled scattering mechanism.

#### **4.6.3 Antenna Scattering Property in Chipless Sensor Tag Design**

The scattering of an antenna occurs due to two phenomena, induction of current in the structure of the antenna, known as structural-mode scattering, and mismatch between the impedances of the antenna and load, known as antenna-mode scattering. The structural-mode scattering is an inherent property and does not vary for a given antenna. On the other hand, the antenna-mode scattering is a load dependant property and varies along with the variation in the impedance of the load. Antenna-mode scattering has been the central part of the chip-based passive RFID technology, where the impedance presented to the antenna is switched to different impedance states to vary the amount of scattered power, and convey the desired information. This technique is known as backscatter modulation. The fact that the total backscattered signal consists of the structural-mode scattered signal and antenna-mode scattered signal and that the structural-mode scattering does not depend on the load while the antenna-mode scattering depends on the load, opens up the possibility of extracting the load information from the antenna-mode scattering, if the individual scattering behavior and their relationship are known. For such a case, the load can be replaced with a sensor load and a chipless sensor tag can be realized. Thus, due to the importance of the scattering properties of an antenna used for chipless RFID sensor tags, the analysis, measurement, and characterization of the scattering properties of the antenna is discussed in Chapter 5.

## **CHAPTER 5**

### **RFID TAG ANTENNA SCATTERING PARAMETERS: THEORY AND EXPERIMENTATION FOR A NEW MEASUREMENT METHOD**

The parameters of antennas that are critical for integration into chipless RFID sensor tags have been discussed in Section 4.6. Antenna scattering (also known as antenna backscattering) is one of the most important parameters, which is defined as a phenomenon by virtue of which an antenna re-radiates some of the incident electromagnetic energy back into space. Generally, passive RFID systems operate on the principle of controlled antenna scattering. In these systems, the reader sends an interrogation signals to the tags, the tag antenna receives the interrogation signal and, based on the load poised to the antenna, it backscatters some part of the received signal into space. The tag changes some parameter of the backscattered signal to convey information to the reader. The backscatter signal is received by the reader for further operations. The wireless range and the efficiency of the system operation depend on the ability of the tag antenna to effectively backscatter the received signal. To achieve the optimum scattering, it is of great importance that all the phenomena involved in the antenna scattering are known, techniques to measure related parameters are developed, and that the relationships between them are established. The backscattering ability of an



RFID tag antenna is measured in terms of radar cross section (RCS). A number of methods to measure RCS of antennas have been used, but the existing techniques require a complicated experimental set up using horn antennas which are not suitable for lower UHF range measurement, such as 915 MHz. Due to the given importance of RCS of an antenna for RFID sensor tags and the complexity of currently available measurement techniques, development and measurement using a new RCS measurement method reported in [89] is discussed in this chapter.

## **5.1 Antenna Backscattering**

The backscattering of an antenna is defined as a phenomenon by which the antenna re-radiates some of the incident electromagnetic energy back into space. When an antenna is irradiated with an electromagnetic wave, the phenomena that takes place at the antenna can be divided into three parts; antenna-mode absorption, the structural-mode scattering, and the antenna-mode scattering. Antennas are generally used for the antenna-mode absorption, by which it absorbs the incident electromagnetic signal and delivers an electrical signal to the load. The structural-mode scattering and antenna-mode scattering are collectively responsible for the antenna backscattering.

### **5.1.1 Structural-Mode Scattering**

The structural-mode scattering occurs at the physical structure of the antenna. When an electromagnetic energy is irradiated on to the surface of an antenna, an electric current is induced on the surface, which flows to the antenna load through the antenna port. But, the fluctuating (induced) current at the antenna surface, before flowing to the load, generates an electromagnetic wave that is radiated back into space as though the current on the surface was induced by a signal to be transmitted [90]. This part of the

energy that immediately escapes into space from the surface of the antenna is called structural-mode scattering.

### **5.1.2 Antenna-Mode Scattering**

The remaining signal energy, after structural-mode scattering, flows out of the antenna port, towards the load. Some part of the signal energy flowing toward the antenna is absorbed at the load, while the remaining part of it is reflected back due to the impedance mismatches between antenna and the load. The part of the signal energy that is absorbed by the load is defined as the antenna-mode absorption. The reflected signal due to impedance mismatch travels back to the antenna and is re-radiated into space. This part of the re-radiated signal is defined as the antenna-mode scattering [91].

### **5.1.3 Properties of Antenna Backscattering**

Structural-mode scattering is an inherent property of an antenna and is independent of the load presented to the antenna. It is because the structural-mode scattering takes place at the surface structure of the antenna, before the signal comes across the load, that the structural-mode scattering is not affected by the load conditions. Antenna-mode scattering takes place at the terminating load. Thus, antenna-mode scattering depends on the type of the load, and both the amplitude and phase of the antenna-mode scattered signal can be controlled by correctly choosing the impedance of the load. Moreover, if a pulse signal is transmitted to an antenna, two pulses will be scattered back due to the two scattering properties of the antenna. The relative time domain position of the pulses scattered due to structural-mode scattering and antenna-mode scattering can be controlled by introducing transmission delay lines in between the

antenna and the load. Additionally, the phase of the antenna mode scattered signal depends on the load which is used to convey sensor information in the sensor tag design.

## 5.2 RCS Parameters of Antenna

The scattering property of an antenna is measured in terms of the radar cross section (RCS) which gives a measure of the ratio of power backscattered to the power transmitted [56]. The RCS of an antenna is represented by  $\sigma$  and defined as the ratio of scattered power by the antenna to the incident power density, as given in Equation (5.1), [91].

$$\sigma = \frac{P_s}{S_i}, \quad (5.1)$$

where,  $P_s$  is the scattered power by the antenna and  $S_i$  is the incident power density. The incident power density at the tag antenna can be written in terms of transmitted power ( $P_t$ ), the gain of transmitting antenna ( $G_r$ ), and the distance of the tag antenna ( $r$ ) as

$$S_i = \frac{P_t G_r}{4\pi r^2}. \quad (5.2)$$

Using Equations (5.1) and (5.2), the received signal at the reader can be expressed in terms of the RCS of the tag antenna as

$$P_r = \frac{P_t G_r^2 \lambda^2}{(4\pi)^3 r^4} \times \sigma. \quad (5.3)$$

Equation (5.3) shows that the received backscattered power is directly proportional to the RCS of the tag antenna. Generally, the overall RCS of the antenna, as given by Equation (5.3), is used for measurement and analysis. However, in some applications, such as RFID sensor tags, a deeper look into the RCS of the antenna is required. The RCS defined in Equation (5.1) can be further divided into three separate

RCS parameters acknowledged to be the power scattered due to structural-mode scattering and antenna-mode scattering, and the relative phase angle between the two scattering phenomena. The RCS related to structural-mode scattering is called structural-mode RCS, denoted by  $\sigma_s$ , and the RCS related to antenna-mode scattering is called antenna-mode RCS and it is denoted by  $\sigma_a$ .

### **5.3 Measurement of RCS Parameters of Antenna**

The RCS of an antenna is usually measured with the aid of Equation (5.3) where measured transmitted power and the received backscattered power are substituted to get the RCS value. Due to the dependence of antenna-mode RCS on load, the overall RCS of the antenna depends on the load presented to the antenna. Usually the RCS for short, open, and matched loads are measured to characterize RFID tag antennas. However, there have been some efforts to measure load independent RCS of an antenna as structural-mode RCS and antenna-mode RCS.

#### **5.3.1 Conventional RCS Measurement Methods and Challenges**

Conventionally, RCS measurements of the antenna were considered for the analysis of antenna properties, such as gain. The more recent analysis and measurement of RCS parameters of antennas has been motivated for application to backscatter based communication technologies, such as RFID systems. However, the previously reported work on antenna scattering properties for backscattering system applications determined the RCS parameters for different loading conditions using conventional RCS relationships, such as shown in Equation (5.3). Various measurement methods for RCS as separate parameters have been reported. For the transmission line analogy method, the

data for standing wave pattern formed by forward traveling waves and backscattered waves are used to extract the scattering properties of the antenna [56]. In other methods and similar variants, RCS parameters are measured for different positions of the short in a transmission line connected to the antenna. The maximum and minimum measured RCS values are used to find the antenna mode and structural mode RCS [58, 59]. Also, the measurement setups for most of the reported methods employ bulky horn antennas, which are usually not suited for lower UHF range measurements, such as at 915 MHz. In another variation, the gain pattern of the antenna is used to find the antenna mode RCS [68]. However, the gain is measured using relative measurement methods and is also limited to antenna mode RCS measurement. A technique to measure RCS for different antenna loads is reported in [65] using RCS equations from [63]. This method measures the two RCS for specific loads but not as independent RCS properties of the antenna.

### **5.3.2 Need for a New RCS Measurement Method**

It should be noted that in a backscatter communication system, such as RFID, the received signal is the superposition of scattered signals by the antenna and the leakage signal. In addition, the superposition of the scattered signal with the leakage signal can be anywhere from in-phase to out-of-phase, depending on the scattering antenna distance from the transmitting antenna, the load, and the wavelength of the signal used [92, 93]. Due to the interference of the scattered signal with the leakage signal, the received signal, as a function of antenna distance, forms a standing wave-like pattern. Thus, the representation of the received power at any scattering antenna distance (as given by Equation (5.3)) should also include the leakage signal and its interference with the scattered signal. However, most of the methods that have been reported represent the

received signal as the only scattered signal from the antenna. Consequently, to suppress the leakage signal, these methods require complex measurement setups using horn antennas and large anechoic chambers [91, 93].

Moreover, the previous works do not consider measuring individual parameters of RCS in the form of structural-mode RCS, antenna-mode RCS, and the relative phase. For antennas used in backscatter communication systems, it is of great importance that individual scattering parameters, including the relative phase, be determined for designing more efficient tags and reader systems.

#### **5.4 A New Method to Measure RCS Parameters of Antennas**

A new method to measure radar cross section (RCS) parameters of antennas is discussed in this section. This method relies on an equation derived for the received signal power, which is represented as the superposition of structural-mode scattered, antenna-mode scattered, and leakage signals. The method also measures relative phase and provides the effect of the load connected to the antenna. The received signal power equation is solved using minimum mean square error estimation, and the solution is used to obtain structural-mode RCS, antenna-mode RCS, and relative phase of an antenna by applying short, open, and match load cases. A measurement example of RCS parameters of a microstrip patch antenna using a simple experimental setup is discussed. The present method requires less lengthy experimental measurements, while providing results that are more informative and accurate as compared to that obtained from previous methods.

##### **5.4.1 Theory**

For a system consisting of a transmitting antenna, a microstrip patch antenna in the far field region as a scattering object (hereafter called a scattering antenna), and a

transmitting/receiving antenna, all placed in an anechoic chamber, the received signal consists of superposition of three major signal components. The first component is the signal scattered by the scattering antenna; the second component is the leakage signal (direct signal from the transmitting antenna in bistatic measurement configuration or the signal due to the return loss of the transmitting antenna in a monostatic configuration), and the third component is the signal reflected from the walls of the anechoic chamber [58, 68, 92, 93]. As the strength of the reflected signal from the walls of the anechoic chamber is negligible compared to the scattered signal and leakage signal [92, 93], it is considered that the leakage signal is the only source of received non-scattered signal. The scattered signal from the scattering antenna consists of two parts, namely, structural-mode scattered signal and antenna-mode scattered signal. The structural-mode scattering is defined as the energy scattered by an antenna when it is terminated to a matched load, and the antenna-mode scattering is defined as the energy scattered by the antenna solely due to the impedance mismatch between antenna and the load connected to it [57, 58, 66, 68, 91].

The RCS parameters of the scattering antenna can be extracted by analyzing the received signal at the receiver end, as observed at the receiver load, with the knowledge of the transmitted signal. It is assumed that the transmitter transmits a continuous sinusoidal signal, the received signal is the superposition of scattered signals and the leakage signal, the anechoic chamber is perfect, and no other form of signal source is present in the system. It is also assumed that the structural-mode scattering and antenna mode scattering are independent [58, 66]. Let,  $v_s$ ,  $v_a$  and  $v_l$  represent the received instantaneous time dependant structural-mode scattered signal, antenna mode scattered

signal, and leakage signal, respectively. By taking the transmitting instance at the transmitting antenna as the reference, the leakage signal ( $v_l$ ) is considered to be delayed by an angle  $\alpha$  with respect to the reference. The relative phase ( $\phi$ ) between the structural-mode scattered signal and antenna-mode scattered signal is  $\phi = \phi_0 + \phi_a$ , where  $\phi_0$  is the constant initial phase, and  $\phi_a$  is the load dependant phase. If the scattering antenna is considered to be located at a distance  $r$  from the transmitting and receiving antenna (hereafter called a transmitting antenna, which implies a transmitting and receiving antenna for a bistatic system and a transmitting/receiving antenna for a monostatic system), then  $v_s$ ,  $v_a$ , and  $v_l$  can be written as

$$v_s = V_{s_{peak}} \sin(\omega t - 2\beta r), \quad (5.4)$$

$$v_a = V_{a_{peak}} \sin(\omega t - 2\beta r - \phi), \quad (5.5)$$

and,

$$v_l = V_{l_{peak}} \sin(\omega t - \alpha), \quad (5.6)$$

where,  $\beta = 2\pi / \lambda$ ,  $V_{s_{peak}}$ ,  $V_{a_{peak}}$ , and  $V_{l_{peak}}$  are the peak values of  $v_s$ ,  $v_a$ , and  $v_l$  respectively, and  $\lambda$  is the wavelength of the signal. In Equation (5.3),  $v_s$  is delayed by  $(2\beta r)$  with respect to the reference, as  $v_s$  travels a distance  $2r$  before arriving at the receiving end. In Equation (5.4),  $v_a$  is delayed by  $\phi$  with respect to  $v_s$ , that results in the total delay of  $(2\beta r + \phi)$  with respect to the reference. As the signals are independent, the total instantaneous received signal ( $v_r$ ) can be written as the sum of  $v_s$ ,  $v_a$ , and  $v_l$  as

$$v_r = V_{s_{peak}} \sin(\omega t - 2\beta r) + V_{a_{peak}} \sin(\omega t - 2\beta r - \phi) + V_{l_{peak}} \sin(\omega t - \alpha). \quad (5.7)$$

The root mean square of  $v_r$  [94] can be obtained as



$$V_{rms} = \left[ (1/2\pi) \cdot \int_0^{2\pi} v_r^2 d\omega t \right]^{\frac{1}{2}}. \quad (5.8)$$

Substituting  $v_r$  from Equations (5.7) in (5.8) and solving we get Equation (5.9).

$$\begin{aligned} V_{rms}^2 = (1/2) \cdot & \left( V_{s_{peak}}^2 + V_{a_{peak}}^2 + V_{l_{peak}}^2 \right. \\ & + 2V_{s_{peak}} V_{a_{peak}} \cos \phi \\ & + 2V_{s_{peak}} V_{l_{peak}} \cos(2\beta r - \alpha) \\ & \left. + 2V_{a_{peak}} V_{l_{peak}} \cos(2\beta r + \phi - \alpha) \right) \end{aligned} \quad (5.9)$$

Since,  $V_{rms}^2 = P \times Z$  and  $V_{peak}^2 = 2(P \times Z)$ ,  $P$  and  $Z$  being the power and impedance [94], Equation (5.9) can be written in terms of respective powers as

$$\begin{aligned} P_r = P_s + P_a + P_l + 2\sqrt{P_s P_a} \cos \phi \\ + 2\sqrt{P_s P_l} \cos(2\beta r - \alpha) \quad , \\ + 2\sqrt{P_a P_l} \cos(2\beta r + \phi - \alpha) \end{aligned} \quad (5.10)$$

where  $P_r$ ,  $P_s$ ,  $P_a$ , and  $P_l$  represent total received signal power, structural-mode scattered signal power, antenna-mode scattered signal power, and leakage signal power, respectively. The individual received signal powers can be defined in terms of transmitted power  $P_t$ , distance of the scattering antenna from the transmitting antenna  $r$ , structural-mode RCS  $\sigma_s$ , and antenna-mode RCS  $\sigma_a$ , as shown in Equations (5.11) and (5.12), [58, 64, 68, 91].

$$P_s = P_t \frac{G_t G_r \lambda^2}{(4\pi)^3 r^4} \sigma_s \quad (5.11)$$

$$P_a = P_t \frac{G_t G_r \lambda^2}{(4\pi)^3 r^4} \sigma_a \tau_a^2 \quad (5.12)$$

where  $G_t$  and  $G_r$  are transmitting and receiving antenna gains, respectively, and  $\tau_a$  is the antenna and load impedance mismatch reflection coefficient of the scattering antenna [58]. If  $Z_a$  and  $Z_L$  represent the antenna and load impedances,  $\tau_a$  and  $\phi_a$  are given as

$$\tau_a = \left| \frac{Z_a - Z_L}{Z_a + Z_L} \right| \text{ and } \phi_a = \angle \left( \frac{Z_a - Z_L}{Z_a + Z_L} \right). \quad (5.13)$$

Substitution of Equations (5.11) and (5.12) in Equation (5.10) gives

$$\begin{aligned} \frac{P_r}{P_t} = & \Gamma^2 + \frac{k^2}{r^4} \left( \sigma_s + \tau_a^2 \sigma_a + 2\tau_a \sqrt{\sigma_s \sigma_a} \cos \phi \right) \\ & + \frac{2k\Gamma}{r^2} \left( \sqrt{\sigma_s} \cos(2\beta r - \alpha) \right. \\ & \left. + \tau_a \sqrt{\sigma_a} \cos(2\beta r + \phi - \alpha) \right) \end{aligned} \quad (5.14)$$

where,

$$\Gamma^2 = P_l / P_t \text{ and } k^2 = \frac{G_t G_r \lambda^2}{(4\pi)^3}. \quad (5.15)$$

Equation (5.14) represents the total received power as the superposition of the scattered signal and leakage signal. For an antenna of known RCS parameters, Equation (5.14) gives the received scattered signal power as a function of the load connected to the antenna and its distance from the transmitting antenna. For ideal measurement conditions, the received signal does not contain any leakage signal component and, thus, the received power consists of only the scattered signals from the antenna under measurement. In such a case, the terms containing the leakage signal component  $\Gamma$  in Equation (5.14) vanish, resulting in the relation shown in Equation (5.16).

$$\frac{P_b}{P_t} = \frac{k^2}{r^4} \left( \sigma_s + \tau_a^2 \sigma_a + 2\tau_a \sqrt{\sigma_s \sigma_a} \cos \phi \right). \quad (5.16)$$

Equation (5.16) also represents the actual backscattered signal part ( $P_b$ ) in Equation (5.14). Using Equation (5.16) the total RCS ( $\sigma_T$ ) of the antenna can be written as

$$\sigma_T = \left( \sigma_s + \tau_a^2 \sigma_a + 2\tau_a \sqrt{\sigma_s \sigma_a} \cos \phi \right). \quad (5.17)$$

Equation (5.17) gives the total RCS of an antenna in terms of the structural-mode RCS, antenna-mode RCS, load, and relative phase.

#### **5.4.2 Determination of RCS Parameters using Minimum Mean Square Error Estimation**

In this section, Equation (5.14) is solved using minimum mean square error estimation (also called least squares estimation), and the solution is used to obtain the RCS parameters of an antenna by applying short, open, and match load cases. Using the derived RCS solutions, a measurement example of the RCS parameters of a microstrip patch antenna is demonstrated. Equation (5.14) can be divided into three different parts. The first part contains only  $\Gamma$  (leakage signal), and is independent of  $\tau_a$  (antenna load) and  $r$  (antenna distance). The second part varies only with  $\tau_a$  and  $r$ , and is independent of  $\Gamma$ . The third part contains all three components,  $\tau_a$ ,  $r$ , and  $\Gamma$ , and is responsible for the oscillation in the received signal as a function of antenna distance.  $\Gamma$  is independent of the antenna load and antenna distance. Thus, the first part of Equation (5.14) is constant for a given measurement system. Many signal cancellation techniques for keeping leakage signal ( $\Gamma$ ) minimum and determining RCS parameters from the measured received signal data have been reported [69, 92, 93]. However, a signal cancellation method can effectively cancel the first part of the equation, but cannot cancel out the third part which varies with load ( $\tau_a$ ) as well as antenna distance ( $r$ ). Therefore, RCS parameters

determined without considering the superposition of scattered signal with leakage signal tend to include errors associated with the third part of Equation (5.14), if the first part is accurately eliminated. In this section, a more accurate method to determine the RCS parameters of an antenna that accounts for the superposition of scattered signals with leakage signals is presented.

Expanding the sine and cosine terms in Equation (5.14) and rearranging the like terms gives

$$\frac{P_r}{P_t} = a_0 + \frac{1}{r^4} x_1 + \frac{\cos(2\beta r)}{r^2} x_2 + \frac{\sin(2\beta r)}{r^2} x_3 \quad (5.18)$$

where,

$$a_0 = \Gamma^2, \quad (5.19)$$

$$x_1 = k^2 \left( \sigma_s + \tau_a^2 \sigma_a + 2\tau_a \sqrt{\sigma_s \sigma_a} \cos \phi \right), \quad (5.20)$$

$$x_2 = 2k\Gamma \left( \sqrt{\sigma_s} \cos \alpha + \tau_a \sqrt{\sigma_a} \cos(\alpha - \phi) \right), \quad (5.21)$$

and,

$$x_3 = 2k\Gamma \left( \sqrt{\sigma_s} \sin \alpha + \tau_a \sqrt{\sigma_a} \sin(\alpha - \phi) \right). \quad (5.22)$$

If  $d_i$  are measured data for  $(P_r/P_t)_i$  with measurement (observation) error  $e_i$ , Equation (5.18) can be written in terms of  $d_i$  and  $e_i$  in the form of a regression as

$$d = a_0 + \frac{1}{r^4} x_1 + \frac{\cos(2\beta r)}{r^2} x_2 + \frac{\sin(2\beta r)}{r^2} x_3 + e, \quad (5.23)$$

where the dependent variable  $d$  is referred to as response, the independent variables  $x_1$ ,  $x_2$ , and  $x_3$ , are called predictors, and the difference between predicted response  $(P_r/P_t)_i$  and observed response  $d_i$ , denoted by  $e_i$ , is called residue. The model has three predictor

variables  $x_1, x_2$ , and  $x_3$  ( $p = 3$ ), [95, 97]. For a set of  $n$  measured data  $\underline{d}$  ( $d_1, d_2, \dots, d_n$ ) at  $n$  distances  $\underline{r}$  ( $r_1, r_2, \dots, r_n$ ), Equation (5.23) can be written as a system of equations as

$$\begin{pmatrix} d_1 \\ \vdots \\ d_n \end{pmatrix} = \begin{pmatrix} a_{01} \\ \vdots \\ a_{0n} \end{pmatrix} + \begin{pmatrix} \frac{1}{r_1^4} & \frac{\cos(2\beta r_1)}{r_1^2} & \frac{\sin(2\beta r_1)}{r_1^2} \\ \vdots & \vdots & \vdots \\ \frac{1}{r_n^4} & \frac{\cos(2\beta r_n)}{r_n^2} & \frac{\sin(2\beta r_n)}{r_n^2} \end{pmatrix} \times \begin{pmatrix} x_1 \\ x_2 \\ x_3 \end{pmatrix} + \begin{pmatrix} e_1 \\ \vdots \\ e_n \end{pmatrix}. \quad (5.24)$$

Equation (5.24) can be written in matrix form as

$$\underline{E} = (\underline{d} - \underline{a}_0) - \underline{A}\underline{X} \quad (5.25)$$

where,

$$\underline{E} = \begin{pmatrix} e_1 \\ \vdots \\ e_n \end{pmatrix}, \underline{a}_0 = \begin{pmatrix} a_{01} \\ \vdots \\ a_{0n} \end{pmatrix}, \text{ and } \underline{A} = \begin{pmatrix} \frac{1}{r_1^4} & \frac{\cos(2\beta r_1)}{r_1^2} & \frac{\sin(2\beta r_1)}{r_1^2} \\ \vdots & \vdots & \vdots \\ \frac{1}{r_n^4} & \frac{\cos(2\beta r_n)}{r_n^2} & \frac{\sin(2\beta r_n)}{r_n^2} \end{pmatrix}. \quad (5.26)$$

In Equation (5.25),  $\underline{A}$ ,  $\underline{E}$ , and  $\underline{X}$  denote the coefficient vector, residual vector, and design matrix, respectively. The sum of square error (squared residual),  $\xi$ , in Equation (5.24) can be written as [93, 94]

$$\xi = e_1^2 + e_2^2 + \dots + e_n^2 = \underline{E}^T \underline{E} \quad (5.27)$$

Substituting Equation (5.25) into (5.27) gives Equation (5.28).

$$\begin{aligned} \xi &= \underline{E}^T \underline{E} = (\underline{d} - \underline{a}_0)^T (\underline{d} - \underline{a}_0) - \underline{X}^T \underline{A}^T (\underline{d} - \underline{a}_0) \\ &\quad - (\underline{d} - \underline{a}_0)^T \underline{A} \underline{X} + \underline{X}^T (\underline{A}^T \underline{A}) \underline{X} \end{aligned} \quad (5.28)$$

A minimum mean square error estimate of  $\underline{X}$  is obtained by applying minimum mean square error condition,  $\frac{\partial \xi}{\partial \underline{X}} = 0$  to Equation (5.28), [95, 96].

$$\frac{\partial \xi}{\partial \underline{X}} = [\underline{A}^T (\underline{d} - \underline{a}_0)]^T - (\underline{d} - \underline{a}_0)^T \underline{A} + 2 \underline{X}^T (\underline{A}^T \underline{A}) = 0 \quad (5.29)$$

Which gives,

$$\underline{X}^T (A^T A) = (\underline{d} - \underline{a}_0)^T A \quad (5.30)$$

Transposing Equation (5.30) and rearranging like terms gives

$$\underline{X} = (A^T A)^{-1} A^T (\underline{d} - \underline{a}_0). \quad (5.31)$$

Equation (5.31) is called the normal equation, which is solved to find the minimum mean square error estimates. Using measured data (observed responses)  $\underline{d}_{short}$ ,  $\underline{d}_{open}$ , and  $\underline{d}_{match}$ , at distances  $\underline{r}$ , the  $\underline{X}_{short}$ ,  $\underline{X}_{open}$ , and  $\underline{X}_{match}$  (predictors), respectively are determined using Equation (5.31). Substituting the short load ( $Z_L = 0$ ,  $\tau_a = 1$ ,  $\phi_a = 0$ ,  $\phi = \phi_0$ ), open load ( $Z_L = \infty$ ,  $\tau_a = 1$ ,  $\phi_a = \pi$ ,  $\phi = (\phi_0 + \pi)$ ), and match load ( $Z_L = Z_{av}$ ,  $\tau_a = 0$ ,  $\phi_a = 0$ ,  $\phi = \phi_0$ ) cases into Equation (5.20), we get Equations (5.32), (5.33), and (5.34), respectively.

$$x_{1short} = k^2 (\sigma_s + \sigma_a + 2\sqrt{\sigma_s \sigma_a} \cos \phi_0) \quad (5.32)$$

$$x_{1open} = k^2 (\sigma_s + \sigma_a - 2\sqrt{\sigma_s \sigma_a} \cos \phi_0) \quad (5.33)$$

$$x_{1match} = k^2 (\sigma_s) \quad (5.34)$$

Equations (5.31-5.34) can be solved by substitution and elimination techniques to obtain the RCS parameters of the antenna ( $\sigma_s$ ,  $\sigma_a$ ,  $\phi_0$ ) as shown in Equations (5.35-5.37).

$$\sigma_s = \frac{x_{1match}}{k^2} \quad (5.35)$$

$$\sigma_a = \frac{x_{1short} + x_{1open}}{2k^2} - \sigma_s, \text{ and} \quad (5.36)$$

$$\cos \phi_0 = \frac{x_{1short} - x_{1open}}{4k^2 \sqrt{\sigma_s \sigma_a}} \quad (5.37)$$

Equations (5.31) and Equations (5.35-5.37) give the solution for the RCS parameters of an antenna in terms of the observed responses  $\underline{d}$ .

As the return loss of an antenna can be measured easily with a network analyzer, it is used as the approximation of the observed ratio of received power over transmitted power and, thus, as the approximation for a measured response  $d_i$ , as shown in Equation (5.38), [69].

$$d_i \approx |S_{11}|_i^2 \quad (5.38)$$

### **5.4.3 Measurement Setup**

A measurement example of RCS parameters of a microstrip patch antenna is demonstrated using the relation shown in Equation (5.38). Figure 5.1 highlights a simple experimental setup consisting of a network analyzer (Agilent 4396B), an anechoic chamber (chamber dimensions: 1.8 m  $\times$  0.72 m  $\times$  0.9 m, absorbing material: C-RAM SFC-8, reflectivity at 1 GHz:  $-30$  dB, manufacturer: Cuming Microwave), and a transmitting antenna, used to measure return losses of a transmitting antenna in the presence of a loaded scattering antenna. Circular disc monopole antennas fabricated on a PCB substrate (substrate: FR4, permittivity: 4.7, substrate height: 0.15 cm, circular patch diameter radius: 5.4 cm, feed width: 0.37 cm, ground-plane dimensions: 13.54 cm  $\times$  5.38 cm) are used as the transmitting and scattering antennas. The antennas are placed at the same elevation and face to face with each other (zero azimuth angle). During the calibration, a transmitting antenna is used as the load to keep the effect of the leakage signal small [69].

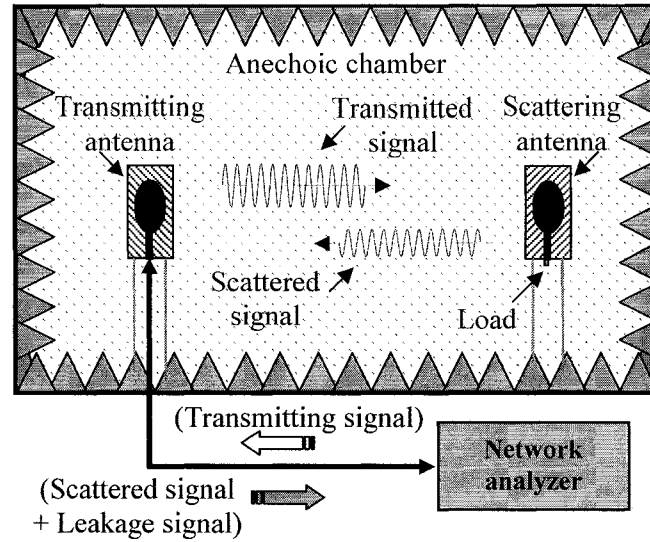


Figure 5.1 Experimental setup for measuring the return loss of the transmitting antenna at 912 MHz in the presence of a scattering antenna with various loads.

The scattering antenna is placed at different distances in the far field region (minimum separation 16 cm [99]) and the return losses of the transmitting antenna is measured at 912 MHz (the resonating frequency of the scattering antenna) for a short load ( $|S_{11short}|$ ), open load ( $|S_{11open}|$ ), and match load ( $|S_{11match}|$ ). The data  $d_{1short}$  corresponds to the return loss  $|S_{11short}|$  measured at distance  $r_1$ . Similarly, data  $d_{1open}$ ,  $d_{1match}$ ,  $d_{2short}$ , ... are related to the respective measured return losses for various cases of loads and distances in the same fashion. The return loss measured without the scattering antenna present in the chamber gives the leakage signal ( $I$ ).

#### 5.4.4 Results and Discussions

Using the measured data (observed responses)  $d_{short}$ ,  $d_{open}$ , and  $d_{match}$  at distance  $r$ , the predictor variables,  $X_{short}$ ,  $X_{open}$ , and  $X_{match}$  are calculated from Equation (5.31). The calculated values are then substituted in Equations (5.35-5.37) to obtain the scattering parameters of the antenna ( $\sigma_s$ ,  $\sigma_a$ , and  $\cos\phi$ ). Result A in Table 5.1 shows the RCS



parameters obtained using the experimental setup shown in Figure 5.1. The minimum mean square error ( $\zeta$ ) is obtained using Equations (5.28, 5.31), and observed responses ( $d$ ).  $\zeta$  gives the standard deviation in the observed response which is used to get the standard deviations of the RCS parameters using Equation (5.31) and Equations (5.35-5.37). The obtained standard deviations of the parameters are shown in parentheses for Result A in Table 5.1. In addition, Result B in Table 5.1 shows the antenna-mode RCS and structural-mode RCS obtained using the method described in [58, 59]. The total RCS of the antenna is measured for different positions of a short along a transmission line connected to the antenna, and the maximum and minimum values are used to calculate antenna-mode RCS and structural-mode RCS. The results shown in B, Table 5.1, are obtained by taking measurements for twenty different positions of the short. The accuracy of the results obtained in this method depends on the accuracy of the measured maximum and minimum RCS, which in turn depends on the step size taken while sliding the short along the transmission line. It can be noted that the Results A and B compare closely with each other. Moreover, Result A also includes the relative phase of an antenna which is not the case for Result B.

Table 5.1 Measured RCS Parameters Obtained using Method Presented in this Paper (A) Shown with the Results Obtained using Method Similar to that Described in [56] and [57] (B). Also using the Standard Deviations Shown in Result A,  $\sigma_s \pm 2\Delta\sigma_s = (-18.129, -18.493)$  and  $\sigma_s$ .

<i>Result</i>	<i>Structural-mode RCS (<math>\sigma_s</math>) (dBsm)</i>	<i>Antenna-mode RCS (<math>\sigma_a</math>) (dBsm)</i>	$\cos\phi_0$
A.	-18.307 ( $\Delta\sigma_s = 2.1\%$ )	-20.386 ( $\Delta\sigma_a = 6.4\%$ )	0.970 ( $\Delta\cos\phi_0 = 6.8\%$ )
B.	-18.114	-19.99	-

In some of the other RCS measurement techniques as in [65], an idealistic case where no leakage signal is present is usually considered. The RCS values are determined from the data measured at only one distance. These techniques do not give RCS parameters as properties of the antenna. Rather, they determine either total RCS or structural-mode RCS and antenna mode RCS in terms of different loads to the antenna. However, the equations used are similar to Equation (5.16), where leakage signals and measurement (observation) errors are considered to be null. Due to the similarity between principal equations used in other common techniques and Equation (5.16), the variation in the results obtained with Equation (5.16) at different antenna distances are highlighted in Table 5.2. The variation of results obtained at different measurement distances show that the determined RCS values are influenced by leakage signals and measurement errors.

Table 5.2 RCS Parameters Obtained Considering Idealistic Measurement Conditions.

<i>Antenna distance (cm)</i>	<i>Structural-mode RCS (<math>\sigma_s</math>) (dBsm)</i>	<i>Antenna-mode RCS (<math>\sigma_a</math>) (dBsm)</i>	<i><math>\cos(\phi_0)</math></i>
30.48	-19.184	-21.281	0.958
40.64	-17.308	-19.527	0.979
52.01	-16.553	-19.160	0.952

#### **5.4.5 Comparison with Previous Measurement Methods**

The method discussed uses Equation (5.14) derived for the backscattered signal that takes into account leakage signals and observation errors, which are not considered in previously reported measurement methods. The inclusion of the interference due to leakage signal and observation errors into the regression model used to solve the derived equation makes the new RCS measurement method more tolerant to the presence of a leakage signal in the measurement setup and observation errors. Thus, with the current method, observations made in a practical measurement setup give more accurate results than the previously reported methods. This has been demonstrated in Table 5.1 where results obtained with the new method are compared with the results obtained with a lengthy and rigorous method reported in [58] and [59]. It is observed that the new method gives as accurate a result as the previous methods. In Table 5.2, where the results obtained considering an ideal condition generally used in conventional methods is shown, it is observed that the results vary with the measurement distance, showing the considerable influence of leakage signals and measurement errors on the RCS results. Moreover, unlike most of the previously reported methods, which provide partial

information on RCS parameters relative to the antenna load, the current method provides these parameters independent of antenna load conditions, and it additionally determines the relative phase.

## **5.5 Application of RCS Parameters of Antennas in RFID System Design**

Antenna scattering has been used extensively in many passive communication technologies, radio frequency identification (RFID) being one of the most new and rapidly growing technologies [1]. The scattering properties of an antenna are defined by the RCS parameters. These parameters signify the amount of scattered power relative to the incident power and represent the ability of the antenna to perform backscatter communication [91]. RFID systems work on the principal of controlled backscattering of the interrogation signal by the tags. Thus, the knowledge of complete and accurate information on the scattering parameters of the antenna has a great importance in the design and development of RFID systems.

### **5.5.1 Estimation of Received Backscattered Power using Derived Equation**

The received signal power for a measurement setup that closely compares with a practical backscatter based reader device is shown in Figure 5.2. A continuous 912 MHz signal from the signal generator is fed to an antenna and the reflected signal is received by the same antenna. The forward signal path and the reflected signal path are isolated with the help of a high isolation circulator. The received signal power, without the scattering antenna present in the anechoic chamber, gives a measure of the leakage signal in the system.

With the measured leakage signal ( $I$ ) of the system and RCS parameters of the scattering antenna shown in Table 5.1, the received signal power for various antenna distances and different loads to the antenna can be predicted using Equation (5.14). The predicted results for short load, open load, and match load are compared with the observed results in Figure 5.2. Therefore, the results obtained using Equation (5.14) show the practical scheme of the measurement system where the received signal oscillates as a function of antenna distance (forming a standing wave like pattern) caused by superposition of scattered signals with leakage signal.

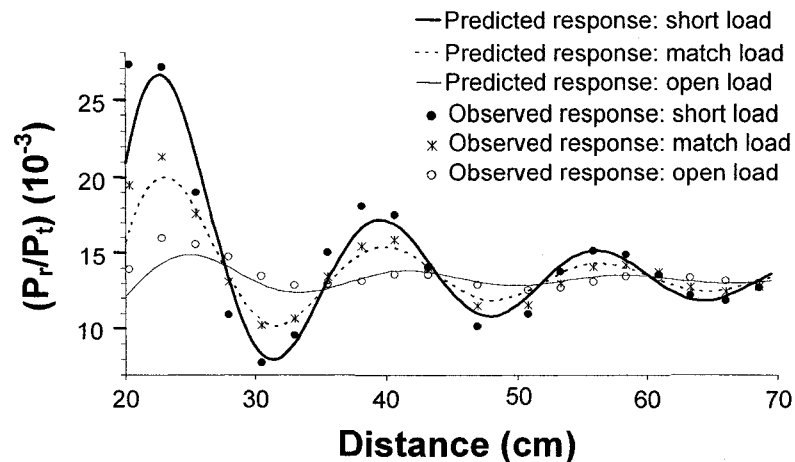


Figure 5.2 Predicted responses ( $P_r/P_t$ ) given by Equation (11) and observed response in a practical reader like experimental setup.

### 5.5.2 Chip-based RFID Systems

In the passive RFID tags, the communication is accomplished by switching the antenna into two different (usually short and match) RCS states. The performance of these devices greatly depends on the antenna properties and on the employed load integration techniques. The availability, from the discussed new method, of more complete information on RCS parameters (load independent) aids in the accurate

prediction of the backscattered signal by an antenna, and is believed to be of great value in the design and development of efficient RFID systems.

### **5.5.3 RFID Reader Design**

The new RCS measurement method provides complete information on RCS properties of a tag antenna. Using Equation (5.14), the received backscattered signal for any tag, in the presence of a leakage signal, can be estimated using Equation (5.14). An estimation and measurement example is discussed in Section 5.5.1, and the result is shown in Figure 5.2. The derived equation shown in Equation (5.14), gives the estimation of received backscattered power as the function of antenna scattering parameters, antenna distance, load, and the leakage signal. The information on received backscattered power aids in the design of RFID reader.

### **5.5.4 Chipless Sensor Tag Design using Scattering Properties of Antenna**

The chipless sensor tags do not contain any memory chip on the tag, and the tag and sensor information are conveyed to the reader through the instantaneous variation in some parameters of the backscattered signal. Changes in antenna resonance frequency with a change in stimulant concentration is reported in [34, 41, 70]. The change in resonance frequency changes the power of the signal scattered by the antenna, which is detected by the reader to detect the change in stimulant concentration. Having complete information on the antenna scattering properties aids in the design of innovative and efficient sensor tags. A new chipless sensor tag design using the relative delay between the structural-mode scattered signal and the antenna-mode scattered signal for ID code generation, and relative phase between the two scattered signals for sensor information extraction, is discussed in Chapter 6.

## CHAPTER 6

### CHIPLESS SENSOR TAGS

Design, fabrication, and testing of passive chipless RFID sensor tags are discussed in this chapter. The sensor tags utilize different antenna scattering modes and their dependence on the load to generate ID code and communicate sensor information. Two configurations of the developed chipless passive RFID sensor tags (conf-I and conf-II) that allow a broad range of sensor types for consideration are presented. The first configuration of the tags (conf-I) consist of a sensor connected as a load to the antenna. The second configuration (conf-II) consists of an antenna, microstrip transmission delay line (ID generation circuit), and a sensor. The tags communicate with the reader using load modulated backscattered communication techniques, at 915 MHz carrier signal. Using a conf-I temperature sensor tag, a demodulated received signal amplitude change of 28% is observed at the reader when the temperature changes from 27 °C to 140 °C at the tag. The presented conf-II tag prototype allows generation of eight different ID codes. The sensor tag experiment with discrete capacitors as the sensor resulted in an average of 26.51° /pF phase change in the antenna-mode scattered signal, when the load capacitance (sensor) of the tag changes between 1 to 5 pF. The experiment with the integrated ethylene sensor resulted in a 33° phase shift in the antenna-mode scattered signal when the ethylene concentration is changed from 0 to 100 ppm.

## **6.1 Sensor Integrated Antenna Tags (Conf-I Sensor Tags)**

A sensor tag configuration (conf-I) consisting of a resistive sensor connected as a load to a microstrip patch antenna is discussed in this section. The sensor tag is based on the fact that the amplitude of the antenna-mode scattered signal depends on the mismatch between the impedances of the antenna and the load connected to it. The theory of operation, design, fabrication methodologies, and experimental results are discussed.

### **6.1.1 Theory**

When an antenna is illuminated with an RF signal, some part of the incident signal is backscattered due to the inherent scattering properties of the antenna. The overall scattering from an antenna can be divided as structural-mode scattering and antenna-mode scattering. Antenna-mode scattering depends on the impedance of the load connected to it. Thus, the received antenna-mode scattered signal at the reader depends on the load connected to the antenna, as given by Equation (5.12). In the case of a sensor tag, with a sensor connected as a load to the antenna, the antenna-mode scattering depends on the mismatch between the antenna impedance ( $Z_a$ ) and the connected sensor load impedance ( $Z_s$ ). Using Equation (5.12), for a given reader system, the antenna mode received scattered power ( $P_a$ ) from a tag at a known distance is directly related to the square of the impedance mismatch factor ( $\tau_a$ ) as

$$P_a \propto \tau_a^2 \quad (6.1)$$

where,

$$\tau_a = \frac{Z_a - Z_s}{Z_a + Z_s} \quad (6.2)$$



For a resistive temperature sensor with a negative temperature coefficient, having impedance  $Z_s$  close to  $Z_a$  at room temperature, and the impedance mismatch factor ( $\tau_a$ ), thus, the power  $P_a$  at room temperature is small. When the temperature at the tag is increased above room temperature, the impedance of the sensor decreases and the scattered power increases. The power of a signal is related to the square of its amplitude and as the received scattered power, as shown by Equations (6.1) and (6.2), is related to the impedance of the sensor, the amplitude of the backscattered signal from the tag gives an account of the change in the sensor impedance, and, thus, the change in temperature at the tag. For the case of a negative temperature coefficient sensor, the increase in temperature at the tag results in an increase in the amplitude of the backscattered signal, while a decrease in temperature results in a decrease in the amplitude. This effectively modulates the sensor signal into the amplitude of the backscattered signal, which is received by the reader and the sensor information is extracted.

### **6.1.2 Design and Fabrication**

A triangular microstrip patch antenna with slotted ground is used for the sensor tag [46]. The sensor is designed in Ansoft Designer [86] and fabricated on Pyralux FR9151 CU CLAD substrate [79] using standard photolithographic techniques (antenna dimensions: 5.54 cm  $\times$  5.34 cm, ground slot dimensions: 6.09 cm  $\times$  5.19 cm, input impedance: 50  $\Omega$ , VSWR: 1.2, radiation pattern: omnidirectional, polarization: linear). A negative temperature coefficient thermistor having 47  $\Omega$  resistance at 25  $^{\circ}\text{C}$  is used as the temperature sensor (manufacturer: EPCOS, part no: B57311V2470J060) which is connected across the feed and the ground plate of the antenna, making the sensor a load to the antenna. The picture of a fabricated sample is shown in Figure 6.1.

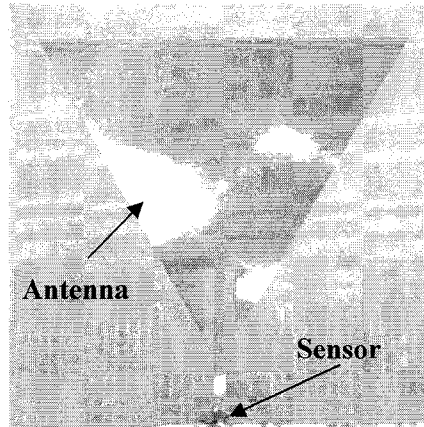


Figure 6.1 A fabricated temperature sensor tag sample (antenna dimensions: 5.54 cm  $\times$  5.34 cm).

### 6.1.3 Experimental Setup

The experimental setup used for the system testing is shown in Figure 6.2. The setup consists of reader system, temperature sensor tag, heating system, digital thermometer, and anechoic chamber. The anechoic chamber is a rectangular wooden box of dimensions: 1.8 m  $\times$  0.72 m  $\times$  0.9 m (length  $\times$  width  $\times$  height) with RF absorbing materials on all six sides (absorbing material: C-RAM SFC-8, reflectivity at 1 GHz:  $-30$  dB, manufacturer: Cuming Microwave). The experiments are performed in the anechoic chamber so as to isolate the experiment from the external noise and reduce the reflections from the walls. The reader antenna and the sensor tag, along with the heating system, are placed inside the anechoic chamber to prevent the influence of an unwanted signal on the experiment. The thermocouple of the thermometer is placed at the same position as the sensor tag in reference to the heating system to measure the temperature at the sensor. The reader system is connected to a switch and accessed from a computer in the network to observe the amplitude of the received backscattered signal.

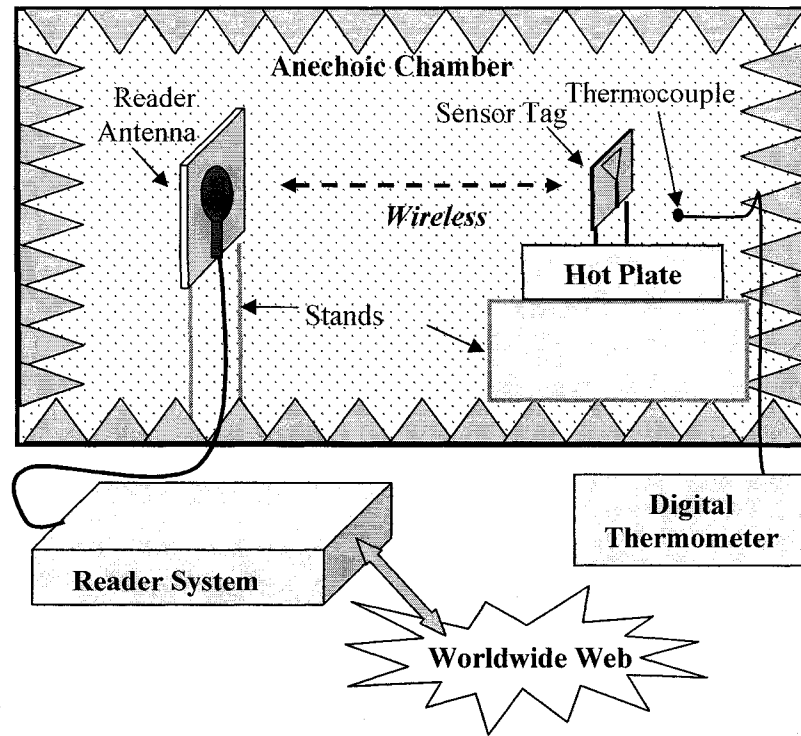


Figure 6.2 Experimental setup for the system testing (anechoic chamber dimensions:  $1.8 \text{ m} \times 0.72 \text{ m} \times 0.9 \text{ m}$ , reflectivity at 1 GHz:  $-30 \text{ dB}$ ).

#### 6.1.4 Results and Discussions

The received backscattered signal amplitude for different temperatures at the tag is measured. The temperature at the tag is measured by using a digital thermometer. Observation at the reader is taken ten minutes after changing the temperature at the heater. The observed variation in the received backscattered signal amplitudes, when the temperature at the tag changes from  $27 \text{ }^\circ\text{C}$  to  $140 \text{ }^\circ\text{C}$ , is shown in Figure 6.3. It is observed that the received backscattered signal amplitude increases linearly with increasing temperature at the tag. The experiment is repeated for the decreasing temperature, and the results are also shown in Figure 6.3. It is observed that the plot for the decreasing temperature follows the same path as the increasing temperature.

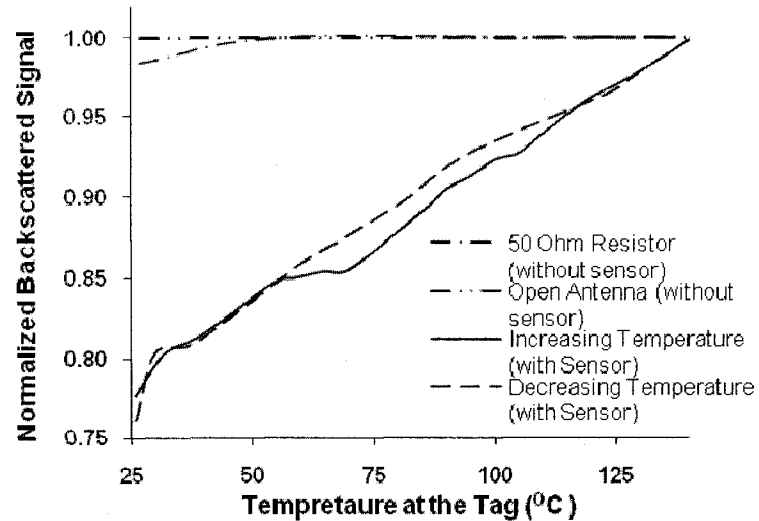


Figure 6.3 Normalized backscattered signal amplitudes observed at the reader measured for various temperatures at the sensor tag (17 °C-140 °C).

Similar experiments are carried out for two different tags without the sensor to verify that the change in the received backscattered signal is only due to the change in the resistance of the sensor and not due to the any changes in the substrate or other parameters. In the first case, the sensor is replaced with a 50  $\Omega$  resistor, and, in the second case, the sensor is removed and the antenna is kept open. For both cases, it is observed that (as also seen in Figure 6.3) the backscattered signal does not change with the change in temperature at the tag.

## **6.2 Antenna Scatterings Based ID Generation and Sensor Information Extraction Scheme**

The reflection and delay in a transmission line was discussed in Chapter 3. The ID generation techniques using reflection and delay in multiple microstrip transmission lines were discussed in Chapter 4. The different parameters of antenna scattering and their measurement were discussed in Chapter 5. In this section the use of the delay and reflection in a transmission line and different scattering modes of an antenna for the

generation of ID code and extraction of sensor information in a chipless sensor tags (for conf-II tags) is discussed. The conf-II tags use a single transmission line to generate PPM represented ID code and utilize phase change in the antenna-mode scattered pulse to detect sensor information.

### **6.2.1 Antenna Scatterings**

When an antenna is illuminated with an RF signal, some part of the signal is scattered back into space which constitutes two parts, the structural-mode scattered signal and the antenna-mode scattered signal. Structural-mode scattering takes place at the surface of the antenna and is not dependent on the load presented to the antenna. On the other hand, the antenna-mode scattering comes from the part of the signal that travels to the load through the antenna feed and is reflected due to the mismatch between the impedances of the antenna and the load presented to the antenna. Thus, the relative delay between the two types of scattering depends on the signal path length the antenna-mode scattering travels before it is re-radiated. The amplitude as well as the phase of the antenna-mode scattering depends on the load presented to the antenna. Also, the relative phase between the two types of scattering is dependent on the load.

### **6.2.2 Relative Time Domain Delay between Structural-Mode and Antenna-Mode Scattered Pulse Signals**

When an antenna is incident by a sinusoidal pulse signal, the scattered signal by the antenna consists of two scattered pulses which stem from the two scattering modes of the antenna. The first pulse originates from the surface of the antenna, due to structural-mode scattering, and the second pulse originates from the signal reflected at the load, due to the antenna-mode scattering. Due to the fact that the antenna-mode scattered pulse is

reflected at the load, it is delayed in the time domain relative to the structural-mode scattered pulse. The relative delay can be increased by adding a long transmission line in-between the antenna feed and the load. The transmission line introduces signal propagation delay in the antenna mode scattered pulse and, thus, increases the delay relative to the structural-mode scattered pulse.

### **6.2.3 ID Code Generation using Relative Time Domain Delay**

As discussed in the Section 6.2.2, the relative time domain delay between the two types of scattered pulses can be increased by introducing a transmission line between the antenna and the load. The relative delay can be precisely controlled, and the scattered pulse signals can be placed at any desired position by properly designing the length of the transmission line. This method is utilized to generate a pulse position modulated (PPM) signal pattern representing a unique ID code. The relative position of the antenna-mode scattered pulse with respect to the structural-mode scattered pulse is varied by varying the transmission line length. The structural-mode scattered pulse is taken as the reference pulse, and the relative delay in antenna-mode scattered pulse is used for the code generation, as illustrated in the schematic diagram shown in Figure 6.4. The first backscattered pulse is due to structural-mode scattering, and the second pulse is due to the antenna-mode scattering. As seen in Figure 6.4, the time axis is divided into eight time slots, each slot representing a bit in the ID code. For example, the presence of the second pulse in the third slot represents the ID code **011**, while the presence of this pulse in seventh time slot represents the ID code **110**. Thus, with eight time slots, eight different combination of bits representing a three bit ID can be generated.

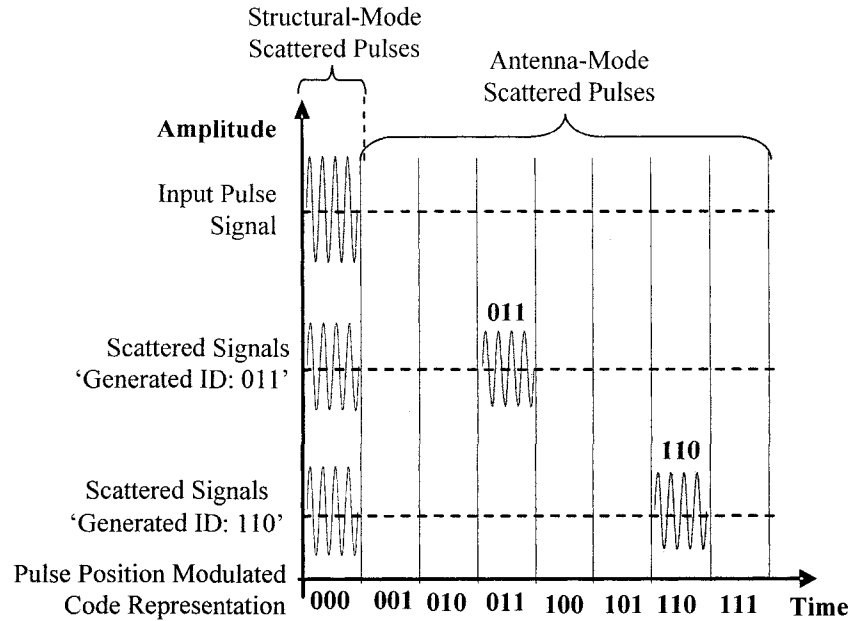


Figure 6.4 Schematic illustration of code generation using structural-mode and antenna-mode scattered pulses.

#### **6.2.4 Relative Phase Difference between Structural-Mode and Antenna-Mode Scattered Pulse Signals**

The structural-mode scattered pulse (first pulse) is independent of the load connected to the antenna, while the amplitude and the phase of the antenna-mode scattered pulse (second pulse) depends on the load impedance. For a given tag with known transmission line and load, the relative phase difference between the two scattered pulses is constant. But, due to the dependence of the antenna-mode scattered signal phase on the load, the relative phase difference changes as the phase of the antenna-mode scattered signal changes with load. Using the structural-mode scattered signal as the reference, for a given tag, the change in the phase in the antenna-mode scattered signal due to the change in load can be measured.

### **6.2.5 Sensor Information** **Extraction using Relative** **Phase Difference**

For a tag consisting of an antenna and a long transmission line (used for code generation) a sensor is connected as a load at the end of the transmission line. The phase of the antenna mode scattered signal depends on the impedances of the transmission line and the sensor as given by

$$\phi_A = \angle \left( \frac{Z_T - Z_S}{Z_T + Z_S} \right), \quad (6.3)$$

where,  $\phi_A$  is the phase of the antenna mode scattered pulse signal due to impedance mismatch,  $Z_T$  is the transmission line impedance, and  $Z_S$  is the sensor impedance. Thus, using the structural mode scattered signal as the reference signal, the change in phase difference between the two scattered pulse signals gives the measure of the change in the sensor impedance.

### **6.3 Sensor Requirements**

The impedance of the sensor can be represented in terms of resistance and reactance as given by

$$Z_s = R_s + jX_s. \quad (6.4)$$

For a transmission line of  $50 \Omega$  impedance, the change in the reactance of the sensor produces more change in the phase of the signal necessary to detect the change in the sensor parameter. Thus, a capacitive sensor has been selected for integration with the tag. It is observed that the change in capacitance between 1 to 5 pF results in a greater change in the phase in the antenna-mode scattered signal [70].



The selected sensor needs to be small in size. The sensor fabrication process is also required to be simple to fabricate on the tag substrate. Due to these requirements, a layer by layer and deep-coating fabrication process has been identified as the suitable process for the sensor tag design.

## **6.4 Freshness Sensor**

A freshness sensor detects the ripening stage of a fruit by detecting the concentration of a particular gas emanated by the fruit at different stages of the ripening. A freshness sensor based on SnO<sub>2</sub> nanoparticles and fabricated with an on-substrate deep-coating technique for integration with the planar chipless tags is discussed in this section.

### **6.4.1 Ethylene Sensor as Freshness Sensor**

Climatic fruits emanate different concentrations of ethylene (C<sub>2</sub>H<sub>4</sub>) gas at the different stages of ripening [70]. The concentration of ethylene emanated by the fruit increases rapidly when fruit is overripe, thus, rapidly increasing the level of ethylene concentration inside an enclosed box of fruit. Thus, an ethylene sensor can be used as a freshness sensor to detect the ripening stages of climatic fruits and also detect the presence of overripe fruit in an enclosed box [70].

### **6.4.2 Tin-dioxide Nanoparticles Based Ethylene Sensor**

Tin dioxide (SnO<sub>2</sub>) is a widely used material for the detection of ethylene gas. Due to the requirements of needing an external heating mechanism and other bulky external activation for bulk SnO<sub>2</sub> based ethylene sensors, they are not applicable for planar chipless RFID sensor tags. A SnO<sub>2</sub> nanoparticles based capacitive ethylene sensor, which does not require any heating or external activation and that can be fabricated on

the tag substrate using the simple fabrication techniques reported in [70], is selected for the chipless sensor tags.

#### **6.4.3 Fabrication of Sensor on the Tag**

The sensor is fabricated on the tag using a dip-coating fabrication technique. The sensor is a parallel plate capacitor where a small copper structure connected to the transmission line is used as the bottom plate. The sensor material is placed as the dielectric material on the top of the bottom plate, and a copper strip is placed on the top which is connected to the ground plane of the tag. The sensor dielectric consists of three layers, an SnO<sub>2</sub> nanoparticles layer, cellulose acetate layer, and a poly diallyl dimethylammonium chloride (PDDA) layer. The schematic of the sensor depicting the different sensor layers is shown in Figure 6.5. The fabrication process and steps are described below [70]:

- The substrate is cleaned with acetone, washed with de-ionized water, and dried with high pressure nitrogen.
- A thin layer of cellulose acetate is fabricated on top of the bottom plate structure of the capacitor. The cellulose acetate layer serves as the insulating layer. The fabrication process includes placing a few drops of the solution on the substrate, draining the substrate, and drying at room temperature in air for five minutes.
- A thin layer of PDDA is fabricated on top of cellulose acetate layer to promote the adhesion of the SnO<sub>2</sub> nanoparticles. The layer is fabricated using the dip-coating technique. The substrate is dried at room temperature in air for five minutes.

- The SnO<sub>2</sub> is the sensing layer of the sensor. A thin SnO<sub>2</sub> layer is fabricated using a solution made by mixing colloidal tin dioxide solution and de-ionized water in equal ratio and using the dip-coating fabrication technique. After the fabrication of the sensor, the substrate is dried at room temperature for five minutes.
- A copper strip is carefully attached on the top of the tin dioxide layer and connected to the ground layer of the tag substrate.

The schematic of the sensor layers is shown in Figure 6.5 and a picture of a fabricated sensor on the tag substrate is shown in Figure 6.6.

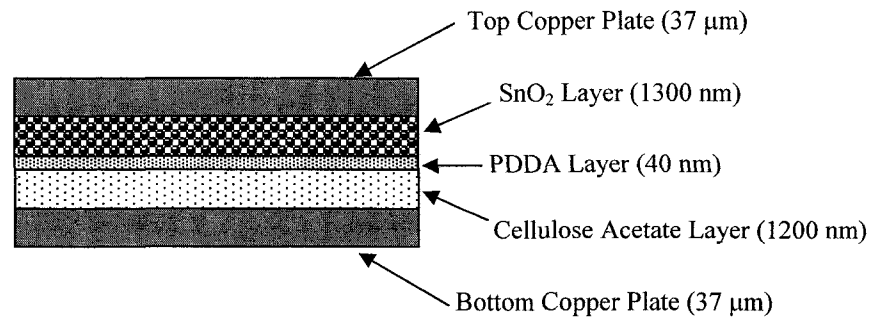


Figure 6.5 Schematic of an ethylene sensor fabricated on the tag.

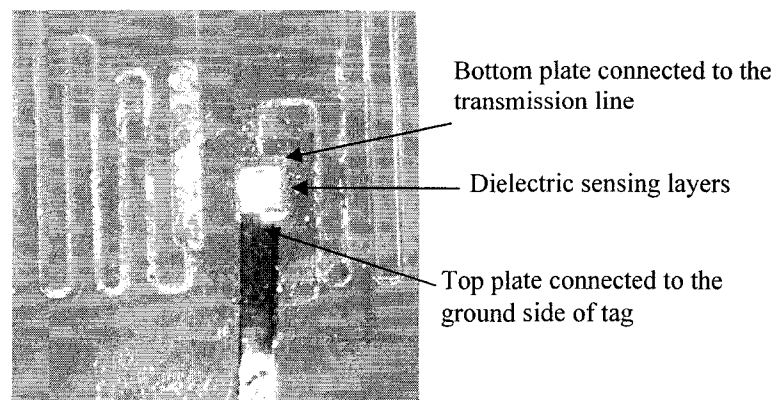


Figure 6.6 A prototype of a fabricated sensor sample on the tag.

#### 6.4.4 Characterization

The capacitance of the fabricated sample is measured on Micromanipulator probe station (serial no. 916776) with two manipulator probes (model 525) and KEITHLEY test system 595 (capacitance-voltage, CV, meter). For the measurement of the capacitance of the ethylene sensor fabricated on a tag, separate sensor samples of same size and structure as of on the tag are fabricated and the capacitances are measured. The results obtained with the test system for two different samples as capacitance on the y-axis and applied voltage from  $-2$  to  $2$  V on the x-axis, are shown in Figure 6.7. The average capacitance for sample 1 is  $4.28$  pF and for sample 2 is  $4.15$  pF.

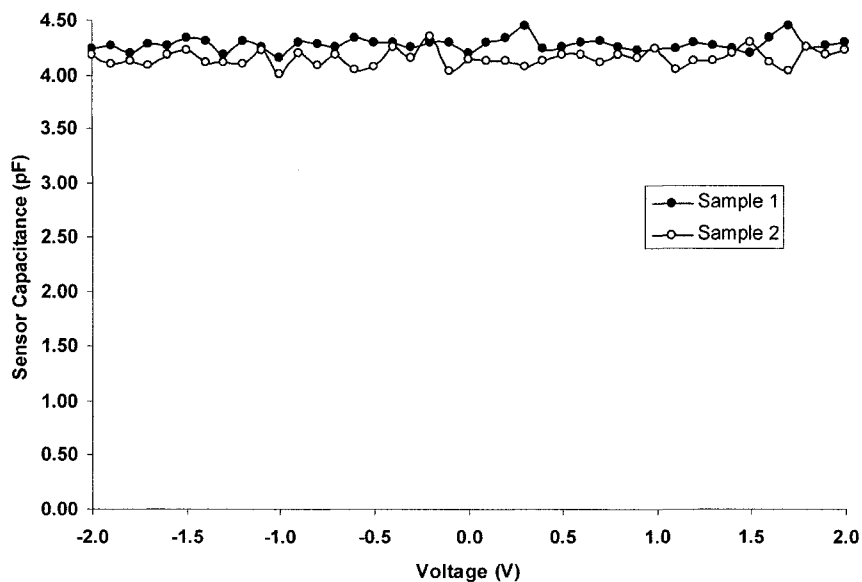


Figure 6.7 Capacitance of two sensor samples measured using KIETHLEY measurement system.

#### 6.5 Design and Simulation of Conf-II Tags

The sensor tag has been designed using a triangular microstrip antenna with slotted ground [46]. A meandered microstrip transmission line that was discussed in Chapter 3 and Chapter 4 is used for the code generation, and the SnO<sub>2</sub> nanoparticles

based ethylene sensor is discussed in Section 6.4. The design and simulation results of the ID code generation and sensor information extraction is discussed in this section.

### **6.5.1 ID Code Generation**

As discussed in the Section 6.2, a transmission line is introduced in between the antenna and the sensor load for the ID code generation. The delay introduced by the transmission line depends on the length of the line and, thus, a specific transmission line length represents a unique code for the tag. The meandered microstrip transmission line designed and tested in Chapter 3 and Chapter 4, is used for the tag design. The ID generation with transmission line represented in PPM is simulated in Ansoft Designer simulation software. The simulated results for the PPM modulated signal pattern generated using two pulses are shown in Figure 6.8, where only five bit positions are shown in eight bit position representation.

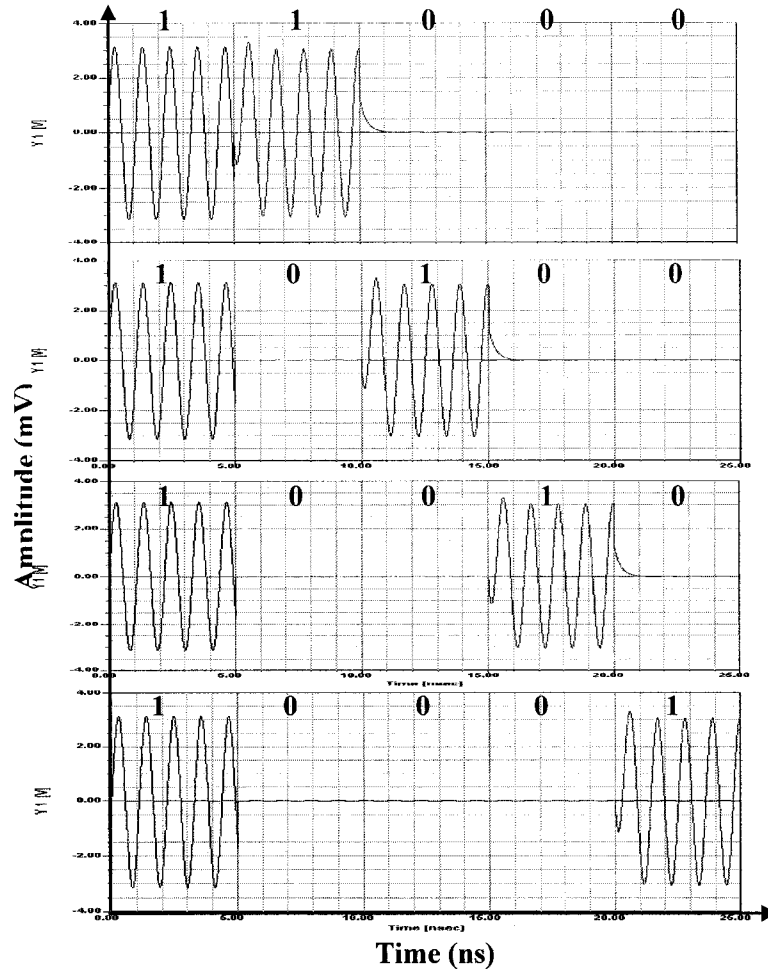


Figure 6.8 PPM represented ID code generation with two pulse signals.

### 6.5.2 Sensor Information Extraction

The sensor tag is designed by placing the capacitive sensor at the end of a transmission line. The sensor is connected across the transmission line and the ground plane. The simulation model of the sensor tag is designed in Ansoft Designer simulation software. The simulation design consists of a transmission line with a variable capacitor placed at the end of the line. A pulse signal is used as the interrogation signal and the phase of the reflected pulse signal is measured for different capacitance values. The shift

in phase of the reflected signal when the capacitance is increased from 2 to 12 pF is shown in Figure 6.9.

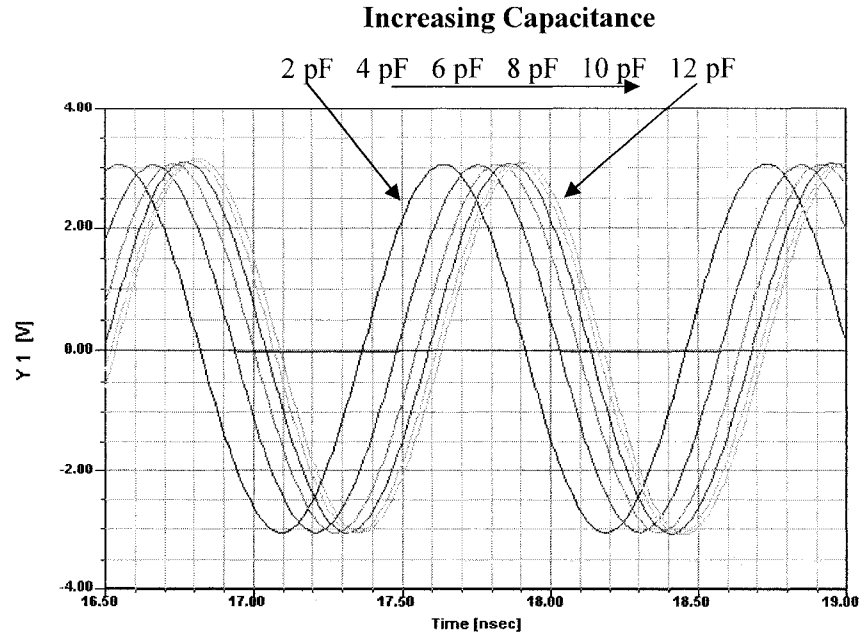


Figure 6.9 Simulated phase shift of the reflected signal due to the change in capacitance of the load.

## 6.6 Fabrication

The sensor tag is designed in Ansoft Designer and the mask is prepared with the help of LinkCad software and printed on a transparent plastic using a mask printer. A simulation of the design of the tag is shown in Figure 6.10. The tag is fabricated on the CUCLAD substrate [79] using a standard photolithographic technique as described in the transmission line fabrication section in Chapter 4. Then, the capacitive ethylene sensor is fabricated on the tag using an SnO<sub>2</sub> nanoparticles solution and the dip-coating fabrication technique, as described under sensor fabrication in Section 6.4. A photograph of a fabricated tag sample is shown in Figure 6.11.

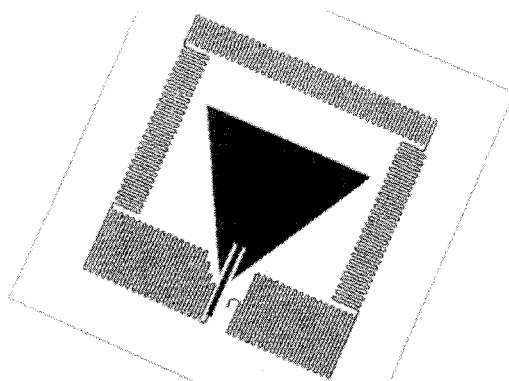


Figure 6.10 Design of sensor tag in Ansoft Designer showing antenna and transmission line ID circuit.

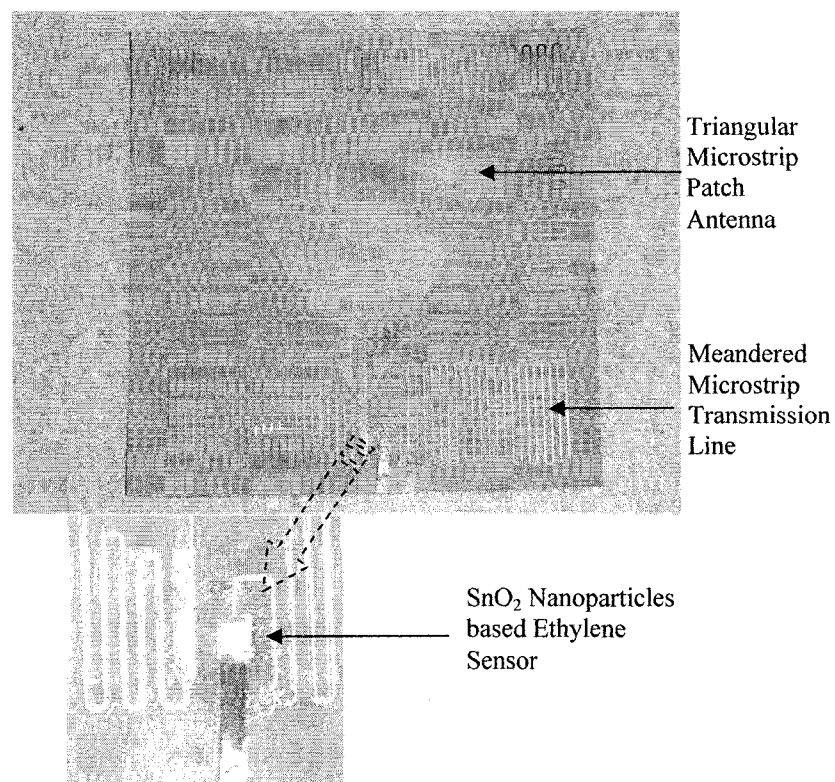


Figure 6.11 A fabricated tag sample showing antenna, transmission line, and sensor.



### 6.7 Measurement Setup

The schematic of measurement setup consisting of reader, reader antenna, oscilloscope, gas chamber, and anechoic chamber is shown in Figure 6.12. The airtight gas chamber contains two pipe connections to facilitate gas flow. The gas chamber is placed inside the anechoic chamber, and the gas inlet pipe is connected to a control knob with two inlets – one connected to an ethylene gas cylinder and the other connected to a dry air source. The outlet is connected to a commercial ethylene sensing instrument, used to measure the concentration of ethylene in the chamber. The reader, oscilloscope, and circulator are connected as shown in Figure 6.12. The sensor tag is placed inside the gas chamber. The reader generates the interrogation signal which is fed to the reader antenna placed inside the anechoic chamber, as shown in Figure 6.12. The oscilloscope is connected to the reader antenna through the circulator.

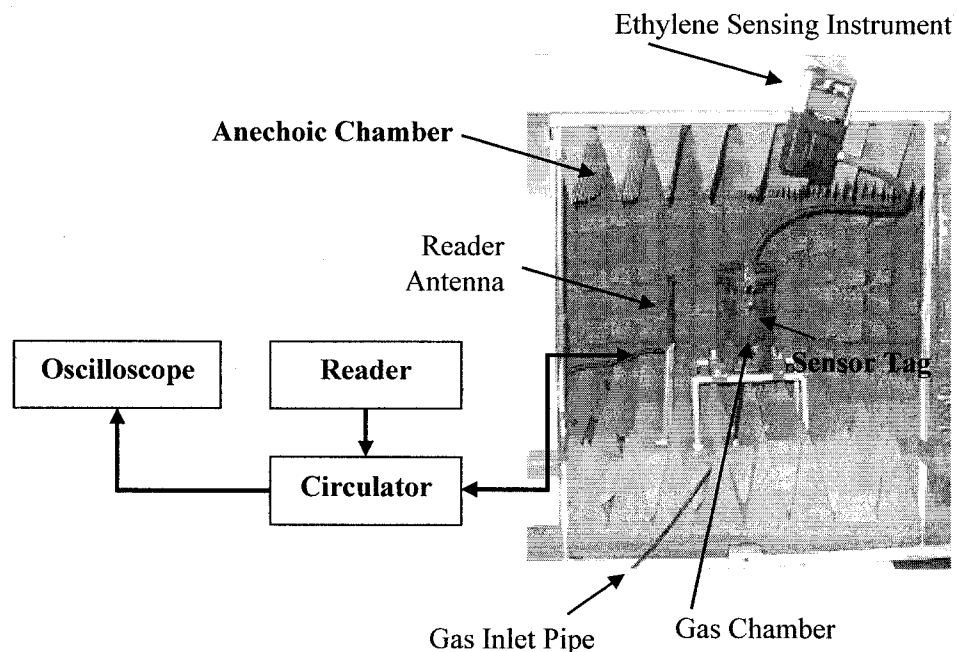


Figure 6.12 Schematic of the sensor tag measurement setup.

## **6.8 Results and Discussions**

A pulsed interrogation signal with a 915 MHz carrier signal is used as the interrogation signal. The pulse signal is generated by the reader which is fed to the reader antenna through the circulator. The antenna transmits the signal to the tag inside the chamber and receives the scattered signal from the tag. The received signal is fed to the oscilloscope for observation through the circulator. The circulator isolates the transmission and reception path of the signal. The received signal is observed and analyzed in the oscilloscope for the generated ID code and the sensor information from the received signal.

### **6.8.1 ID Code Observation**

The experimental results observed with two tags (tag-I and tag-II) showing the generation of ID code **011** and **100** in PPM representation are shown in Figure 6.13, along with the signal observed without the tag present in the chamber. The received signal observed in the absence of the tag represents the leakage signal and the noise present in the system. With tag-I, an additional pulse observed just following the leakage signal is the structural-mode scattered pulse. The second pulse, delayed in time with respect to the structural-mode scattered pulse, is the antenna-mode scattered pulse signal. It is also observed that the structural-mode scattered pulse and the antenna-mode scattered pulse are separated by two pulse positions representing **10010000** binary bits, which is equivalent to ID code **011** in PPM coding. Similarly, two pulses due to structural-mode scattering and antenna-mode scattering are observed with tag-II. In this case, the two pulses are separated by three pulse positions representing **10001000** binary bits, which is equivalent to ID code **100** in PPM coding.

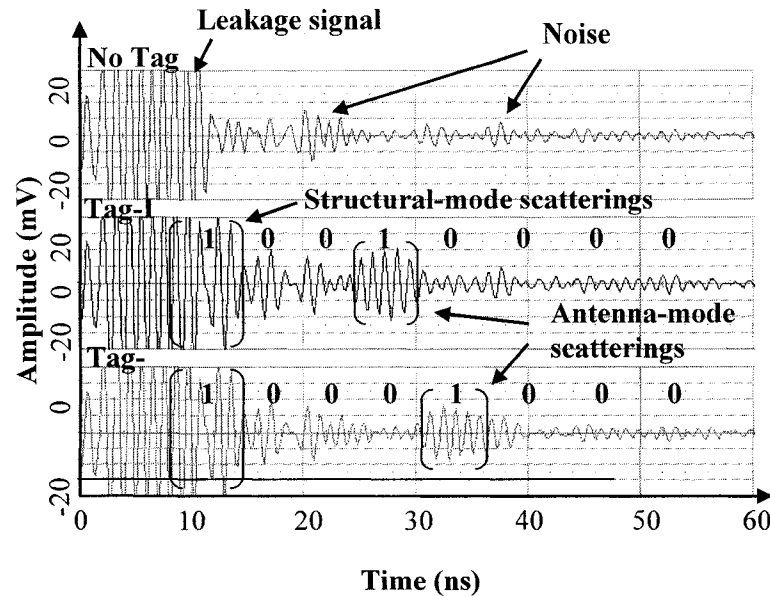


Figure 6.13 Experimental results showing received backscattered signal for the no tag condition (representing leakage signal in the reader and noise), and tag with the ID code 10010000 (Tag-I, 011 in PPM), and 10001000 (Tag-II, 100 in PPM), respectively.

### 6.8.2 Phase Change Observation

Two sets of experiments are carried out to observe the change in the phase of the antenna-mode scattered signal. In the first set of experiments discrete capacitors of various capacitances are placed on the tag, and the phase change in the antenna-mode scattered signal is observed. The second set of experiments are carried out with the actual ethylene sensors on the tag, and the phase change in the antenna-mode scattered signal for various ethylene concentration at the tag is observed.

**6.8.2.1 Results with Discrete Components** In the first set of experiments, discrete capacitors with capacitances of 0.5 to 9 pF are connected across the end of the transmission line and the ground of the tag, as shown in Figure 6.14. The phase change in the antenna-mode scattered pulse is observed in the oscilloscope and the results are shown in Figure 6.15 and Figure 6.16. The results in Figure 6.15 show the observed

phase change for the antenna-mode scattered pulse signal, when the capacitive load of the tag is changed from 2 to 5 pF. The structural-mode and antenna-mode scattered signals are enlarged in the insets. It is observed that the phase of the structural-mode scattered pulse does not vary with a change in load (sensor) capacitance, while the phase of the antenna-mode scattered pulse varies with capacitance.

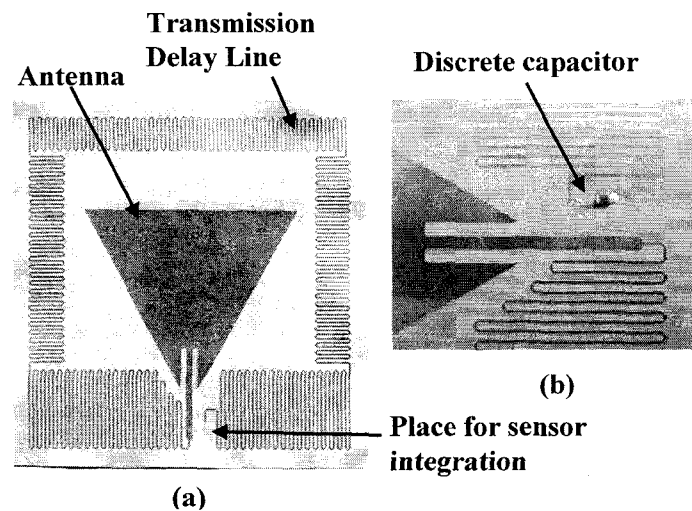


Figure 6.14 (a) Microstrip triangular antenna and meandered transmission line ID circuit for three bit code (110) generation. (b) A (sensor) capacitor integrated at the end of the transmission line.

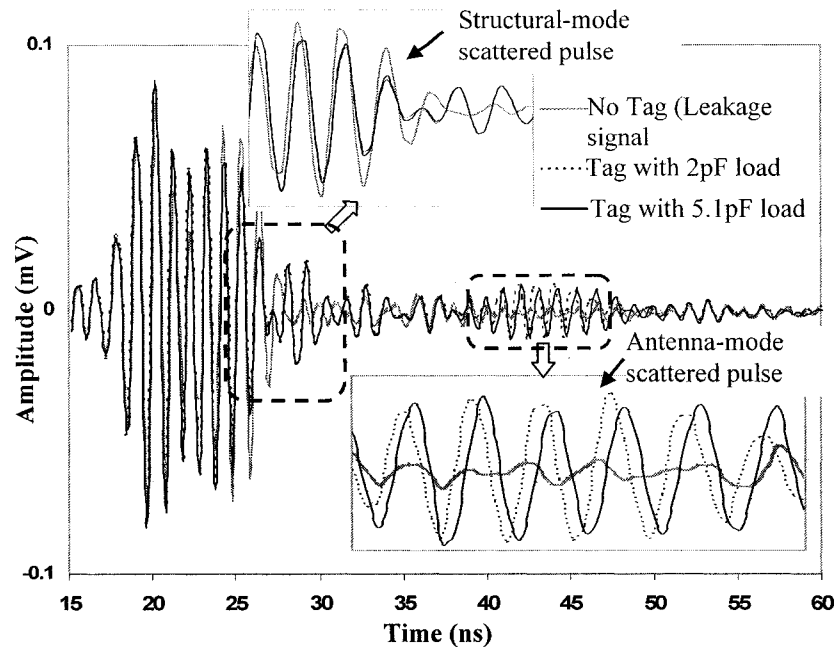


Figure 6.15 Experimental results showing received backscattered signal for no tag present versus tags with 2 and 5 pF capacitive loads.

The variation in the phase of the antenna-mode scattered signal with change in load capacitance is shown in Figure 6.16. It is observed that when the capacitance changes from 0.5 to 9 pF, the phase of the antenna-mode scattered pulse changes by 171.46 degrees. The average change in phase of the antenna-mode scattered pulse is  $26.51^\circ / \text{pF}$ , observed over the load capacitance between 1 to 5 pF. Simulation is performed with Ansoft Designer simulation software where the phase of the reflected signal from a transmission line is measured against the change in capacitance of the terminating load to the line. The simulation result is also shown in Figure 6.16. It is observed that the experimental and simulation results follow the same trend, and a small deviation is observed at higher capacitance values. This deviation is attributed to the fact that the resistance value of the practical sensor load also increases slightly with the increase in capacitance, which is not the case in the simulation where an ideal capacitor is

considered. This change in phase can be further utilized to obtain sensor information. It has been reported that the capacitance of an ethylene sensor changes by 37% when the concentration of the ethylene changes from 0 to 100 ppm [41]. For the sensor of 4.15 pF capacitance, the change in concentration of ethylene from 0 to 100 ppm translates to 1.5 pF change in the sensor capacitance. In the result shown in Figure 6.16, considering a linear change in phase with sensor capacitance in the small section between 4 and 5 pF capacitances, the slope of the phase curve is 20.96 (relating to the phase change of 20.96°/pF sensor change in capacitance). This result translates into 31.44° degrees of phase change in the antenna-mode scattered pulse when the ethylene concentration changes from 0 to 100 ppm.

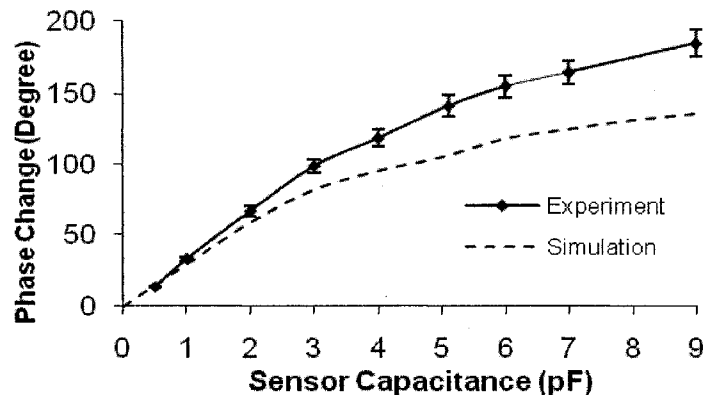


Figure 6.16 Experimental and simulation results showing the variation in the phase of the received antenna mode scattered pulse at the reader for various load (sensor) capacitance at the tag.

**6.8.2.2 Results with Ethylene Sensor** The experiments are carried out with the setup discussed in Section 6.7. The sensor tag with an ethylene sensor fabricated on the tag is placed inside the gas chamber. The flow of the ethylene in the gas chamber is controlled using the gas flow control knob, and the ethylene concentration is measured using the

commercial ethylene sensor connected to the chamber. The ethylene flow for 3 min recorded a 100 ppm ethylene concentration on the ethylene sensing instrument used for the measurement. The signal for 0 ppm ethylene and the 100 ppm ethylene are recorded, which are shown in Figure 6.17. The measurement of phase for the antenna-mode scattered pulse is taken with respect to the structural-mode scattered pulse. The structural mode scattered pulse for both cases are aligned by placing one exactly on the top of the other, and the antenna-mode scattered pulses are compared. It is observed that the antenna-mode scattered signal for the 100 ppm ethylene concentration is shifted to the left by 100 ps compared to the 0 ppm ethylene concentration, representing a  $33^\circ$  phase shift in the antenna-mode scattered pulse signal.

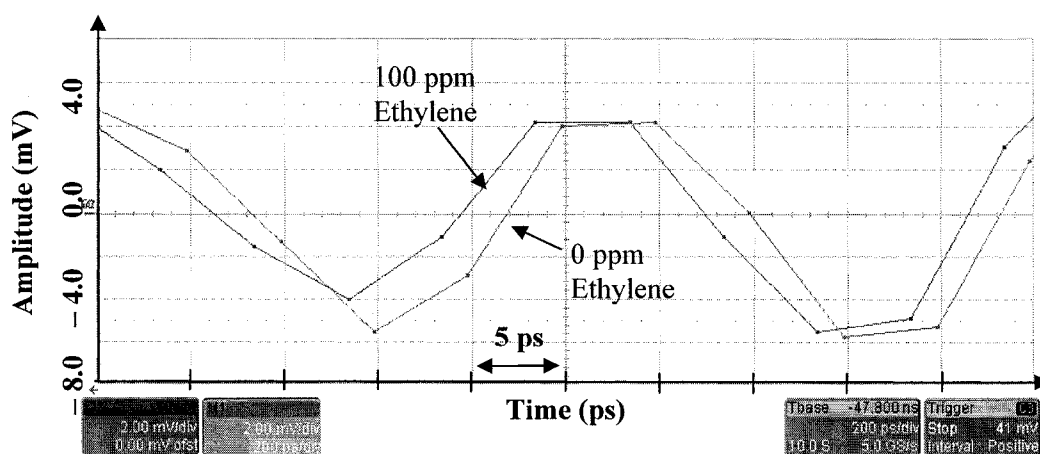


Figure 6.17 Experimental results showing phase change in antenna-mode scattered pulse with two different ethylene concentrations, 0 ppm and 100 ppm. 100 ps time shift is observed which corresponds to a  $33^\circ$  change in phase (200 ps/division on x-axis, 2 mV/division on y-axis).

The gas flow control knob has two inlets, one connected to the ethylene cylinder and the other to a dry air source. Using the flow control knob, the ratio of ethylene to air flow is changed from 0 to 80% and the antenna-mode scattered pulse is observed. The

ratio of the flow is changed every 3 min, and the phase change is measured at the end of each period. The shift in phase of the antenna-mode scattered pulse is measured with the reference to the phase of the structural-mode scattered pulse, which does not change with the change in sensor parameters. A  $13^\circ$  phase change is observed in the antenna-mode scattered pulse when the ethylene flow changes from 0 to 80%, also shown in Figure 6.18.

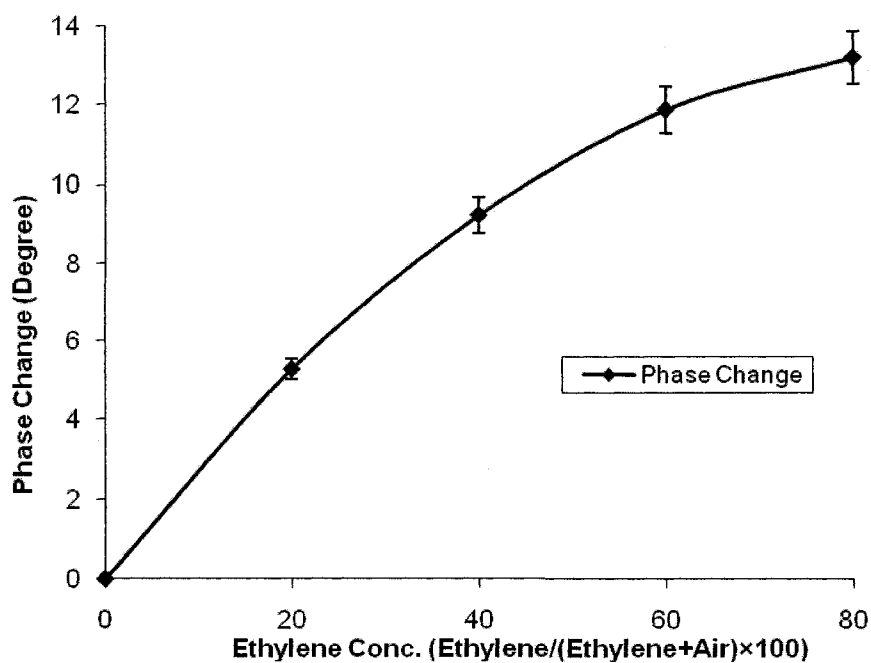


Figure 6.18 Result of phase change in antenna-mode reflected pulse when the ratio of ethylene to air concentration changes from 0 to 80%.



## CHAPTER 7

### READER SYSTEM DESIGN AND IMPLEMENTATION

The reader system design for chipless passive RFID sensor tags, including the work reported in [74], is discussed in this chapter. The designed reader system consists of an analog reader that communicates with the sensor tags by transmitting an interrogation signal and receiving the backscattered signal. The received backscattered signal is demodulated and fed to the single board computer (SBC). The SBC, after receiving signals from an analog reader, computes sensor value, and puts the computed sensor information in an EPC standard RFID tag frame. The SBC also makes the computed sensor value and the RFID tag data frame accessible to the user through a web interface.

#### 7.1 Introduction

The RFID sensor tags discussed in Chapter 6 do not contain any semiconductor chips on the tag, and involve innovative sensor integration as well as ID generation techniques. Compared with chip-based sensor tags, chipless sensor tags are simpler in design and less expensive. Chipless sensor tags do not involve analog to digital conversion, which makes the sensor integration process simpler and cost effective. Additionally, chipless tags can be used in environments where the semiconductor chip would otherwise limit the applications, such as in harsh environments.

The presented chipless sensor tags do not use conventional RFID communication techniques and, thus, the available RFID readers cannot communicate with the chipless tags. While the custom designed chipless sensor tag readers can obtain information from the tags, the readers do not produce output in the RFID standard tag ID format. This prevents the chipless sensor tag system from becoming a part of a conventional RFID system and to connecting with cyberspace, which has been a major challenge in the realization of a commercial chipless sensor tag based RFID system. An RFID system that overcomes the above mentioned impediments and developed for a cyber centric monitoring application is presented and testing with chipless freshness (ethylene) and temperature sensor tags is discussed. However, the application of the discussed system can be further applied to a variety of other sensing applications. The schematic of the presented RFID system is shown in Figure 7.1.

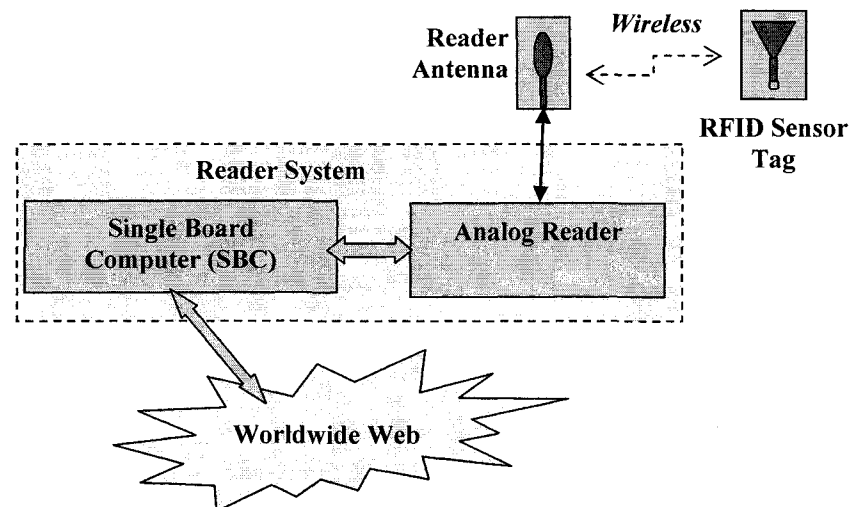


Figure 7.1 Schematic of cyber enabled RFID system.

The reader system encloses an analog reader that transmits a 915 MHz interrogation signal, receives a backscattered signal from the tags, and feeds the

demodulated signal to the analog-to-digital (A/D) converter of the single board computer (SBC). A user friendly web interface has been developed on the SBC accompanied with web server, dynamic host configuration protocol (DHCP) client, user authentication features, and applications programs. The SBC takes input from the analog reader and computes the sensor value. The reader system further constructs an RFID standard tag ID, and allows communication with conventional RFID systems and through cyberspace.

## **7.2 RFID Tag Data Frame Structures**

The RFID tag data format varies with the type of application, tag technology, number of bits available, and also with the different standards used, such as electronic product code (EPC), US department of defense (DOD), and international standard organization (ISO). An example of tag ID classification based on the application, type of memory, power source, and features are shown in Table 7.1 [36]. The EPC classification and the tag format structures are shown in Table 7.2 [100].

Table 7.1 RFID Tag Classifications Based on Tag Capabilities.

<i>Class</i>	<i>Nickname</i>	<i>Memory</i>	<i>Power Source</i>	<i>Features</i>
<b>0</b>	Anti-Shoplift Tags	None	Passive	Article Surveillance
<b>1</b>	EPC	Read-Only	Any	Identification Only
<b>2</b>	EPC	Read-Write	Any	Data Logging
<b>3</b>	Sensor Tags	Read-Write	Semi-Passive or Active	Environmental Sensors
<b>4</b>	Smart Dust	Read-Write	Active	Ad Hoc Networking

Table 7.2 EPC RFID Tag Classifications and Tag Format Structures.

<i>EPC Type</i>	<i>Header Size</i>	<i>First Bits</i>	<i>Domain Manager</i>	<i>Object Class</i>	<i>Serial Number</i>	<i>Total</i>
<b>64 bit type I</b>	2	01	21	17	24	64
<b>64 bit type II</b>	2	10	15	13	34	64
<b>64 bit type III</b>	2	11	26	13	23	64
<b>96 bit and more</b>	8	00	28	24	36	96

The header in the data frame defines the EPC class of the data structure, the first bits define the format version number, the domain manager identifies the manufacturer, the object class defines the product number, and the serial number represents the unique serial number of the product. An example of an EPC 96 bit version tag ID is shown in Figure 7.2 [101].

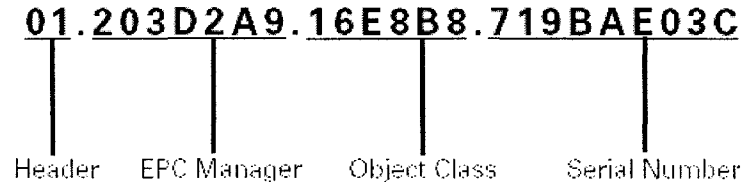


Figure 7.2 An ID tag format example of EPC 96 bit version.

### **7.3 Tag ID Standardization Scheme for Chipless RFID Sensor Tags**

A tag ID standardization scheme to construct an EPC standard RFID tag data, including sensor information and the ID generated by the chipless tags, is discussed in this section. In the present scheme, using the sensor data, the reader system constructs an ID frame in EPC standard RFID tag data structure to communicate through cyberspace as a standardized RFID reader system. The EPC RFID tag data structure starts with an 8 bit header, followed by additional tag data. An example of a serialized global trade item

number-96 (SGTIN-96) data structure is shown in Table 7.3 [102]. Here, the 96 bit long data frame is partitioned into different fields. The header field defines the format of the data frame and informs the reader on how to interpret the rest of the bits in the frame. The company prefix is unique for a given product vendor, and it prevents repeating the same ID for other vendors. The reference field defines the type of item (object) being tagged. The 38 bit long serial number is used for itemized tagging [100, 103] and includes the sensor information in the presented scheme. The designed chipless RFID tags have fewer numbers of ID bits, as compared to commercial RFID tags. This places a limitation on the number of RFID tags that can be realized with unique IDs. For example, an ID generation scheme with three bits ID code allows the realization of eight different RFID tags. When more tags have to be deployed, the ID will be repeated and it is not possible to distinguish between two different tags with the same ID code. To overcome this limitation, a reader domain system technique has been designed and developed. In this technique, each RFID reader is assigned with a unique reader ID.

Table 7.3 A Typical SGTIN-96 EPC RFID Tag Data Structure.

<i>Field Name</i>	<i>Header</i>	<i>Filter Value</i>	<i>Partition</i>	<i>Company Prefix</i>	<i>Item Reference</i>	<i>Serial Number</i>
<b>Frame</b>	8 bits	3 bits	3 bits	20-40 bits	24-4 bits	38 bits
<b>Example</b>	00110000	011	010	34 bits	10 bits	38 bits

Furthermore, as shown in Table 7.4, the 38 bit long serial number field is divided into three subfields, reader ID, tag ID, and sensor information fields. The reader ID is 14 bits long, which allows having up to 163,482 unique readers under the same company prefix and item reference. Moreover, a reader ID defines a reader domain, and any tag

with the same reader ID is considered to belong to a reader domain and is deployed in the range of the same reader. The tag ID field is 8 bits long, where the all-zero code is reserved for no tag ID. This allows having up to 255 unique tag IDs under a given reader domain. The sensor information field is 16 bit, allowing inclusion of the sensor information in the data frame with 16 bit resolution. This representation allows more than 4 million unique RFID sensor tags with 16 bit resolution for sensor information.

Table 7.4 Partitioning of the Serial Number Field to Include Reader ID, Tag ID, Sensor Information.

<i>Field Name</i>	<i>Reader ID</i>	<i>Tag ID</i>	<i>Sensor Information</i>
<b>Frame</b>	14 bit	8 bit	16 bit

The reader domain concept and representation of a unique ID code using reader ID is shown in Figure 7.3. In the given example, two readers with reader IDs 0009 (binary: 00000000001001) and 0003 (binary: 00000000000011) represent two different reader domains. In one reader domain it is not possible to have two tags with the same tag IDs; however it is possible to have two tags with the same ID in different reader domains. In representing the data frame, a reader adds its unique ID into the reader ID field along with the tag and the sensor ID fields. The reader then generates a complete 96 bit long RFID data frame, which also includes predefined header field, filter value, partition, company prefix, and item reference. The final RFID data frame thus generated represents a globally unique ID. When the data frame is accessed from the outside world, it appears as a SGTIN-96 format RFID tag ID, while only the given reader system can extract the reader, tag, and the sensor information. This also provides a means for a more secure transfer of sensor information.

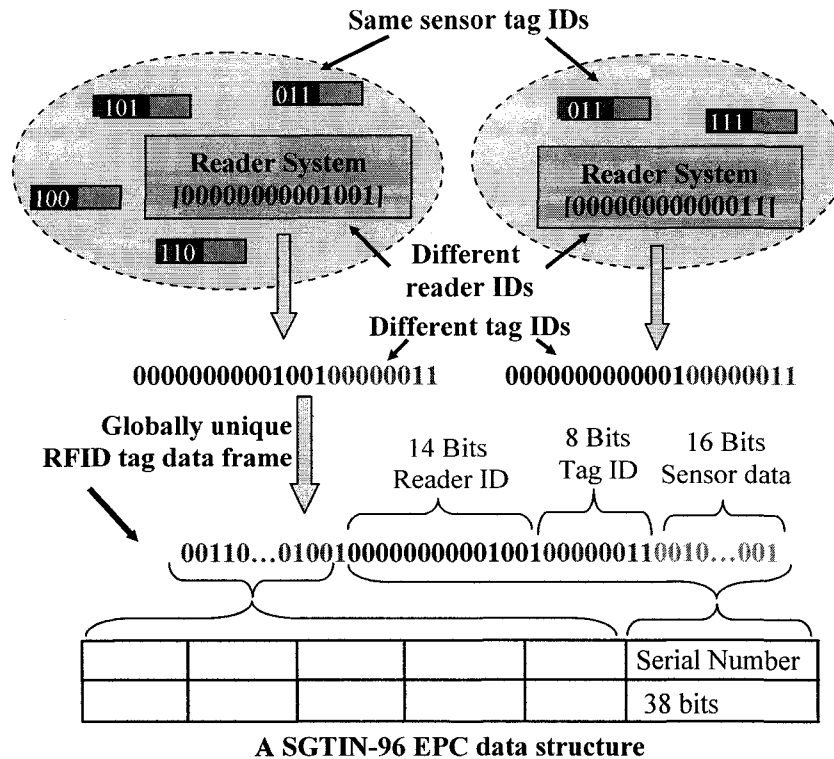


Figure 7.3 Reader domain concept for construction of unique ID code using reader ID.

## 7.4 Reader System Components

The reader system is divided and discussed in two sections as an analog reader and a single board computer. The components of the reader dealing with analog signal are discussed in the analog reader section, and the hardware, software, and the connection of analog reader and single board computer is discussed in the single board computer section.

### 7.4.1 Analog Reader

The analog reader is responsible for performing wireless communication with the tags by sending an interrogation signal and receiving a backscattered signal from the tags, and operates on the analog signal before feeding it to the SBC. The expanded schematic drawing of the reader system is shown in Figure 7.4, which includes both the analog

reader and the SBC. As shown in Figure 7.4, the analog reader is further divided into four sections as transmission, reception, signal cancellation and signal amplification, and demodulation and filtering section. The transmission section consisting of a VCO and a circulator (part no: JCC0800T0960S10 coaxial circulator, manufacturer: JQL Electronics Inc.) generates a continuous 915 MHz signal and transmits it to the tags through the reader antenna. The reader antenna is a circular disc monopole antenna fabricated on a PCB substrate (substrate: FR4, permittivity: 4.7, substrate height: 0.15 cm, circular patch diameter radius: 5.4 cm, feed width: 0.37 cm, ground-plane of dimensions: 13.54 cm × 5.38 cm), [46]. The backscattered signal from the tags is received by the reader antenna and sent to the reception section.

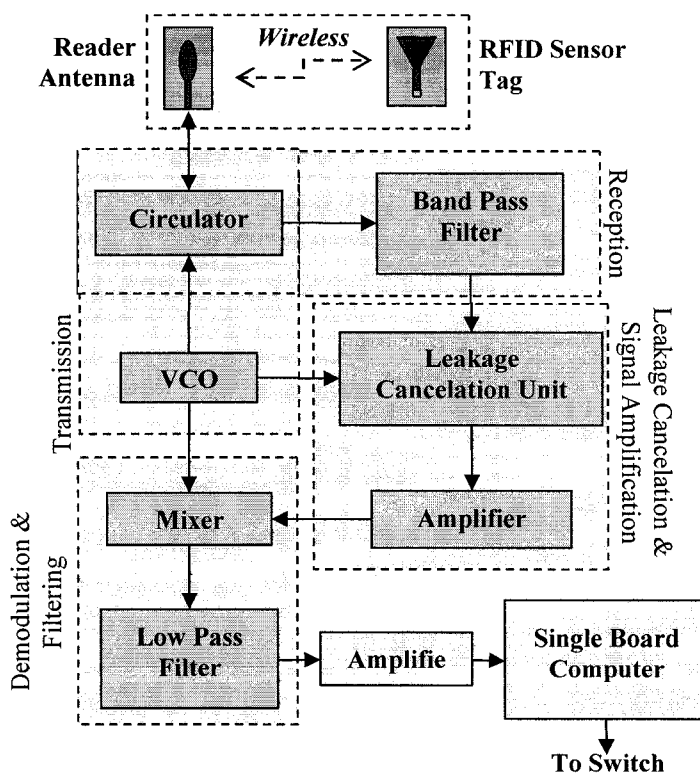


Figure 7.4 Schematic of the reader system showing components of the analog reader and the connection to SBC.



The forward and the returning paths of the signal from the reader antenna are separated by the circulator. The reception section includes a band-pass filter to block unwanted signals. The signal is then passed to the leakage cancelation and signal amplification section. The leakage signal cancellation unit consists of a variable attenuator, a delay line, and a signal combiner (part no: 802-S-1.900-M01, manufacturer: Meca Electronics). The signal received due to the return loss of the reader antenna is called the leakage signal. This is the signal observed at the reception section output when the reader system is placed inside an anechoic chamber with no tags present. The leakage canceling signal is generated with the help of the signal from the VCO, variable attenuator, and the delay line as described in [104]. The canceling signal is added to the original signal with the help of the combiner. The signal from the combiner is amplified by a low noise amplifier (part no: HMC372LP3 Evaluation Board, manufacturer: Hittite Microwave) and passed to the demodulation and filtering section that consists of a mixer (part no: HMC207 Evaluation Board, manufacturer: Hittite Microwave) and a low pass filter (part no: SLP-250, manufacturer: Mini Circuits). The signal is demodulated by mixing the local carrier signal from the VCO with the received signal and passed through the low pass filter, which is then amplified and fed to the A/D converter input of the SBC.

#### **7.4.2 A Single Board Computer**

Single board computers have been an important part of modern signal processing and data analysis systems with size restrictions and the need for resident computing ability. An SBC includes the basic components needed to run a computer and everything fits on a single board. The main components of an SBC are the processor, read only memories (ROM), random access memories (RAM), and input/output (I/O) interfaces.

The read only memory stores the information necessary to start up the computer while the random access memory stores the programs currently being executed. The I/O interfaces connect the computer to the outer world for data acquisition and presentation. The development of a reader system using a single board computer, including hardware aspects, configuration, and programming, is discussed in this section.

**7.4.2.1 Hardware Selection** Hardware selection is made on the basis of the availability of the necessary resources on the board, including I/O interfaces and ethernet interface, flexibility, and ease of configuration and programming. The hardware, configuration, and programming aspects of two selected single board computers, Freescale QUICCstart MPC8248 SBC and BL2500 Rabbit Core Board SBC, are discussed. However, due to the availability of extended libraries with Rabbit Core SBC programming environment and on-board A/D converter, the Rabbit Core SBC is selected for the reader system design.

**7.4.2.1.1 Freescale QUICCstart MPC8248** A Freescale QUICCstart MPC8248 SBC (400 MHz processor, 16 MB RAM, 8 MB flash) is equipped with two serial ports, two ethernet ports, one USB port, a PCI edge, and I/O and bus expansion receptacles [105]. A picture of the SBC showing connection to the ethernet and A/D converter is shown in Figure 7.5. The system runs on a Linux board support package developed with embedded planet Linux development kit and programmed in Code Warrior Integrated Development Environment (IDE) [106, 107].

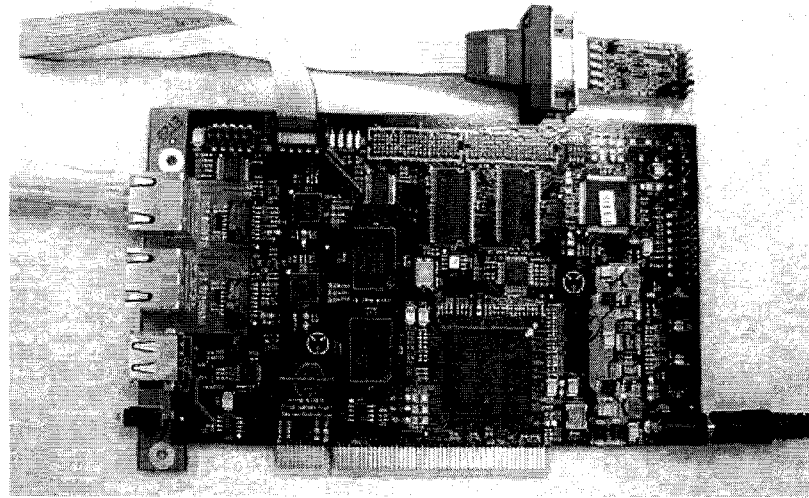


Figure 7.5 Freescale QUICC start MPC8248 single board computer.

**7.4.2.1.2 Rabbit Coyote BL2500** A Rabbit Coyote BL2500 SBC is equipped with 29.4 MHz processor with 256K flash and 128K SRAM, 8 bit A/D analog input channel, one 10baseT Ethernet port, six serial ports, and four user configurable LEDs [108]. A picture of the SBC is shown in Figure 7.6. The Dynamic C Integrated Development Environment is used to program the SBC [109].

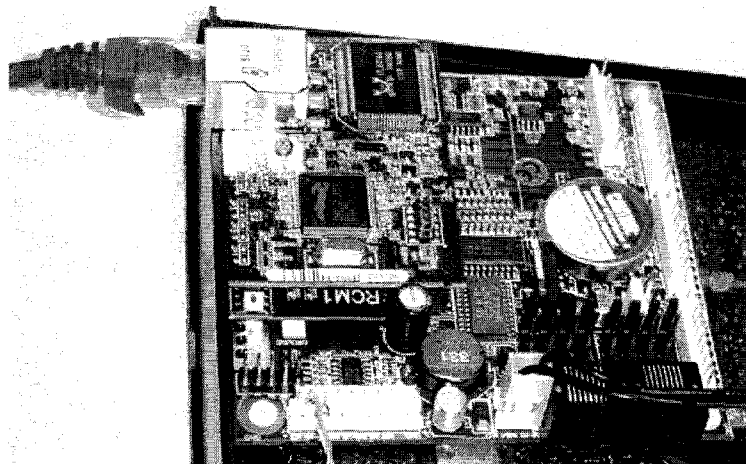


Figure 7.6 Rabbit Coyote BL2500 single board computer.

**7.4.2.2 Configuration and Programming** The SBC is connected to a host computer through the serial interface of the SBC for initial configuration and programming. The Freescale SBC is connected to the USB port of the host computer using a USB TAP, while the Rabbit Core SBC is directly connected to the serial port of the host using a programming cable. After the connection is made with the host computer, the SBCs are programmed using the appropriate programming environment, the Code Warrior for the Freescale SBC and Dynamic C for the Rabbit Core SBC. The SBCs are also connected through the ethernet interface with the host computer for cross checking while running the intermediate programs in the SBC. The schematic of the SBC configuration and programming connection with host computer is shown in Figure 7.7.

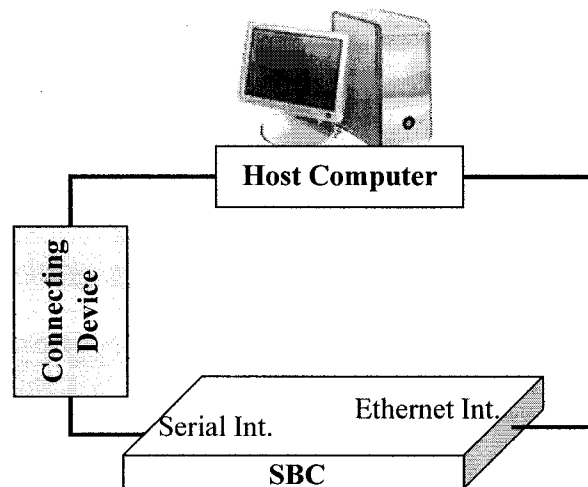


Figure 7.7 Schematic of the SBC connection with the host computer for configuration and programming.

**7.4.2.2.1 Freescale SBC** The Freescale SBC is programmed with Code Warrior IDE. The Code Warrior provides a single platform for toolset, editor, compiler, linker, debugger, and software module operation. The program for the board is written on the Code Warrior IDE. The host computer and the single board computer are linked via USP TAP

through the serial port of the single board computer and USB port of the host computer. The SBC periodically takes input from the serial interface and performs appropriate processing tasks to extract the sensor information from the input data. The change in the sensor parameter is obtained by comparing the current input data with a reference data. Any difference between the received current input and reference data measures the change in the sensor parameter and, thus, provides a measure of the change in the quantity of stimulant at the tag. The flow chart of the procedures is summarized in Figure 7.8.

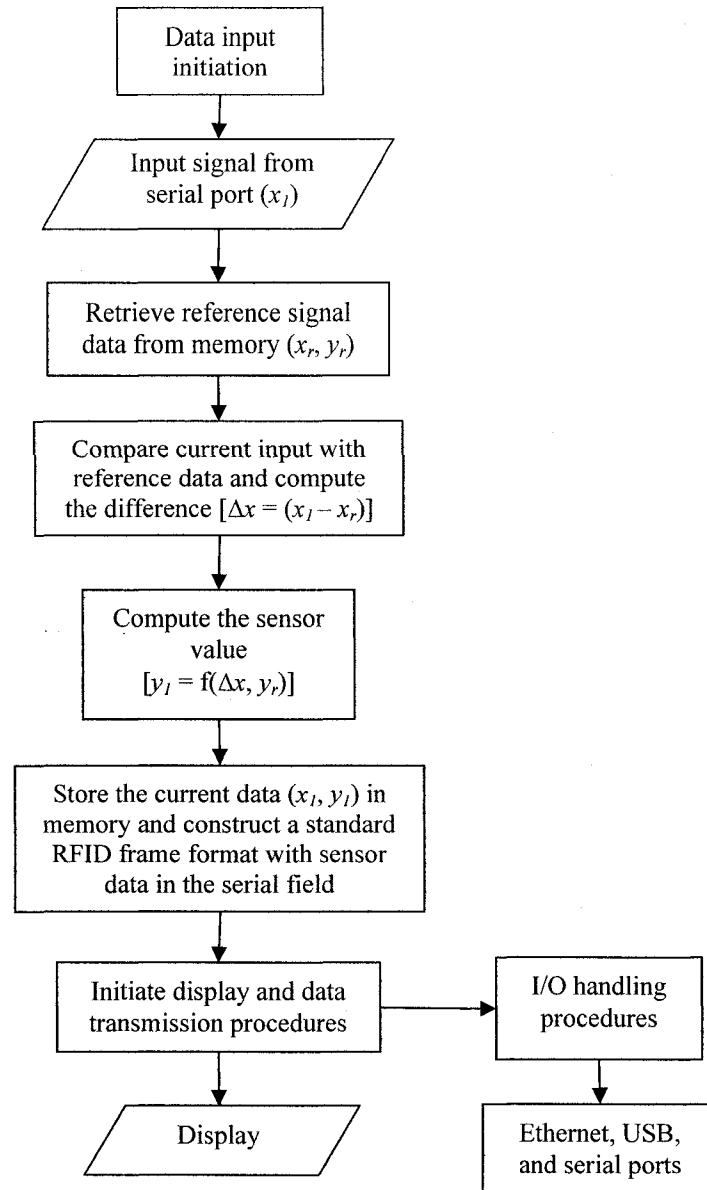


Figure 7.8 Flow chart showing the tasks performed by the SBC to compute the sensor value for an integrated sensor-antenna tag.

As shown in Figure 7.8, the current input data from the analog reader is in the form of a voltage amplitude ( $x_l$ ). The present voltage amplitude is compared with the reference voltage amplitude retrieved from the memory ( $x_r$ ) and the difference between the reference and present voltage amplitudes ( $\Delta x = x_l - x_r$ ) is computed. Based on the sensor characteristics (e.g. linear or exponential change in sensor signal), the change in

voltage is interpreted for the change in the sensed quantity using a predefined function ( $y = f(\Delta x, y_r)$ ). The interpreted sensor data ( $y_l, x_l$ ) is stored in the memory for further operations by the reader system, including construction of the raw sensor data into a standardized RFID tag data format.

**7.4.2.2.2 Rabbit Core SBC** The Rabbit Core SBC is connected directly to the host program using a serial programming cable and programmed with Dynamic C Integrated Development Environment [109]. Dynamic C provides editing, compiling, linking, loading, and debugging facilities in a single environment and allows program execution and debugging on the target hardware. In addition to conventional C libraries, the environment provides additional libraries and extension that makes the reliable multitasking software development simpler and easier. The developed firmware for the Rabbit Core SBC includes web server, DHCP client, and authentication rules to serve the user web interface and to perform computation of equivalent sensor value from the analog reader input signal.

**7.4.2.3 Connection with the Analog Reader** The single board computer and the analog reader discussed in Section 7.2 are connected through an A/D converter. The A/D converter converts the analog signal from the analog reader into a form suitable to use in the digital SBC and is fed through the serial interface. The SBC, after computing the sensor information, eventually communicates the information to the outer world through the ethernet interface of the SBC. Figure 7.9 depicts the connection of the SBC with the analog reader through the A/D converter and with the outside world through the ethernet interface.

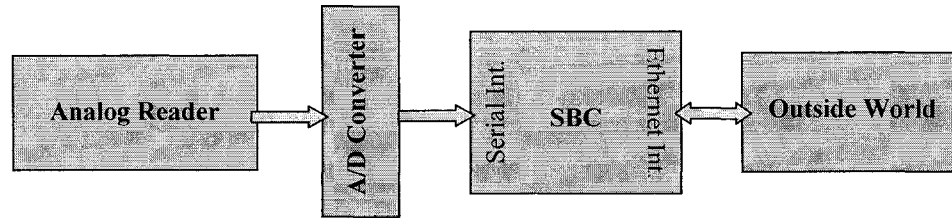


Figure 7.9 Schematic showing connections of the SBC with the analog reader through the A/D converter and outside world through the ethernet interface.

**7.4.2.3.1 Freescale SBC** The laboratory prototype of the reader system using the Freescale SBC and the modular analog reader is shown in Figure 7.10. The SBC is connected to the analog reader through an A/D converter. The computer acquires the information from the analog reader through a serial interface and stores it in the memory for further processing of the sensor information [110, 111]. Once the appropriate program is loaded in the flash memory of the SBC, it can function as an independent system, take input through the serial interface, and communicate to the host computer and outside world through the ethernet interface.



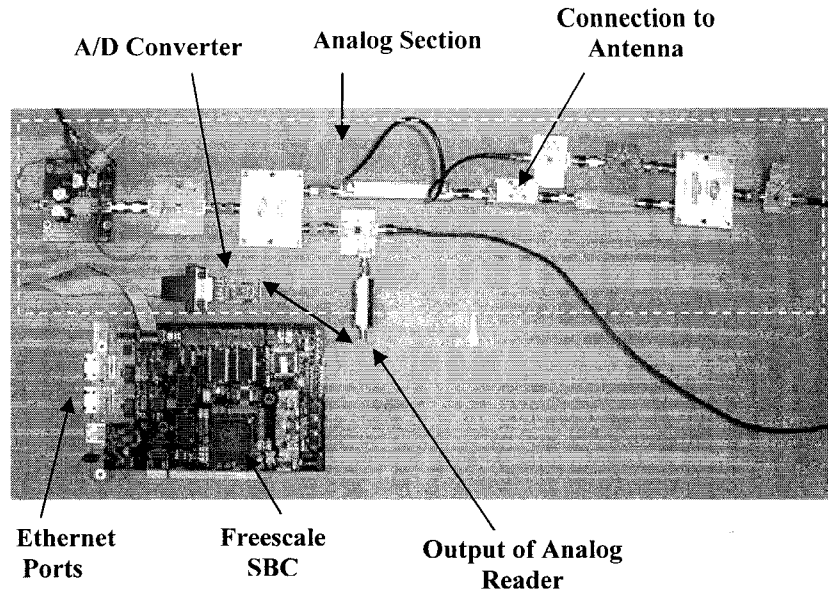


Figure 7.10 A modular laboratory prototype of the reader system using the Freescale SBC.

**7.4.2.3.2 Rabbit Core SBC** The developed reader system prototype using a Rabbit Core SBC is shown in Figure 7.11, which also includes a modular analog reader. The Rabbit Core SBC houses an 8 bit A/D converter and does not need an external A/D converter (unlike Freescale SBC which needs an external A/D converter). Due to this reason and also due to the availability of extended libraries and ease of programming with Dynamic C environment, the Rabbit Core SBC is selected and used for further reader system design and firmware development. The SBC takes analog reader input through the A/D converter. The analog reader output is amplified using an amplifier circuit before feeding to the SBC. With the firmware loaded in the SBC, it periodically takes input from the analog reader and communicates with the outside world through the ethernet interface.

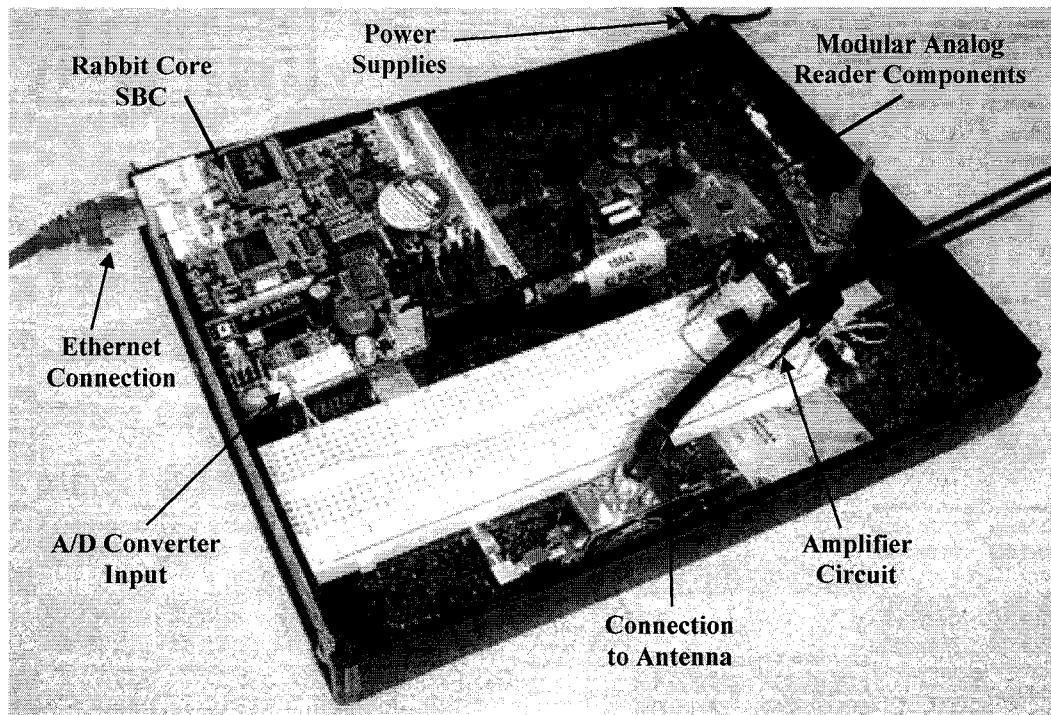


Figure 7.11 Reader system prototype using Rabbit Core SBC.

### **7.5 Reader System Firmware Development with Rabbit Core SBC**

The reader system firmware is developed in the Dynamic C Integrated Development Environment [109]. The developed firmware includes web server, DHCP client, and authentication rules to serve the user web interface and compute equivalent sensor values from the analog reader input signal. After the board, sockets, web server, and necessary variables have been initialized, the DHCP client has been started, and authentication rules have been defined, the process is transferred to the indefinite loop of the instructions shown in Figure 7.12. The main steps of the instruction cycle and the interactions between instructions, memory, and the web interfaces are highlighted in Figure 7.12.

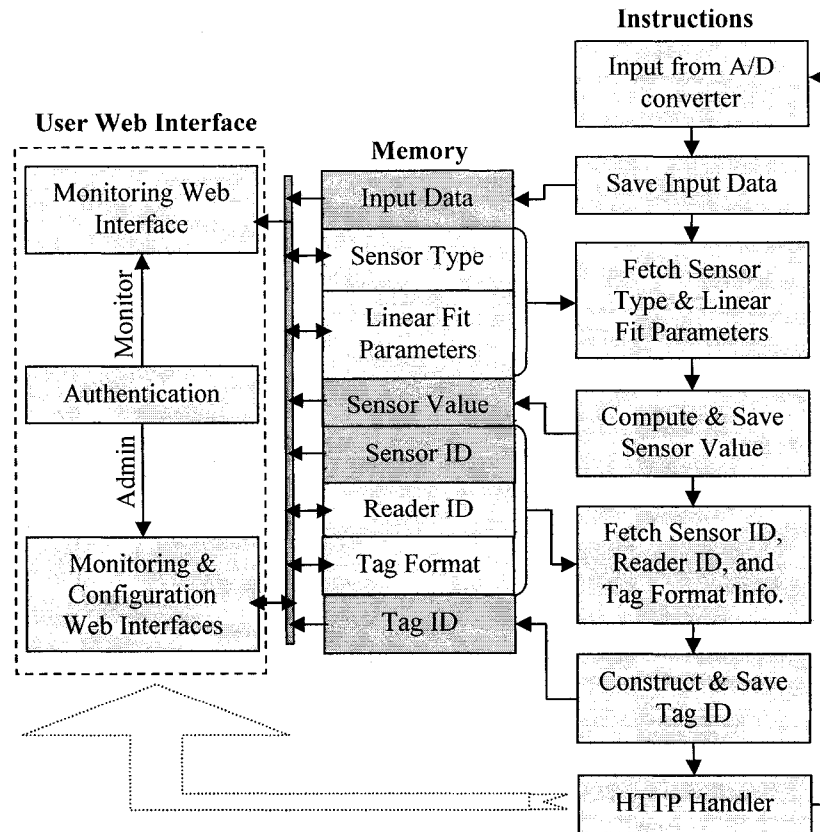


Figure 7.12 Schematic of reader operations highlighting the interaction between instructions, user web interface, and memory.

### 7.5.1 Initializations

The program starts by defining the necessary modules to run the reader system. The DHCP client module is called to assign an IP address to the ethernet interface. The module allows using a static IP address as well as obtaining it from a DHCP server. Here the module is configured to obtain an IP address from a DHCP server in the network and in the case of failure, a static IP address is assigned. Along with the DHCP client module, web (Rabbit web) and authentication modules are also initiated. The web module facilitates an easy transfer of information between the procedures and the web interface by allowing the sharing of variables while the authentication module helps to define the access control to the web content in the SBC. The board, sockets, and the hypertext

transfer protocol (HTTP) handler that serves the web server, are initialized along with the necessary variables and functions.

### **7.5.2 Web Interface Files**

The web interface files are developed in hyper text mark up language (HTML) and dynamic web contents are introduced using ZHTML scripting language [112]. The ZHTML scripting language allows for introducing dynamic content easily on the web pages and provides a simple means of information transfer between the program and the web interfaces through the sharing of variables across the program and the web files. The files are imported to the program and copied into the root directory, which are made accessible from the outside world using the worldwide web.

### **7.5.3 Input from Analog Reader**

After the necessary modules, functions, and hardware have been initialized, the program enters into an infinite instruction cycle shown in Figure 7.12. The instruction cycle starts from the A/D converter input (input data). The input from the analog reader is taken periodically by calling a function that takes the input from the A/D converter input and stores it in the memory.

### **7.5.4 Computation of Sensor Value**

The sensor value is computed from the analog reader input with the help of sensor type information and sensor linear fit parameters obtained from the memory. The memory stores a set of sensor linear fit parameters (provided during reader configuration) for each sensor type, and appropriate parameters are used based on the provided sensor type information. The computation equation used to compute the sensor value from the analog reader input using sensor linear fit parameters, also depends on the sensor type. For example, a set of linear fit parameters for a temperature sensor include two sets of

data with temperature at the tag and the amplitude of the analog reader input signal for the given temperature. The linear fit parameters are provided to the reader during the reader configuration. For the temperature sensor tag, the analog reader input linearly increases with the temperature. Thus, from the sensor fit parameters, intercept and slope is calculated which is used to compute the current temperature at the tag from the analog reader input data.

#### **7.5.5 RFID Tag Data Frame Construction**

The reader is provided with the reader ID and the tag format information to be used while configuring the reader. Using the sensor ID, reader ID, and tag format information obtained from the memory, a 96 bit modified SGTIN-96 EPC format tag ID is constructed and saved. The 96 bits of tag ID consist of 8 bit header, 3 bit filter value, 3 bit partition, 34 bit company prefix, 10 bit item reference, 14 bit reader ID, 8 bit sensor ID, and 16 bit sensor value [103]. For the temperature sensor tag, the first bit of the 16 bit sensor value corresponds to the sign of the temperature (0 = positive and 1 = negative). The temperature is represented up to one decimal point, and it is achieved by multiplying the computed temperature by 10 and discarding the remaining numbers after the decimal point. Thus, the sensor value in the tag ID can hold temperatures ranging from  $-3276.7^{\circ}\text{C}$  to  $3276.7^{\circ}\text{C}$ .

#### **7.5.6 Information Access through Web Interface and User Authentication**

The construction of the tag ID is followed by the process transfer to the HTTP handler which serves the user web interfaces. The user web interfaces allow accessing, monitoring, and configuring the reader through cyberspace. The memory serves both

instructions and the user web interface, providing a platform for information exchange between the user interface and the instructions. The input data, sensor value, and tag ID can only be updated by the instructions, while the sensor type, sensor linear fit parameters, sensor ID, and reader ID are available to the user for modification. It is to be noted that the sensor type, linear fit parameters, and sensor ID are interrelated and each sensor type is associated with a unique sensor ID and a set of sensor linear fit parameters. For example, a temperature sensor is assigned a unique sensor ID (01 in Hex) and is associated with a set of linear fit parameters, initially configured by the user, and later this information is used to compute the temperature in degrees centigrade from the input sensor data in millivolts.

The web interfaces are categorized into monitoring and configuration web interfaces. The monitoring interface displays information about the current analog reader input data, sensor type, computed sensed value, reader ID, and the constructed tag ID in the SGTIN-96 EPC format. The configuration web interface displays as well as allows modifying information on sensor type, sensor linear fit parameters, reader ID, and tag ID format. The web interfaces can be accessed using any standard web browser by typing the IP address of the reader system on the address bar. Whenever a web interface is accessed, the user is asked to authenticate by providing a username and password, and, on the basis of provided information, the users are divided into monitor and administrator groups. The administrator group is allowed to access both monitoring as well as configuration interfaces while the monitor group is allowed access only to the monitoring interface.

## **7.6 System Test Results and Discussions**

The developed firmware is loaded in the SBC flash memory and is used as a stand alone system to monitor the chipless sensor tags. The reader wirelessly communicates with the tags to obtain information and allows accessing of this information from cyberspace using secure web interfaces. Moreover, the reader constructs a globally unique tag ID using the ID construction scheme discussed in Section 7.3 to communicate with the other systems as a standard RFID reader system. An application example of the developed reader system to monitor temperature using a temperature sensor tag by accessing the reader system from the worldwide web is discussed in this section. The system testing setup consists of a reader antenna and the tag with heating system placed inside an anechoic chamber. The reader antenna is connected to the reader through a coaxial cable, and the reader is connected to cyberspace through a switch. The user web interface of the reader system is accessed from a computer connected to the internet by providing the username and password.

### **7.6.1 Reader Configuration**

The reader system is configured by providing linear fit parameters for the temperature sensor before using it to measure the temperature at the sensor tag. The linear fit parameters for the temperature sensor tags consist of two data sets of amplitude and temperature. To obtain the data sets as well as to establish the temperature sensor tag concept, a set of experiments is carried out where the analog reader inputs at the reader versus various temperatures at the tag are measured. The monitoring user interface of the reader system is accessed from a computer connected to the worldwide web, the user name and password are provided, and the backscattered signal amplitudes (displayed on the user interface as current analog reader input) for different temperatures at the tag are

measured. The measurement is discussed in Section 6.1.3 and the results are shown in Figure 6.3. It is observed that the amplitude at the output of the analog reader increases linearly with an increase in temperature at the tag. Thus, the linear fit has been used for the computation of the sensor value for the temperature sensor tag. During the configuration, two experimental data sets of temperature and analog reader input are entered through the configuration web interface.

### **7.6.2 System Testing Results**

Based on the experimental results shown in Figure 6.3, a linear change in temperature versus analog reader input (backscattered signal amplitude) is adopted to compute the temperature from the analog reader input signal. The reader takes two data sets of analog reader input versus temperature (through the configuration interface of the reader system), determines the slope and intercept for the linear fit line, and computes the temperature from the input signal obtained from analog reader (through A/D input). The configuration interface is accessed from a computer connected to the internet and two sets of experimental data points (temperature, analog reader input) are entered on the “Reader and Sensor Settings” tab under the “Sensor Linear Fit Parameters” option. A snapshot of the “Reader and Sensor Settings” tab on the configuration interface is shown in Figure 7.13. Also, the reader ID can be changed on the configuration interface, which is unique among a particular item reference for a given company. The reader ID can vary from 1 to 16,383.



**RFID Sensor Reader System**

**Reader and Sensor Settings**

**Reader Settings:**  
Reader ID(1-16383): 9

**Sensor Settings:**  
Sensor Type: Temperature

**Sensor Linear Fit Parameters:**

Data Set - I:  
Temperature: 40.00 (Degree Centigrade)  
Analog Reader Input: 648.83 (mili-Volts)

Data Set - II:  
Temperature: 100.00 (Degree Centigrade)  
Analog Reader Input: 734.16 (mili-Volts)

Submit

Figure 7.13 The configuration interface used to configure the reader system by providing sensor linear fit parameters for a given sensor type.

The submission of the linear fit parameters takes effect instantly, and the reader can be used to monitor the temperature at the tag. Using the submitted information, the reader computes the sensor value from the reader input signal. As discussed in Section 7.3, the reader constructs a 96 bit RFID tag ID that contains ID format information, reader ID, sensor ID, and computed sensor value. The information can be viewed on the monitoring interface. A snapshot of the monitoring interface is shown in Figure 7.14. From Figure 7.14 it is observed that the current analog reader input is 675.72 mV, the sensor tag under consideration is a temperature sensor tag, and the temperature at the tag is 58.9 °C. The figure also shows that the reader ID is 009 and the constructed tag ID in EPC SGTIN-96 format is 30680000000100400901024d (in Hexadecimal).

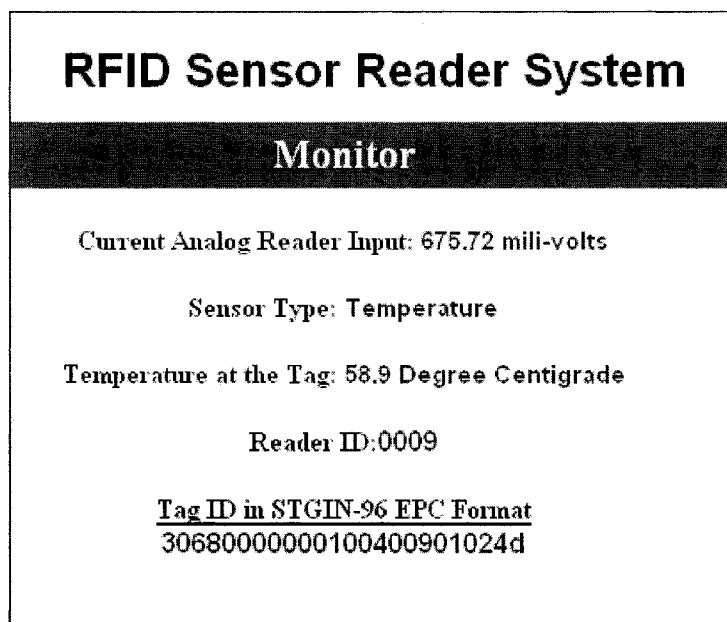


Figure 7.14 The monitoring interface showing sensor tag information that includes sensor type, computed temperature at the tag, and the tag ID.

In the tag ID 30680000000100400901024d, the sensor information consists of the last six digits (01024d). The first two digits (8 bit) of the sensor information correspond to sensor type and the remaining four digits (16 bit) correspond to the sensor information. The sensor ID **01** tells that it is a temperature sensor and, thus, the sensor value is temperature in degrees centigrade. The leading zero in the binary equivalent of the sensor value (0000001001001101) indicates that the sign of the temperature is positive while the remaining 15 bits represent the temperature expressed to one decimal point. The decimal equivalent of the sensor value is 589, thus the temperature at the tag is +58.9 °C.

## **CHAPTER 8**

### **APPLICATIONS**

The battery-free and chipless operating mechanism of passive chipless RFID sensor tags, used in a chipless sensor tag system, provides broad application opportunities for the systems. The system provides a means for the wireless collection of physical information from the environment for various applications, such as product monitoring, health care, and household applications in a reliable and cost effective way. The chipless sensor tags can be applied in harsh environments where the chip-based sensor tags cannot be used because the semiconductor chips do not operate in these environments. The possible applications of the developed chipless ID generation techniques, RCS measurement method, chipless sensor tags, and the chipless sensor tag based system are discussed in this chapter.

#### **8.1 Low Cost Printable RFID Tag Applications**

Chipless printable RFID tag technologies have been a great attraction for tagging and tracking applications. The printable tags can be directly fabricated on the desired object and at very low cost. According to the RFID market research forecast [72], chipless tags are expected to occupy 45% of the RFID market by 2016. The transmission delay line reflection based ID generation technique can be applied to printable RFID tag technology. The RFID tags based on transmission line reflection consist of microstrip

antenna and transmission lines which can be fabricated using inkjet printing technologies. Thus, the tags can be applied using printable tag technologies to achieve very cost effective printable RFID tags as compared to other competing chipless RFID technologies, such as printed electronics and SAW based RFID. While the low number of bits generated by the transmission line based ID generation can be a limiting factor in some applications, the low cost printable RFID tags are useful for low bit applications, such as anti-theft tags and one-bit tags in books, libraries, and archives.

## **8.2 RCS Measurement of Antennas for RFID Tag and Reader Design**

Besides the traditional use of RCS measurement in radio detection and ranging (RADAR) applications, recently, RCS measurement interests are being generated by the emergence of passive wireless communication technologies, such as RFID. The RFID systems function by measuring the scattered signal by the antenna on an RFID tag. The strength of the signal scattered by an antenna is measured in terms of the radar cross section (RCS) of the antenna. An antenna with high RCS scatters more of the incident energy back into space. An RFID tag operates by switching between two RCS states and effectively modulating the scattered signal and the RCS is observed by the remote reader. Conventionally, the RCS of antennas has been measured using methods involving bulky horn antennas and sophisticated and lengthy measurement techniques. The new RCS measurement method presented provides an easy method of RCS measurement without requiring a sophisticated experimental setup while providing more accurate and complete information on the RCS parameters of the antenna. Moreover, due to the larger antenna size requirement, the methods involving a horn antenna cannot be used for lower UHF frequencies, such as 915 MHz where most of the RFID systems are used.

Additionally, using the measured RCS parameters, the received backscattered signal by a reader can be modeled using the derived equation which is applicable to the design of more efficient RFID readers. The complete information provided by the new measurement method on the RCS parameters of antennas as an independent property, including the relative phase between the structural-mode RCS and antenna-mode RCS, are applicable in the design and development of efficient RFID tags and reader systems.

### **8.3 Low Cost Passive Chipless Sensing Applications**

The developed sensor tags do not contain any semiconductor chips on the tag and the sensors are fabricated using low cost on-tag fabrication techniques, such as dip-coating. This allows realization of low cost passive sensor tags that can be used for various sensing application, such as product monitoring, environment monitoring, health care, and household applications. The sensor tags containing only the antenna and the sensors are applicable to continuous product monitoring by applying a sensor tag on the product cases, such as monitoring the freshness of fruits in a shipping container when the fruits are being transported or in storage. Due to the distance constraints, these sensor tags can be read either by using mobile readers where the reader is kept at a certain specified distance range or in a conveyer belt type of application.

The sensor tags containing an ID generation circuit provides a tag identification feature in addition to the sensing feature. This allows different types of sensor tags to be used in any environment and also removes the distance constraints for an integrated antenna sensor tags (conf-I tags). These sensor tags are applicable in areas such as wireless monitoring of different physical parameters in a room or an environment. The chipless sensor tags are applicable to harsh environments where conventional chip-based

sensor tags cannot be used because of potential chip failures. In addition, the ID code is hard written on the tag in the form of transmission lines which cannot be altered without physically altering the length of the transmission lines. This protects the sensor tags from attackers, tag silencing, tag spoofing, virus attacks, information alteration, and other wireless attacks. Moreover, the developed sensor tags send the sensor information to the reader as an instantaneous change in the phase of the scattered signal and not as a digital signal, which protects the sensor tags against alteration of the sensor information by an attacker that could be done in chip-based sensor tags by altering the information stored in the memory. In addition, the chipless sensor tags do not contain any on-board battery, which makes them valuable in applications where changing tag batteries is not possible or feasible, and where continuous service of the tags is critical.

#### **8.4 Cyber Centric Environment Monitoring Applications**

The developed sensor system uses the developed reader system capable of communicating through cyberspace. The reader system communicates with the tag to obtain sensor and tag information and makes the obtained sensor tag information available on a user web interface, which can be securely accessed through the worldwide web. Due to the low cost of the chipless sensor tags and the features developed on the reader system, the sensor system is applicable for cyber centric environment monitoring. An example of such an application is depicted in Figure 8.1. The low number of bits generated by the chipless tags is used for the identification of the sensor type on the tag. This allows deploying different types of sensor tags in a given environment, as shown in Figure 8.1, where an environment contains a reader and a number of tags where each tag

contains a different type of sensor. Thus, by using this system, a number of physical parameters can be monitored in a given environment.

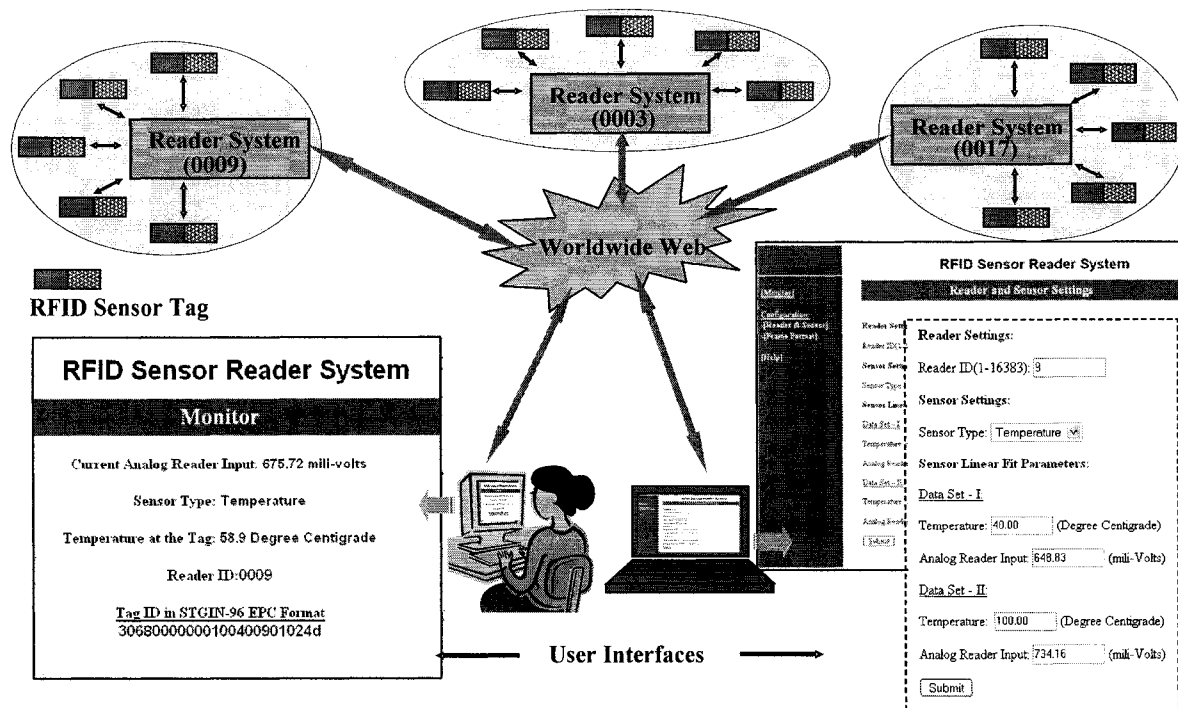


Figure 8.1 The schematic illustration of cyber centric multiple environment monitoring application of the chipless sensor system.

As shown in Figure 8.1, each reader is assigned a unique reader ID which distinguishes that particular reader from other readers. As a reader is associated with a particular environment, the reader ID also uniquely identifies the associated environment. The environment discussed can be a room or an open area covered by the reading range of the reader. The readers are connected to the worldwide web and can thus be accessed and the sensor tags monitored from any computer connected to the worldwide web. The readers provide a unique reader ID which allows the identification of the monitored environment, such that multiple environments can be monitored using multiple readers. For example, if the application shown in Figure 8.1 is a big storage facility with a

particular types of products stored in any storage unit, the system can be used in a storage unit to monitor different parameters, such as temperature, humidity, or any gas present unique to the stored product, such as ethylene in the case of climatic fruits. Here, a storage unit makes an environment and a system can be deployed in each storage unit, thus allowing the environmental condition of all the units to be remotely monitored. The developed sensor system provides a convenient and cost effective method for remote environment monitoring through cyberspace.



## CHAPTER 9

### CONCLUSION AND FUTURE WORK

#### 9.1 Conclusion

A chipless RFID sensor tag system with microstrip transmission line based ID generation schemes is presented. The sensor tag system consists of chipless passive RFID sensor tags and a specialized reader system. The presented system has been designed to be used through cyberspace for wireless environment monitoring applications. Moreover, the developed system provides a cost-effective approach for the realization of RFID sensor systems. System testing with temperature and ethylene sensor tags has been demonstrated.

A novel passive ID generation scheme that utilizes reflection and delay in a transmission line has been discussed in Chapter 4. The pulse reflection due to impedance mismatch in a transmission line has been utilized to construct OOK modulated signal patterns for ID generation. The generation of OOK modulated signal patterns using multiple reflections of an input pulse signal in a two transmission line system and a step impedance transmission line system have been demonstrated. Ten different ID codes generated by placing three reflected pulses in six different bit positions have been demonstrated. However, the scheme allows for the generation of higher combinations of bits.

Most of the passive RFID systems are used at the 915 MHz or 2.4 GHz ISM frequency bands. Due to the use of horn antennas and lengthy measurement process involved, existing RCS measurement methods are not practical for lower UHF range antennas, such as 915 MHz and 2.4 GHz. Moreover, these methods do not provide complete and accurate information on the scattering properties of antennas, which is needed for chipless sensor tag design. Thus, a more accurate and practical measurement method that provides complete RCS information for the antenna, including the relative phase factor, has been presented in Chapter 5. An equation for the received backscattered signal power, which takes leakage signals and observation errors into account, and has not been considered in previously reported methods, has been derived. The equation is solved using minimum mean square error estimation, and the solution is used to obtain structural-mode RCS, antenna-mode RCS, and relative phase of an antenna by applying short, open, and match load cases.

A measurement example of the scattering parameters of a microstrip patch antenna using the developed method has also been demonstrated. The structural-mode RCS, antenna-mode RCS, and the relative phase factor  $\cos(\phi_0)$  of the antenna are measured as  $-18.307$  dBsm,  $-20.386$  dBsm, and  $0.970$ , respectively. The measured results have also been compared with the results obtained with other commonly used measurement techniques. It has been observed that the results obtained with methods based on a single antenna vary with distance, indicating considerable error in the measured parameters.

The design, fabrication, and testing of the chipless sensor tags have been presented in Chapter 6. Two configurations of the developed chipless passive tags (conf-I

and conf-II) that provide a range of sensor types for consideration have been discussed. For the testing of the conf-I temperature sensor tag (consisting of a temperature sensor connected as a load to the antenna), a 28% amplitude change in demodulated received signal is observed when the temperature at the tag was changed from 27 °C to 140 °C. With the conf-II tags (consisting of an antenna, a microstrip transmission line for ID generation, and a sensor) generation of eight different ID codes using a PPM modulated signal pattern has been demonstrated. Testing of the conf-II sensor tag with discrete capacitors (as sensors) resulted in an average of 26.51° /pF phase change in the antenna-mode scattered signal, when the load capacitance (sensor) of the tag was changed between 1 to 5 pF. The experiment with the integrated ethylene sensor resulted in a 33° phase shift in the antenna-mode scattered signal when the ethylene concentration was changed from 0 to 100 ppm.

The reader system discussed in Chapter 7 encloses an analog reader and an SBC. The hardware, software, and the implementation of the reader system have been discussed. In the as presented reader system, the analog reader communicates with the sensor tags at a 915 MHz signal frequency and feeds the received signal to the SBC. The SBC then computes the sensor value from the input signal, constructs a unique ID code, and makes the information available to the user through a user interface accessible from cyberspace. Compared to active RFID sensor tags, the proposed tags generate a fewer number of bits. However, due to the passive chipless ID generation technique used, the new tags have a longer life time and are more cost effective. Compared to the limited types of sensor tags realizable with SAW based RFID, the proposed sensor tags provide a wide range of sensor types for consideration.

## 9.2 Future Work

With the knowledge gained from theoretical analysis, simulation results, and observation of the experimental results, the research work can be used to further increase the quality, efficiency, and applications of the developed sensor tag system, which is planned as future work. A planned outline for future work is presented in this section.

### 9.2.1 Substrate with Higher Delay for Higher Number of Bits

The presented schemes use transmission line reflection and delay for ID generation. These schemes require a longer transmission line to generate a higher number of bits. However, due to the size and signal loss constraints, using a longer transmission line approach for a higher number of bits is not practical. On the other hand, the number of bits can also be increased by increasing the propagation delay in the transmission line. As given by Equation (3.17) the speed of a signal in a transmission line is inversely related to the square root of the dielectric constant of the substrate material. Thus, the signal propagation delay in the transmission line can be increased by using a substrate of higher dielectric constant. In Equation (3.17), if the dielectric constant is increased by four fold, the delay increases by two fold, thus allowing the ID circuit to generate twice as many number of codes (bit combinations) as with the original substrate. The increase in code combination corresponds to the increase by 1 bit of the ID code (8 binary combinations is equivalent to 3 bits and 16 binary combinations is equivalent to 4 bits). Thus, for a given transmission line length, considering that other parameters do not change, every four fold increase in dielectric constant increase 1 bit of the generated tag ID. Some of the high dielectric constant materials that have been used in microelectronic devices and possess applicability to the presented schemes are listed in Table 9.1.

Table 9.1 High Dielectric Constant Materials.

<i>Material</i>	<i>Dielectric Constant</i>
Hafnium Oxide (HfO <sub>2</sub> )	25
Zirconium Oxide (ZrO <sub>2</sub> )	20-25
Hafnium Silicate (HfSiO <sub>4</sub> )	15-18
Zirconium silicate (ZrSiO <sub>4</sub> )	15
SrTa <sub>2</sub> O <sub>6</sub>	35-45
Titanium Oxide (TiO <sub>2</sub> )	100

### 9.2.2 More Flexible Substrates

The tags have been fabricated on a copper-clad flexible substrate with 177  $\mu\text{m}$  (dielectric = 127  $\mu\text{m}$  and adhesive = 50  $\mu\text{m}$ ) thick dielectric material. To further increase the flexibility and reduce the price of the tags, other thin and flexible substrates can be used. Some of the more flexible substrates useful for sensor tag fabrication are listed in Table 9.2.

Table 9.2 More Flexible Substrates for Sensor Tag Fabrication.

<i>Substrate</i>	<i>Thickness (<math>\mu\text{m}</math>)</i>	<i>Dielectric Material</i>	<i>Flexibility</i>
Pyralux® AC Copper-clad Laminate	Dielectric = 12	Polyimide	High Flexural Endurance
Pyralux® AX Copper-clad Laminate	Dielectric = 25	Polyimide	High Flexural Endurance
Nikaflex® F-20V Epoxy Adhesive based Clad	Dielectric = 12.5 Adhesive = 13	Polyimide	Excellent Flexural Endurance
Shin-Etsu MicroSi RNS22D58	Dielectric = 69 Adhesive = 10	Polyimide	Excellent Flexural Endurance

### **9.2.3 Tag Printing Techniques**

The sensor tags have been fabricated using standard photolithographic techniques used for semiconductor device fabrication. The use of photolithographic techniques for tag fabrication can produce precise devices useful for prototyping. However, alternative techniques, such as ink-jet printing technologies, are more cost effective for commercial applications. Ink-jet printing techniques have been extensively researched and used for microstrip lines and device fabrication. Thus, the continuing study and implementation of various tag printing technologies have the potential of greatly reducing the cost of the sensor tags.

### **9.2.4 Automatic ID Code and Phase Decoding**

In the presented sensor tag, the ID generation has been accomplished using signal pulses of several nanoseconds duration and the sensor information is introduced as the phase change of such signal pulses. The smaller pulse width helps to reduce the size of the tag for a given number of generated bits. However, due to the smaller pulse width used, the reading of the generated ID and the sensor introduced phase change have been achieved through the manual observation of the signal on the oscilloscope. An ID decoding and phase detection circuit can be integrated into the developed reader system platform for automatic ID code decoding and phase reading. This can be achieved by using a fast analog to digital converter and adding an application program in the reader, to input the signal from the A/D converter, decode the ID and compute the phase change from the input data. Additionally, the reader should include a functionality to switch between the two modes of reading for conf-I and conf-II tags. The schematic of a reader system showing an extension to provide automatic ID code and phase information

reading capabilities is shown in Figure 9.1, where the additional functionalities needed are indicated with dotted lines.

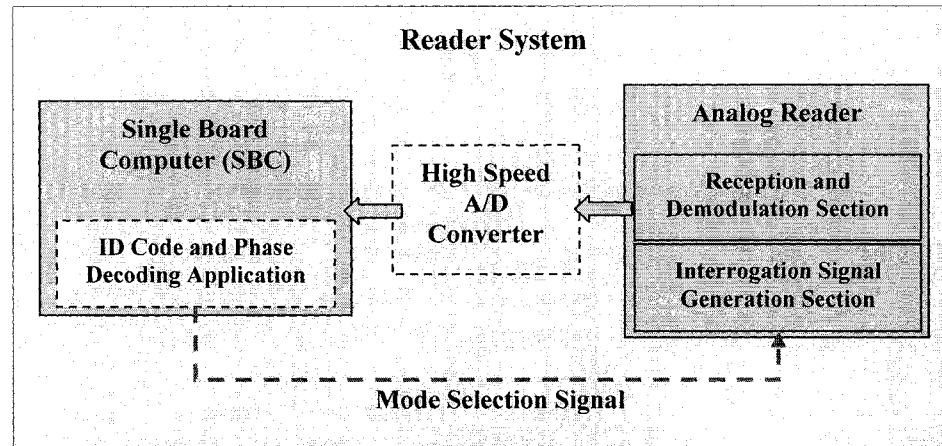


Figure 9.1 Schematic of the reader system showing extension for automatic ID and phase reading capability.

### **9.2.5 Cellular RFID Sensor Tag Deployment Scheme using Mobile Readers**

The cyber centric monitoring of the environment using the chipless sensor tag system was discussed in Section 8.4 with the aid of Figure 8.1. In the discussed implementation, as also illustrated by Figure 8.1, a reader is always associated with a particular tag environment called the reader domain. This requires having a reader in each domain. For a more cost effective and large scale sensor deployment, mobile readers with a location or cell ID concept can be used. The implementation of the cellular concept is illustrated in Figure 9.2 using examples of temperature and gas sensor IDs. In the implementation model shown, the sensor deployment field is divided into a large number of cells or locations and each cell is assigned a unique cell ID. A reader can move from cell to cell and read the sensor tags. The reader in a particular cell constructs an RFID tag

data frame, including the cell ID. In the example shown in Figure 9.2, the tag ID constructed for a temperature sensor (1) by a reader 009 in cell 1248 is “prefix + 009 + 1248 + 1 + sensor info” while the tag ID constructed by the same reader (009) for another temperature sensor tag (1) in a different cell 1246 differs from the previous one as “prefix + 009 + 1246 + 1 + sensor info.” Thus, the inclusion of the cell ID in the data frame makes it unique among the tag IDs constructed by the same reader and the same kind of sensor tag in a different cell.

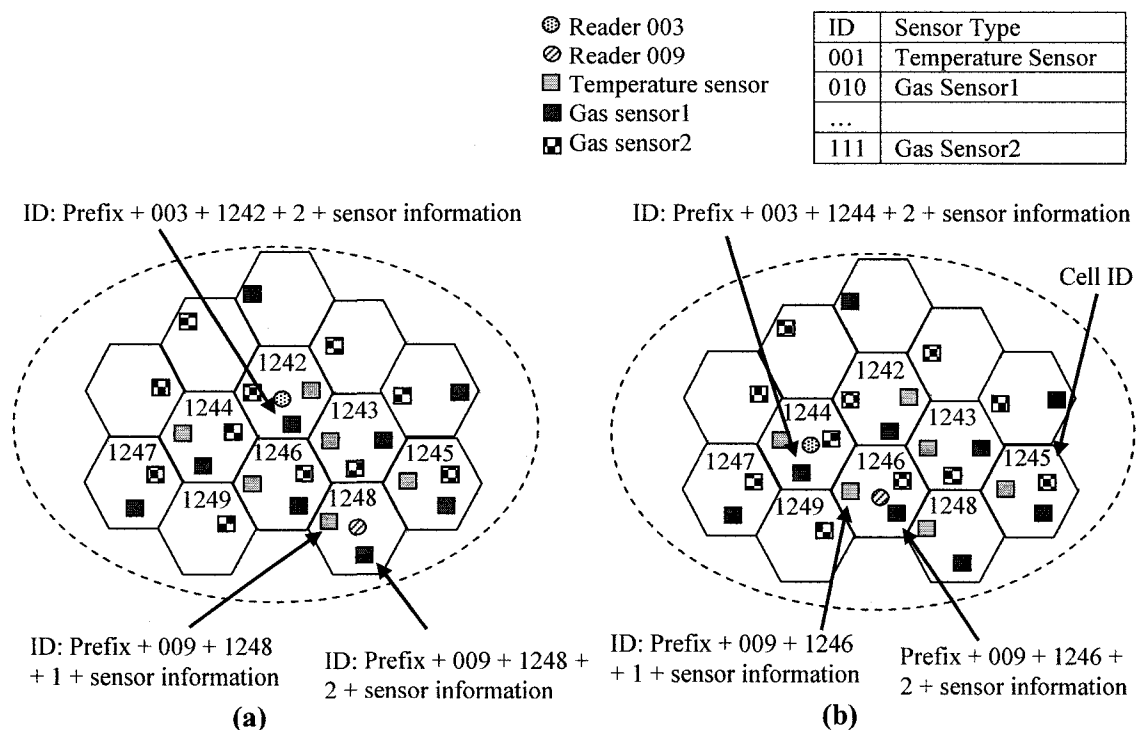


Figure 9.2 The cellular RFID sensor tag deployment concept. (a) Example for reader 003 located in cell 1242 and 009 in cell 1248. (b) Reader 003 moves to cell 1244 and 009 moves to cell 1246.

The reader can obtain the cell ID from a fixed device in the cell, for example a passive chip-based tag with stored cell ID or through a global positioning system (GPS) integrated into the reader system. In this case, the reader needs an additional capability to



convert the location information obtained from the GPS into the cell ID. Here, the ID code generated by the tag is used to identify the sensor on the tag. For example, an ID code **001** indicates that the tag contains a temperature sensor, while **010** indicates a gas sensor. Thus, if two temperature sensor tags are deployed in a given cell, it is not possible to uniquely identify the tags. However, two similar tags can be deployed in a cell to improve reliability. The size of a cell and the numbers of readers determine the cost and performance of the system. A smaller cell size and more readers give better performance but at higher cost.

## REFERENCES

- [1] K. Finkenzeller, *RFID handbook fundamentals and applications in contactless smart cards and identification*, 2nd ed. West Sussex, U.K.: Wiley, 2004.
- [2] C. W. Pobanz and T. Itoh, "Microwave noncontact identification transponder using subharmonic interrogation," *IEEE Transactions on Microwave Theory and Techniques*, vol. 43, no. 7, pp.1673-1679, 1995.
- [3] I. D. Robertson and I. Jalaly, "RFID tagging explained," *IEE Communications Engineer*, vol. 1, no. 1, pp.20-23, 2003.
- [4] J. P. Curty, M. Declercq, C. Dehollainand, and N. Joehl, *Design and optimization of passive UHF RFID systems*, New York: Springer, 2007.
- [5] R. Weinstein, "RFID: A technical overview and its application to the enterprise," *IT Professional*, vol. 7, no. 3, pp. 27-30, May-Jun. 2005.
- [6] P. G. Ranky, "Engineering management-focused radio frequency identification (RFID) model solutions," *IEEE Engineering Management Review*, vol. 35, no. 2, pp. 20-30, 2007.
- [7] A. Cangialosi, J. E. Monaly, and S. C. Yang, "Leveraging RFID in hospitals: Patient life cycle and mobility perspectives," *IEEE Communications Magazine*, vol. 45, no. 9, pp. 18-23, Sep. 2007.
- [8] Y. Ekinci, U. Ekinci, and U. Gunaydin, "The application of UHF passive RFID technology for the effectiveness of retail/consumer goods supply chain management," *1st Annual RFID Eurasia*, Istanbul, Turkey, Sep. 2007, pp. 1-6.
- [9] O. Atsushi and Y. Kentaro, "A temperature-managed traceability system using RFID tags with embedded temperature sensors," *NEC Technical Journal*, vol. 1, no. 2, pp. 82-86, 2006.
- [10] M. Roberti, "Navy revs up RFID sensors," *RFID Journal*, Jun. 18, 2004. [Online]. Available: <http://www.rfidjournal.com/article/view/990/1/1>. [Accessed Oct. 14, 2005].
- [11] S. C. Mukhopadhyay, A. Gaddam, and G. S. Gupta, "Wireless sensors for home monitoring - A review," *Recent Patents on Electrical Engineering*, vol. 1, no. 1, pp. 32-39, 2008.

- [12] J. Brusey and A. Throne, "Aero-ID sensor integration: Scope of work," *Aerospace ID*, Feb. 1, 2006. [Online]. Available: [http://www.aero-id.org/research\\_reports/AEROID-CAM-003-Sensors.pdf](http://www.aero-id.org/research_reports/AEROID-CAM-003-Sensors.pdf). [Accessed Sep. 2, 2006].
- [13] H. Shen, L. Li, and Y. Zhou, "Fully integrated passive UHF RFID tag with temperature sensor for environment monitoring," *Proc. 7th International Conference on ASIC*, Guilin, China, Oct. 2007, pp. 360-363.
- [14] J. Mitsugi, T. Inaba, B. Patkai, L. Theodorou, J. Sung, and T. S. Lopez et al., "Architecture development for sensor integration in the EPCglobal network," *Auto-ID Labs White Paper*, WP-SWNET-018, Jul. 2007.
- [15] S. Haller and S. Hodges, "The need for a universal smart sensor network," *Auto-ID Center*, Nov. 1, 2002. [Online]. Available: <http://autoid.mit.edu/whitepapers/cam-autoid-wh-007.pdf>. [Accessed Sep. 2, 2006].
- [16] D. C. Ranasinghe, K. S. Leong, M. L. Ng, D. W. Engles, and P. H. Cole, "A distributed architecture for a ubiquitous RFID sensing network," *Intelligent Sensors, Sensor Networks and Information Processing Conference*, Australia, Dec. 2005, pp. 7-12.
- [17] E. Jovanov, A. O. Lords, D. Raskovic, P. G. Cox, R. Adhami, and F. Andrasik, "Stress monitoring using a distributed wireless intelligent sensor system," *IEEE Engineering in Medicine and Biology Magazine*, vol. 22, no. 3, pp. 49-55, May 2003.
- [18] H. H. Asada, P. Shaltis, A. Reisner, S. Rhee, and R. C. Hutchinson, "Mobile monitoring with wearable photoplethysmographic biosensors," *IEEE Engineering in Medicine and Biology Magazine*, vol. 22, no. 3, pp. 28-40, May 2003.
- [19] A. D. DeHennis and K. D. Wise, "A wireless microsystem for the remote sensing of pressure, temperature, and relative humidity," *Journal of Microelectromechanical Systems*, vol. 14, no. 1, pp.12-22, Feb. 2005.
- [20] F. Rahman, A. Kumar, and G. Nagendra, "Network approach for physiological parameters measurement," *IEEE Transactions on Instrumentation and Measurement*, vol. 54, no. 1, pp. 337-346, Feb. 2005.
- [21] "Embedsense wireless sensor," *Micro Strain Inc.*, Jun. 1, 2007. [Online]. Available: [http://www.microstrain.com/pdf/wireless-sensors/embedsense/EmbedSense\\_Rev1\\_datasheet.pdf](http://www.microstrain.com/pdf/wireless-sensors/embedsense/EmbedSense_Rev1_datasheet.pdf). [Accessed Apr. 2, 2008].
- [22] A. Ogasawara and K. Yamasaki, "A temperature-managed traceability system using RFID tags with embedded temperature sensors," *NEC Technical Journal*, vol. 1, no. 2, pp. 82-86, 2006.

- [23] I. Zalbide, J. Vicario, and I. Velez, "Power and energy optimization of the digital core of a gen2 long range full passive RFID sensor tag," *Proc. IEEE International Conference on RFID*, Nevada, USA, Apr. 2008, pp. 126-133.
- [24] G. Chen, L. Li, H. Shen, and Y. Zhou, "Design of a low-power digital core for passive UHF RFID sensor," *International Conference on ASIC*, Toowoomba, Australia, Oct. 2007, pp. 886-889.
- [25] L. Lofgren, B. Lofving, T. Pettersson, B. Ottosson, C. Rusa, and C. Haas et al., "Low-power humidity sensor for RFID applications," *Proc. M42008 Conference*, Cardiff, UK, Sep. 2008.
- [26] M. Christian, M. Florian, and F. Elgar, "Ambient energy scavenging for sensor-equipped RFID tags in the cold chain," *Lecture Notes in Computer Science*, Springer Berlin/Heidelberg, vol. 4793, pp. 255-269, Oct. 2007.
- [27] T. Kaya, "A new batteryless active RFID system: Smart RFID," *1st Annual RFID Eurasia*, Istanbul, Turkey, Sep. 2007, pp. 1-4.
- [28] P. Sample, D. J. Yeager, P. S. Powledge, A. V. Mamishev, and J. R. Smith, "Design of an RFID-based battery-free programmable sensing platform," *IEEE Transaction on Instrumentation and Measurement*, vol. 57, no. 11, pp. 2608-2615, Nov. 2008.
- [29] N. Cho, S.-J. Song, J.-Y. Lee, S. Kim, S. Kim, and H.-J. Yoo, "A 8-mW, 0.3mm<sup>2</sup> RF-powered transponder with temperature sensor for wireless environment monitoring," *IEEE International Symposium on Circuits and Systems*, vol. 5, May 2005, pp. 4763-4766.
- [30] J. R. Smith, B. Jiang, S. Roy, M. Philipose, K. S. Rajan, and A. Mamishev, "ID modulation: Embedding sensor data in an rfid timeseries," *Proc. Information Hiding*, LNCS 3727, pp. 234-246, 2005. [Online]. Available: <http://web.media.mit.edu/~jrs/WISP-IHW.pdf>. [Accessed Oct. 5, 2006].
- [31] R. Want, "Enabling ubiquitous sensing with RFID," *IEEE Computer*, vol. 37, no. 4, pp. 84-86, Apr. 2004.
- [32] M. Philipose, J. R. Smith, B. Jiang, A. Mamishev, R. Sumit, and K. Sundara-Rajan, "Battery-free wireless identification and sensing," *IEEE Pervasive Computing*, vol. 4, no. 1, pp. 37-45, Jan.-Mar. 2005.
- [33] K. Opasjumruskit, T. Thanthipwan, O. Sathusen, P. Sirinamarattana, P. Gadmanee, and El Pootarapan et al., "Self-powered wireless temperature sensors exploit RFID technology," *IEEE Pervasive Computing*, vol. 5, no. 1, pp. 54-61, Jan.-Mar. 2006.

- [34] K. Chang, Y. H. Kim, Y. J. Kim, and Y. J. Yoon, "Functional antenna integrated with relative humidity sensor using synthesised polyimide for passive RFID sensing," *IEE Electronic Letters*, vol. 43, no. 5, Mar. 2007.
- [35] J. Siden, X. Zeng, T. Unander, A. Koptuyug, and H.-E. Nilsson, "Remote moisture sensing utilizing ordinary RFID tags," *Proc. IEEE Sensors Conference*, Atlanta, USA, Oct. 2007, pp. 308-311.
- [36] C. M. Robert, "Radio frequency identification (RFID)," *Computers & Security*, no. 25, pp. 18-26, 2006.
- [37] M. R. Rieback, B. Crispo, and A. S. Tanenbaum, "Is your cat infected with a computer virus?," in *4th Annual IEEE International Conference on Pervasive Computing and Communications*, Pisa, Italy, Mar. 2006.
- [38] T. Phillips, T. Karygiannis, and R. Kuhn, "Security standards for the RFID market," *IEEE Security & Privacy Magazine*, vol. 3, no. 6, pp. 85-89, Nov.-Dec. 2005.
- [39] A. Chamarti, W. Mohammad, S. Ramisetti, J. Vemagiri, U. Dandgey, and K. Varahramyan, "A low cost flexible-substrate wireless sensor tag based on sensor switch element," *55th Electronic Components and Technology Conference*, Florida, United States, May 2005, pp. 523-527.
- [40] S. Mukherjee, "Passive sensors using RF backscatter," *Microwave Journal*, vol. 47, no. 11, pp. 96, Nov. 2004.
- [41] M. D. Balachandran, S. Shrestha, M. Agarwal, Y. Lvov, and K. Varahramyan, "SnO<sub>2</sub> capacitive sensor integrated with microstrip patch antenna for passive wireless detection of ethylene gas," *IEE Electronic Letters*, vol. 44, no. 7, Mar. 2008.
- [42] S. Mukherjee, "Chipless radio frequency identification (RFID) device," *1st Annual RFID Eurasia*, Istanbul, Turkey, Sep. 2007, pp. 1-4.
- [43] A. Chamarti and K. Varahramyan, "Transmission delay line-based ID generation circuit for RFID applications," *IEEE Microwave and Wireless Components Letters*, vol. 16, no. 11, pp.588-590, Nov. 2006.
- [44] J. Vemagiri, A. Chamarti, M. Agarwal, and K. Varahramyan, "Transmission line delay-based radio frequency identification (RFID) tag," *Microwave and Optical Technology Letters*, vol. 49, no. 8, pp. 1900-1904, 2007.
- [45] A. Chamarti, "Delay line based passive radio frequency identification tags," Ph.D. Dissertation, Louisiana Tech University, 2006.
- [46] J. K. Vemagiri, "Design and development of microstrip antenna," Ph.D. Dissertation, Louisiana Tech University, 2006.

- [47] J. C. Liu and J. H. Yao, "Wireless RF identification system based on SAW," *IEEE Transaction on Industrial Electronics*, vol. 55, no. 2, pp. 958-961, Feb. 2008.
- [48] L. Shujian, M. Lin, and W. Danzhi, "A remote wireless identification system based on passive surface acoustic wave (SAW) devices," *Proc. of International Conference on Communications, Circuits and Systems*, vol. 2, May 2005, pp. 1113-1116.
- [49] S. Harma, V. P. Plessky, C. S. Hartmann, and W. Steichen, "Z-path SAW RFID tag," *IEEE Transactions on Ultrasonic, Ferroelectronics, and Frequency Control*, vol. 55, no. 1, pp. 208-213, Jan. 2008.
- [50] S. Harma and V. P. Plessky, "Extraction of frequency-dependent reflection, transmission, and scattering parameters for short metal reflectors from FEM-BEM simulations," *IEEE Transactions on Ultrasonic, Ferroelectronics, and Frequency Control*, vol. 55, no. 4, pp. 883-889, Apr. 2008.
- [51] S. Harma, W. G. Arthur, C. S. Hartmann, R. G. Maev, and V. P. Plessky, "Inline SAW RFID tag using time position and phase encoding," *IEEE Transactions on Ultrasonic, Ferroelectronics, and Frequency Control*, vol. 55, no. 8, pp. 883-889, Aug. 2008.
- [52] M. Schussler, C. Damm, M. Maasch, and R. Jakoby, "Performance evaluation of left handed delay line for RFID backscatter applications," *IEEE MTT-S International Microwave Symposium Digest*, Georgia, United States, Jun. 2008, pp. 177-180.
- [53] L. M. Reindl and I. M. Shrena, "Wireless measurement of temperature using surface acoustic waves sensors," *IEEE Transactions on Ultrasonic, Ferroelectronics, and Frequency Control*, vol. 51, no. 11, pp. 1457-1463, Nov. 2004.
- [54] A. Stelzer, S. Scheiblhofer, S. Schuster, and M. Brandl, "Multi reader/multi-tag SAW RFID systems combining tagging, sensing, and ranging for industrial applications," *IEEE International Frequency Control Symposium*, Hawaii, USA, May 2008, pp. 263 – 272.
- [55] C. Hausleitner, A. Pohl, M. Brandl, and F. Seifert, "New concepts of wireless interrogable passive sensors using nonlinear components," *IEEE International Symposium on Applications of Ferroelectrics*, Honolulu, HI, pp.851-854, 2000.
- [56] D. D. King, "The measurement and interpretation of antenna scattering," *Proc. IRE*, vol. 37, no. 7, pp. 770-777, Jul. 1949.
- [57] J. A. McEntee, "A technique for measuring the scattering aperture and absorption aperture of an antenna," *Antenna Laboratory, Ohio State University, Columbus, OH*, Rep. no. 612-14, 1957.

- [58] J. Appel-Hansen, "Accurate determination of gain and radiation patterns by radar cross-section measurements," *IEEE Transaction on Antennas and Propagation*, vol. AP-27, no. 5, pp. 640-646, Sep. 1979.
- [59] K. M. Lambert, R. C. Rudduck, and T. H. Lee, "A new method for obtaining antenna gain from backscatter measurements," *IEEE Transaction on Antenna and Propagation*, vol. 38, no. 6, pp. 896-902, Jun. 1990.
- [60] J. T. Mayhan, A. R. Dion, and A. J. Simmons, "A technique for measuring antenna drive port impedance using backscatter data," *IEEE Transaction on Antenna and Propagation*, vol. 42, no. 4, pp. 526-533, Apr. 1994.
- [61] W. Wiesbeck and E. Heidrich, "Wide-band multiport antenna characterization by polarimetric RCS measurements," *IEEE Transactions on Antenna and Propagation*, vol. 46, no. 3, pp. 341-350, Mar. 1998.
- [62] R. B. Green, "Scattering from conjugate-matched antennas," *IEEE Transaction on Antennas and Propagation*, vol. AP-14, no. 1, pp. 17-21, Jan. 1966.
- [63] R. C. Hansen, "Relationship between antennas as scatterers and as radiators," *Proc. of the IEEE*, vol. 77, no. 5, pp. 659-662, May 1989.
- [64] T. M. Au, Y. W. M. Chia, and M. S. Leong, "Backscattering characteristics of finite narrow rectangular loop," *IEEE Antenna and Propagation Society International Symposium*, Montreal, Canada, pp. 294-297, Jul. 1997.
- [65] K. Penttila, M. Keskilammi, L. Sydanheimo, and M. Kiviloski, "Radar cross-section analysis for passive RFID system," *Proc. IEEE Microwave Antenna and Propagation*, vol. 153, no. 1, pp. 103-109, Feb. 2006.
- [66] K. J. Lee, D. Kim, M. Kim, M. Tanak, and K. Matsugatani, "A 2.4-GHz dual-patch RFID tag antenna scattering analysis," *Microwave and Optical Technology Letters*, vol. 48, no. 11, pp. 2241-2244, Nov. 2006.
- [67] S. Hu, H. Chen, C. K. Law, Z. Shen, L. Zhu, and W. Zhang et al., "Back scattering cross section of ultra-wideband antennas," *IEEE Antennas and Propagation Letters*, vol. 6, pp. 70-73, 2007.
- [68] Y. Liu, S. X. Gong, and D. M. Fu, "A novel model for analyzing the RCS of microstrip antenna," *IEEE Antenna and Propagation Society International Symposium*, vol. 4, Jun. 2003, pp. 835-838.
- [69] P. V. Nikitan and K. V. S. Rao, "Theory and measurement of backscattering from RFID tags," *IEEE Antenna and Propagation Magazine*, vol. 48, no. 6, pp. 212-218, Dec. 2006.

- [70] M. D. Balachandran “Tin dioxide nanoparticle based sensor integrated with microstrip antenna for passive wireless ethylene sensing,” Ph.D. Dissertation, Louisiana Tech University, 2008.
- [71] “IDTechEx RFID market projections 2008 to 2018,” *IDTechEx.com*, Feb. 4, 2008. [Online]. Available: [http://www.idtechex.com/research/articles/idtechex\\_rfid\\_market\\_projections\\_2008\\_to\\_2018\\_00000813.asp](http://www.idtechex.com/research/articles/idtechex_rfid_market_projections_2008_to_2018_00000813.asp). [Accessed Nov. 5, 2008].
- [72] “Chipless RFID - the end game,” *IDTechEx.com*, Feb. 20, 2006. [Online]. Available: [http://www.idtechex.com/research/articles/chipless\\_rfid\\_the\\_end\\_game\\_00000435.asp](http://www.idtechex.com/research/articles/chipless_rfid_the_end_game_00000435.asp). [Accessed Nov. 5, 2008].
- [73] R. Das, “Chip versus chipless for RFID applications,” *Proc. Joint Conference on Smart Objects and Ambient Intelligence*, Grenoble, France, pp. 23-26, Oct. 2005.
- [74] S. Shrestha, M. D. Balachandran, M. Agarwal, V. V. Phoha, and K. Varahramyan, “Chipless RFID Sensor System for Cyber Centric Monitoring Applications,” *IEEE Transaction on Microwave Theory and Techniques*, submitted on Jan. 2008.
- [75] S. Y. Liao, *Microwave Devices and Circuits*, 3rd ed., New Jersey, USA: Prentice Hall, 1990.
- [76] F.D. Paolo, *Networks and Devices Using Planar Transmission Lines*, Boca Raton, Florida, USA: CRC Press, 2000.
- [77] I. A. Glover, S. R. Pennock, and P. R. Shepherd, *Microwave Devices, Circuits and Subsystems for Communications Engineering*, West Sussex, UK: Wiley, 2005.
- [78] S. R. Seshadri, *Fundamentals of Transmission Line and Electromagnetic Fields*, Massachusetts, USA: Addison-Wesley, Sep. 1971.
- [79] “Pyralux FR copper-clad laminate,” *DuPont*, Jul. 2004. [Online]. Available: [http://www2.dupont.com/Pyralux/en\\_US/assets/downloads/pdf/FRclad\\_H-73233.pdf](http://www2.dupont.com/Pyralux/en_US/assets/downloads/pdf/FRclad_H-73233.pdf). [Accessed Oct. 18, 2006].
- [80] J. Grzyb, I. Ruiz, and G. Troster, “Extraction of material complex permittivity for composite substrate MCM-L technologies,” *Proc. 7th IEEE Workshop on Signal Propagation on Interconnects*, pp. 143-146, May 2003.
- [81] M. Kobayashi “A dispersion formula satisfying recent requirements in microstrip CAD,” *IEEE Transactions on Microwave Theory and Techniques*, vol. 36, no. 8, pp.1246-1250, 1988.



- [82] R. L. Veghte and C. A. Balanis, "Dispersion of transient signals in microstrip transmission lines," *IEEE Transactions on Microwave Theory and Techniques*, vol. 34, no. 12, pp.1427-1436, 1986.
- [83] S. R. Best, "Shunt-stub-line impedance matching: A wave reflection analysis tutorial," *IEEE Antennas and Propagation Magazine*, vol. 44, no. 1, pp.76-86, 2002.
- [84] H. A. Wheeler, "Reflection characteristic relating to impedance matching," *IEEE Transactions on Microwave Theory and Techniques*, vol. MTT-32, no. 9, pp.1008-1021, 1984.
- [85] C. E. Abernethy, A. C. Cangellaris, and J. L. Prince, "Novel method of measuring microelectronic interconnect transmission line parameters and discontinuity equivalent electrical parameters using multiple reflections," *IEEE Transactions on Components, Packaging, and Manufacturing Technology Part B: Advanced Packaging*, vol. 19, no. 1, pp.32-39, 1996.
- [86] "Ansoft designer," *Ansoft Corporation*, ver. 2. [Online]. Available: [http://www.ansoft.com/products/hf/ansoft\\_designer](http://www.ansoft.com/products/hf/ansoft_designer). [Accessed Nov. 5, 2006].
- [87] S. Shrestha, J. Vemagiri, M. Agarwal, and K. Varahramyan, "Transmission line reflection and delay-based ID generation scheme for RFID and other applications," *International Journal on Radio Frequency Identification Technology and Applications*, vol. 1, no. 4, pp. 401–416, 2007.
- [88] "LinkCAD," *Gehriger Engineering*, ver. 5. [Online]. Available: <http://www.linkcad.com>. [Accessed Nov. 5, 2006].
- [89] S. Shrestha, M. Balachandran, M. Agarwal, L.-H. Zou, and K. Varahramyan, "A method to measure radar cross section parameters of antennas," *IEEE Transaction On Antenna and Propagation*, vol. 56, no. 11, pp. 3494-3500 , Nov. 2008.
- [90] P. Y. Ufimtsev, "Scattering of electromagnetic waves by a metallic object partially immersed in a semi-infinite dielectric medium," *IEEE Transactions Antennas and Propagation*, vol. 49, no. 2, pp. 223-233, 2001.
- [91] E. F. Knott, J. F. Shaeffer, and M. T. Tuley, *Radar Cross Section*, 2nd ed., New York: Springer, 2004.
- [92] J. Zhang, Z. Xie, S. Lai, and Z. Wu, "A design of RF receiving circuit of RFID reader," *Proc. 4th International Conference on Microwave and Millimeter Wave Technology*, Beijing, China, Aug. 2004, pp. 406-409.
- [93] Y. Liu, Q. Zhang, and M. Zheng, "Signal analysis and design criteria for UHF RFID reader," *Proc. 6th International Conference on ITS Telecommunication*, Chengdu, China, Jun. 2006, pp. 233-236.

- [94] “Agilent Fundamentals of RF and Microwave Power Measurements (Part 1) Introduction to Power, History, Definitions, International Standards & Traceability,” *Agilent Technologies Inc.*, USA, application note 1449-1, literature no. 5988-9213EN, Apr. 2003.
- [95] S. V. Vaseghi, *Advanced Digital Signal Processing and Noise Reduction*, 2nd ed. West Sussex: Wiley, 2000.
- [96] M. Kuropatwinski and W. B. Kleijin, “Minimum mean square error estimation of speech short-term predictor parameters under noisy conditions,” *IEEE International Conference on Acoustics, Speech, and Signal Processing*, vol. 1, Apr. 2003, pp. I-96-99.
- [97] D. C. Agnew and C. Constable, “Least squares estimation,” *Web Page for SIO223A*, ver. 1.1, chapter 7, 2004. [Online]. Available: <http://mahi.ucsd.edu/cathy/Classes/SIO223/Part1/sio223.chap7.pdf>. [Accessed: Apr. 2, 2007].
- [98] R. L. Mason, R. F. Gunst, and J. L. Hess, *Statistical Design and Analysis of Experiments with Applications to Engineering and Science*, 2nd ed. New Jersey: Wiley, 2003.
- [99] R. G. Kouyoumjian and L. Peters, “Range requirements in radar cross-section measurements,” *Proc. IEEE*, vol. 53, no. 8, pp. 920-928, Aug. 1965.
- [100] “Draft protocol specification for a 900 MHz class 0 radio frequency identification tag,” *MIT Auto ID center*, Feb. 23, 2003. [Online]. Available: [www.epcglobalinc.org](http://www.epcglobalinc.org). [Accessed Apr. 12, 2006].
- [101] “Global commerce initiative EPC roadmap,” *Global Commerce Initiative/IBM*, Nov. 2003. [Online]. Available: [www.fmi.org/docs/supply/gci\\_epc\\_report.pdf](http://www.fmi.org/docs/supply/gci_epc_report.pdf). [Accessed Nov. 5, 2007].
- [102] “EPC generation 1 tag data standards,” *EPC Global Standard Specification*, ver. 1.1, rev. 1.27, May 2005. [Online]. Available: [http://www.epcglobalinc.org/standards/tds/tds\\_1\\_1\\_rev\\_1\\_27-standard-20050510.pdf](http://www.epcglobalinc.org/standards/tds/tds_1_1_rev_1_27-standard-20050510.pdf). [Accessed Nov. 5, 2007].
- [103] J. Sung, T. S. Lopez, and D. Kim, “The EPC sensor network for RFID and WSN integration infrastructure,” *Proc. IEEE Computer and Society, 5th Annual IEEE International Conference on Pervasive Computing and Communication Workshops*, New York, USA, pp. 618-621, Mar. 2007.
- [104] Y. Liu, Q. Zhang, and M. Zheng, “Signal analysis and design criteria for UHF RFID reader,” in *6th International Conference on ITS Telecommunication*, Chedgu, China, pp. 233-236, 2006.

- [105] "QUICCStart MPC8248 evaluation system," *Freescale Semiconductor Inc.*, rev. B, 2006. [Online]. Available: [http://www.freescale.com/files/soft\\_dev\\_tools/doc/data\\_sheet/950-00102.pdf?pspl=1](http://www.freescale.com/files/soft_dev_tools/doc/data_sheet/950-00102.pdf?pspl=1). [Accessed Feb. 20, 2008].
- [106] "Embedded planet linux development kit," *Embedded Planet*. [Online]. Available: [http://www.embeddedplanet.com/products/bsp\\_linux.asp](http://www.embeddedplanet.com/products/bsp_linux.asp). [Accessed Feb. 20, 2008].
- [107] "Code warrior development studio," *Freescale Semiconductor Inc.*, 2004. [Online]. <http://www.freescale.com/webapp/sps/site/homepage.jsp?nodeId=012726>. [Accessed Feb. 20, 2008].
- [108] "BL 2500 single board computer," *Rabbit Inc.* [Online]. Available: <http://www.rabbit.com/products/bl2500/#specs>. [Accessed Apr. 5, 2008].
- [109] "Dynamic C," *Rabbit Inc.*, ver. 9.62. [Online]. Available: <http://www.rabbit.com/products/dc/index.shtml>. [Accessed Apr. 5, 2008].
- [110] H. Austerlitz, *Data Acquisition Techniques Using PCs*, 2nd ed. San Diego, California: Academic Press, 2002.
- [111] W. P. Birmingham, A. Brennan, A. P. Gupta, and D. P. Siewiorek, "MICON: A single-board computer synthesis tool," *IEEE Circuits and Devices Magazine*, vol. 4, no. 1, pp. 37-46, Jan. 1988.
- [112] "Dynamic C TCP/IP user's manual," *Rabbit Inc.*, vol. 2. [Online]. Available: <http://www.rabbit.com/documentation/docs/manuals/TCPIP/UsersManualV2/index.html>. [Accessed Apr. 5, 2008].